UNIVERSITY OF ALBERTA
LIBRARY

Regulations Regarding Theses and Dissertations

Typescript copies of theses and dissertations for Master's and Doctor's degrees deposited in the University of Alberta Library, as the official Copy of the Faculty of Graduate Studies, may be consulted in the Reference Reading Room only.

A second copy is on deposit in the Department under whose supervision the work was done. Some Departments are willing to loan their copy to libraries, through the inter-library loan service of the University of Alberta Library.

These theses and dissertations are to be used only with due regard to the rights of the author. Written permission of the author and of the Department must be obtained through the University of Alberta Library when extended passages are copied. When permission has been granted, acknowledgement must appear in the published work.

This thesis or dissertation has been used in accordance with the above regulations by the persons listed below. The borrowing library is obligated to secure the signature of each user.

Please sign below:

Date	Signature	Institution

THE UNIVERSITY OF ALBERTA

PRELIMINARY STUDY OF HYDRAULIC JUMP FORMATION ON ADVERSE SLOPES

A THESIS

SUBMITTED TO THE FACULTY OF GRADUATE STUDIES

IN PARTIAL FULFILMENT OF THE REQUIREMENTS FOR THE

DEGREE OF MASTER OF SCIENCE

DEPARTMENT OF CIVIL ENGINEERING

by

KRISHAN KAMRA, P. ENG.

EDMONTON, ALBERTA

JANUARY, 1966

UNIVERSITY OF ALBERTA

FACULTY OF GRADUATE STUDIES

The undersigned certify that they have read, and recommend to the Faculty of Graduate Studies for acceptance, a thesis entitled "Preliminary Study of Hydraulic Jump Formation on Adverse Slopes", submitted by Krishan Kamra, in partial fulfilment of the requirements for the degree of Master of Science.

ABSTRACT

This thesis presents a preliminary study of hydraulic jump formation on adverse slopes. The jump formations on horizontal and negative slopes are first briefly reviewed. Then two types of jumps are considered: i) jumps that form completely on the reverse slope (termed A-1), and ii) jumps that begin on the horizontal and end on the reverse slope (termed A-2). Chapter III presents a theoretical solution for the first type of jump. The form of solution for second is also proposed. Twenty-five sets of experiments have been conducted with five distinct adverse slopes. In general, these show that jumps on adverse slopes are extremely unstable. Information has been obtained regarding the boundary layer and the free mixing regions of the jump. The order of magnitude of the momentum and energy correction factors at the end of the roller, has also been estimated.

ACKNOWLEDGEMENTS

The author wishes to extend his appreciation to:

Dr. T. Blench, Professor of Civil Engineering, for his encouragement of this work.

Mr. J.P. Verschuren, Associate Professor of Civil Engineering, for his general supervision of research and much valuable criticism.

Dr. N. Rajaratnam of Department of Civil Engineering for his considerable help and detailed guidance with the experiment, the preparation of manuscript, derivation of mathematical relationships and generous lending of publications from his personal library.

Mr. W.A.B. Saunders, Principal, Northern Alberta Institute of Technology, for permission to use the Hydraulics Laboratory and facilities at N.A.I.T., in carrying out this investigation.

Mr. R. Alexander, Head, Photographic Technology Section, Northern Alberta Institute of Technology, for his very considerable help in developing suitable photographic techniques in obtaining experimental data.

Messrs. J. Nemeth, and R. Strembecki, then students of Photographic Technology at N.A.I.T., for their very diligent and patient assistance in obtaining photographic recordings.

K.K.

EDMONTON

January, 1966

TABLE OF CONTENTS

		Page
Abstract		i
Acknowledgements		ii
Table of Contents		iii
List of Figures		vi
Glossary of Symbols		viii
CHAPTER I	THE PROBLEM AND SCOPE OF RESEARCH	1
	Introduction	1
	Jump Formation in Level Rectangular Channels	4
	Jump Formation in Sloping Channels	10
CHAPTER II	HYDRAULIC JUMP ON NEGATIVE SLOPES	11
	Introduction	11
	Historical Review	12
	Types of Jump	14
	Type C-Jump	16
	Fixing the Type of Jump	22
	Energy Loss in the Sloping Channel Jump	26
	Type E-Jump	26

		Page
CHAPTER III	HYDRAULIC JUMP ON POSITIVE (OR ADVERSE) SLOPES	33
	Theoretical Analysis	
	Introduction	33
	Types of Jump	34
	A-1 Jump: General Solution	34
	Approximate Solution for Small Adverse Slopes	42
	A-2 Jump	45
CHAPTER IV	THE EXPERIMENT, TEST PROCEDURE, AND ANALYSIS	46
	General Aims of the Experiment	46
	Experimental Arrangement	47
	Stability of the Jump on Adverse Slopes	52
	Experimental Details	56
	Length of A-2 Jump	56
	Experimental Data - Table I	57
	Velocity Distribution in the Boundary Layer Portion	58
	Free Mixing Region	63
	Variation of the Parameter δ_1/y_1	63
	Decay of the Maximum Velocity	66
	Momentum and Energy Coefficients at the End of the Roller	66

		Page
CHAPTER V	CONCLUSIONS AND RECOMMENDATIONS	71
	Conclusions	71
	Recommendations for Future Research	72
BIBLIOGRAPHY		73
APPENDIX A	SURFACE PROFILE RECORDINGS	75
APPENDIX B	VELOCITY DISTRIBUTION PLOTS	100

LIST OF FIGURES

Figure		Page
1.1	The Classical Hydraulic Jump	3
1.2	Momentum Equation for the Classical Jump	6
1.3	Length of the Classical Jump	7
1.4	Length of the Roller (Classical Jump)	8
2.1	Hydraulic Jump in Sloping Channels (A, B, C & D Jumps)	15
2.2	Hydraulic Jump in Sloping Channels (E & F Jumps)	17
2.3	Hydraulic Jump in Sloping Channels	17
2.4	Variation of Γ_1 with α	21
2.5	Chart for the Lengths of C and D Jumps	23
2.6	B Jump - Variation of $\frac{y_2}{y_2^*}$ with $1/y_2^*$	24
2.7	Type Fixing Chart for A, B, C & D Jumps	25
2.8	Plot of Relative Energy Loss	27
2.9	Variation of n with $\tan \alpha$	28
2.10	Variation of ε with $1/L$ for B Jump	29
2.11	Variation of $\frac{E_L}{y_c}$ with $\frac{E_2}{y_c}$	30
2.12	Variation of ψ_1 with α (Type E Jump)	32
3.1 (a & b)	A-1 & A-2 Jump	35
3.2	Study of Function $\frac{J}{F_1} = \left[\sqrt{\frac{\cos \alpha}{1 + n \tan \alpha}}\right]$	39
3.3	Study of Equation 3.21: $\psi = \sqrt{1 + 8 J^2} - 1$	40
3.4	Comparison of Present Solution with Stevens' Solution	41

Figures		Page
3.5	Solution for Channels of Small Adverse Slope	44
4.1	Experimental Arrangement (Photograph)	48
4.2	Schematic Line Diagram of the Reverse Slope	49
4.3	Surface Profile Recording for Run A-1	50
4.4	Photograph of Measuring Grid	51
4.5 (a) to 4.5 (c)	Sequential Photographs of Unstable Jump	53
4.6	Variation of $\frac{L_{rj}}{y_1}$ with F_1	59
4.7	Variation of $\frac{y_r}{y_1}$ with F_1	60
4.8	Velocity Distribution Plot	61
4.9	Velocity Distribution (Boundary layer Portion)	62
4.10	Velocity Distribution (The Free Mixing Region)	64
4.11	Variation of δ_1/y_1 with x/y_1	65
4.12	Variation of $\frac{U_m}{U_1}$ with x/y_1	67
4.13	Velocity Distribution in the Classical Wall Jet	68

GLOSSARY OF SYMBOLS

A, B, C, D, E & F	Hydraulic jump types
A-1, A-2	Types of hydraulic jumps investigated
E_1	Specific energy of the supercritical stream
E_L	Loss of specific energy in the jump
F_1	Froude Number
g	Acceleration due to gravity
G_1	Function of Froude number and slope
H	Function of Froude number and slope
J	Function of Froude number and slope
K, K′	Empirical parameters
l	Horizontal distance of toe of A-2 jump from junction section
L	Length of the jump parallel to bed
L_j	Horizontal distance between the beginning and the end of the jump
L_{rj}	Length of the surface roller in the jump
M, M_1 & M_2	Momentum rates
n	Surface slope factor
N_1	Function of Froude number and slope
P, P_1 & P_2	Pressure forces
q	Discharge intensity
U	Mean velocity at depth y above the bed
U_1	Initial velocity of the supercritical stream
U_m	Maximum mean velocity

V	Mean velocity
V_1	Mean supercritical velocity
V_2	Mean subcritical velocity
W	Weight of the body of the jump
x	Horizontal distance from initial section
x'	Empirical parameter for E jump
y	Vertical depth normal to the bed
y_1	Supercritical depth measured normal to the bed, before the hydraulic jump
y_1'	Supercritical vertical depth before the jump
y_2	Subcritical depth measured normal to the bed, after the hydraulic jump
y_2^*	Subcritical sequent depth of the classical jump
y_r	Depth of flow at the end of the surface roller
y_r^*	Depth of flow at the end of the surface roller for the classical jump
y_t	Tailwater depth
α	Angle of the slope with the horizontal
α'	Coriolis energy coefficient
β	Boussinesq momentum correction factor
γ	Specific weight of water
δ	Boundary layer thickness
δ_1	Reference length
Γ_1	Function of slope
ψ, ψ_1	Functions of Froude number and slope
ε'	Integrated bed shear in non-dimensional form
η	Non-dimensional ordinate

CHAPTER I

THE PROBLEM AND SCOPE OF RESEARCH

INTRODUCTION:

Hydraulic Jump is one of the most interesting phenomena in the field of Hydraulic Engineering. Under suitable conditions in an open channel the flow at a depth less than the critical may, over a short length, change to a flow at a depth greater than the critical. With this increase in depth, there is a corresponding reduction in velocity, accompanied by dissipation of energy. The hydraulic jump phenomenon is somewhat similar to the sudden expansion of fluids* in a conduit, in which there is a rapid increase in flow area, a corresponding decrease in velocity, and a loss in available mechanical energy or to the phenomena of shock waves in gas flow.

*In this case, an analogy exists between the behaviour of gases and liquids: In liquids, the supercritical stream changes to the subcritical, and there is a corresponding change in depth; in gases, the supersonic stream changes to subsonic stream, with a corresponding change in density. The Froude number $(\frac{\text{Inertia Force}}{\text{Gravity Force}})$ for dynamic similitude in liquid flow, corresponds with the Mach number $(\frac{\text{Inertia Force}}{\text{Elastic Force}})$ in gaseous flow.

The hydraulic jump may occur in several different forms, which may be classified broadly as direct or undular. The hydraulic jump of the direct type i.e., the jump in a level, smooth, wide, rectangular channel (in literature often referred to as the "classical jump", because of its earlier development) is shown in Figure 1.1. At the beginning of the jump, the water surface rises abruptly, and reaches a steady maximum mean level at the end of the jump. There is a surface roller and an eddying region at the face of the jump. The direct form is characteristic of jumps of relatively large height. In the undular form, (not shown) the surface is wavy but not broken, and there is no roll back. This form is typical of jumps of relatively low height.

It has been shown that an undular jump will form if the Froude number of the incoming flow is in the range of 1.0 to 1.7; whereas the direct jump will occur for Froude numbers greater than about 1.7.

If y_1 is the supercritical depth before the jump, and y_2 is the subcritical depth after the jump, these two depths are known as the sequent depths. The jump is completely defined by the supercritical depth y_1 and the supercritical Froude number: $F_1 = \frac{V_1}{\sqrt{gy_1}}$ where V_1 is the mean supercritical velocity, and g is the acceleration due to gravity. The ratio of the two sequent depths $\frac{y_2}{y_1}$ is related to the Froude number F_1 by the well known "Momentum Equation",

$$\frac{y_2}{y_1} = \tfrac{1}{2} \left[\sqrt{1 + 8 F_1^2} - 1 \right]$$

(This equation is discussed in most text books, and is generally attributed to Belanger).

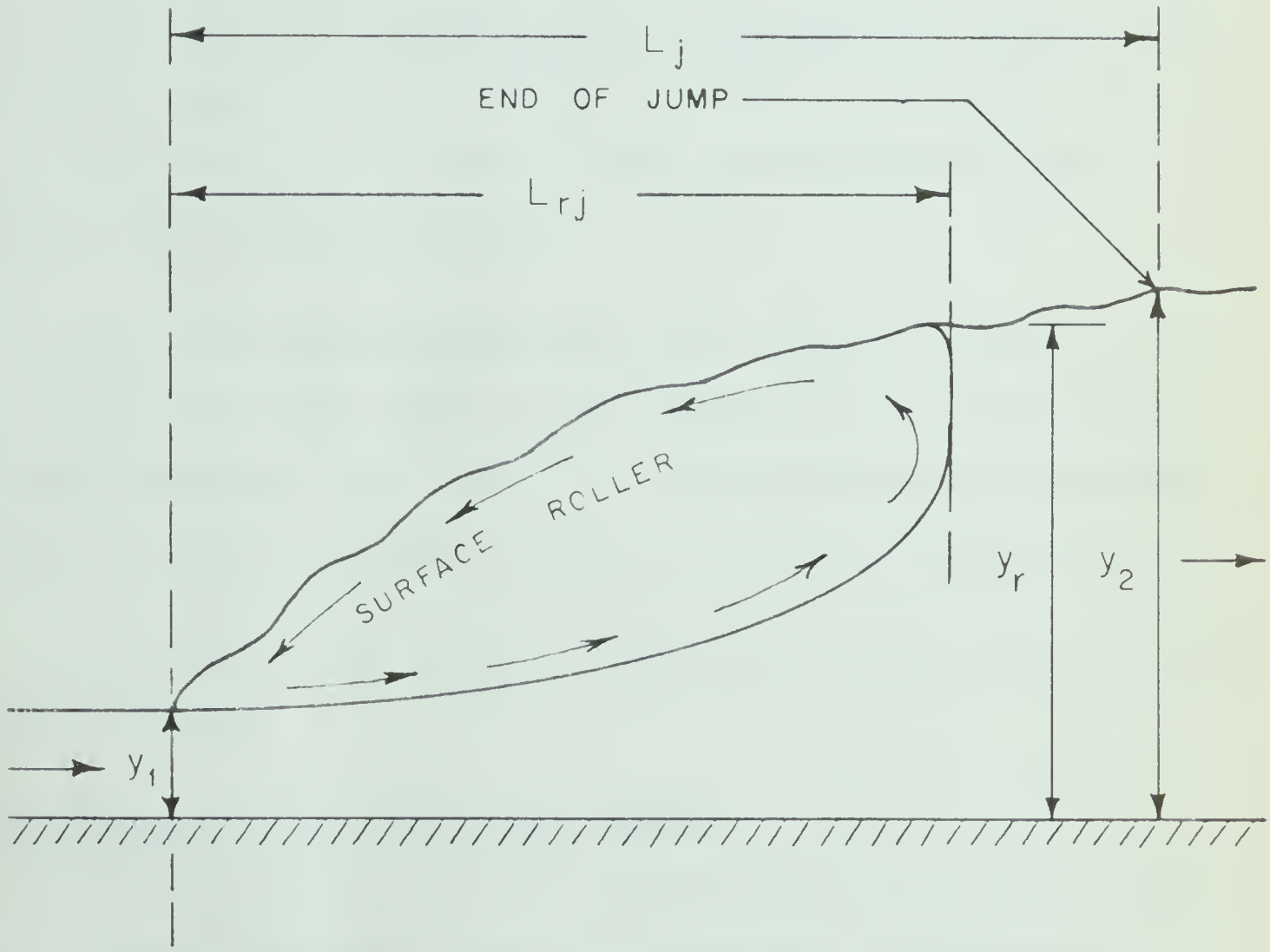

FIGURE 1.1 THE CLASSICAL HYDRAULIC JUMP

The horizontal distance between the beginning and the end of the jump is known as the length of the jump and is denoted by L_j. There is a violent surface roller in the jump, the length of which is denoted L_{rj}.

Because of the considerable energy dissipation, the jump is often used as an energy dissipator at the foot of spillways and other outlet works. Also, because of the efficient mixing produced in the jump, it is used sometimes, for mixing chemicals.

While the theory and experimental data relating to jump in a level wide channel (where side effects can be neglected) are well established, the jump formation in other cases e.g., sloping channels, non-rectangular channels, or narrow rectangular channels, is only partially understood.

The subject of this thesis is a preliminary study of jump formation on adverse slopes.

JUMP FORMATION IN LEVEL RECTANGULAR CHANNELS:

As discussed earlier, the two sequent depths y_1 and y_2 are related to the supercritical Froude number F_1 by the Belanger momentum equation:

$$\frac{y_2}{y_1} = \frac{1}{2}\left[\sqrt{1 + 8\,F_1^2} - 1\right] \qquad (1.01)$$

This equation neglects the shear force on the bottom. It has been experimentally verified for jumps with a fully developed supercritical stream, by Bradley and Peterka (1), and others. In the case of jumps with an almost uniform supercritical stream, the integrated shear force on the bed is appreciable, and equation (1.01) needs a correction, as has been

established recently by Harleman (2), and Rajaratnam (3). The corrected momentum equation can be written as:

$$\frac{y_2}{y_1} = \tfrac{1}{2}\left[\sqrt{1 + 8\,F_1^2 + 4\varepsilon'} - 1\right] \qquad (1.02)$$

where ε' represents the integrated bed shear in a non dimensional form, and is a function only of F_1. Equations 1.01 and 1.02 are shown plotted in Figure 1.2.

If y_r is the depth of flow at the end of the surface roller (see Figure 1.1), it has been found (3), that

$$\frac{y_r}{y_2} = 0.834 + 0.012\,F_1 \qquad (1.03)$$

The length of the jump L_j, made non-dimensional by dividing with y_2, has been found experimentally by Rajaratnam and others, to be a function of F_1, and Figure 1.3 is a plot of the well known curve of Bradley and Peterka, with the recent results of Rajaratnam (3), showing length of jump as a function of F_1. The length of the surface roller is shown in Figure 1.4 with the three curves of Safranez (4), Rouse et al (5), and Rajaratnam (3). The ratio $\frac{L_{rj}}{L_j}$ is essentially a function F_1, and using Rajaratnam's results, is approximately given by the equation (3):

$$\frac{L_{rj}}{L_j} = 0.25 + 0.05\,F_1 \qquad (1.04)$$

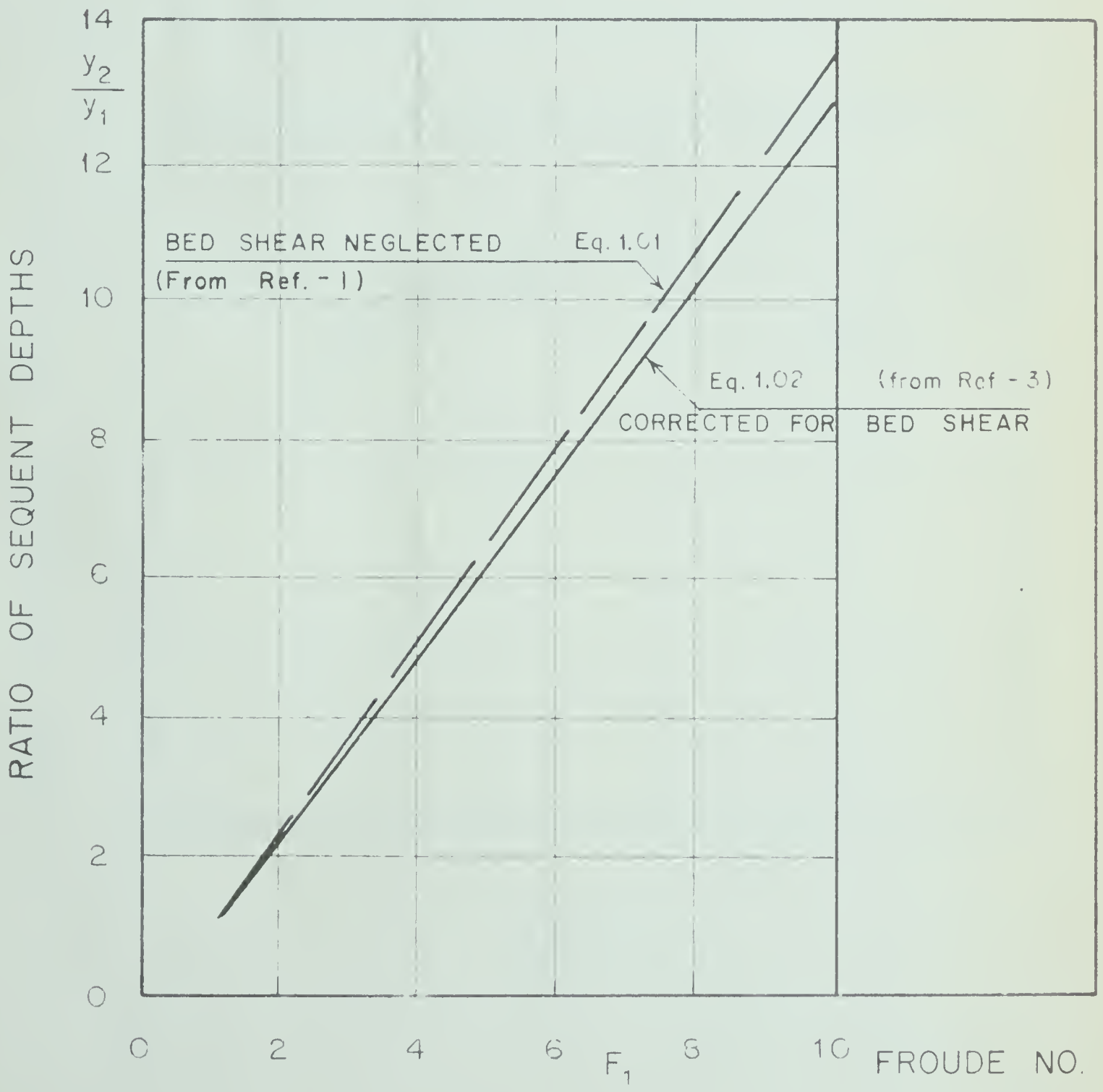

FIGURE 1.2 MOMENTUM EQUATION FOR THE CLASSICAL JUMP

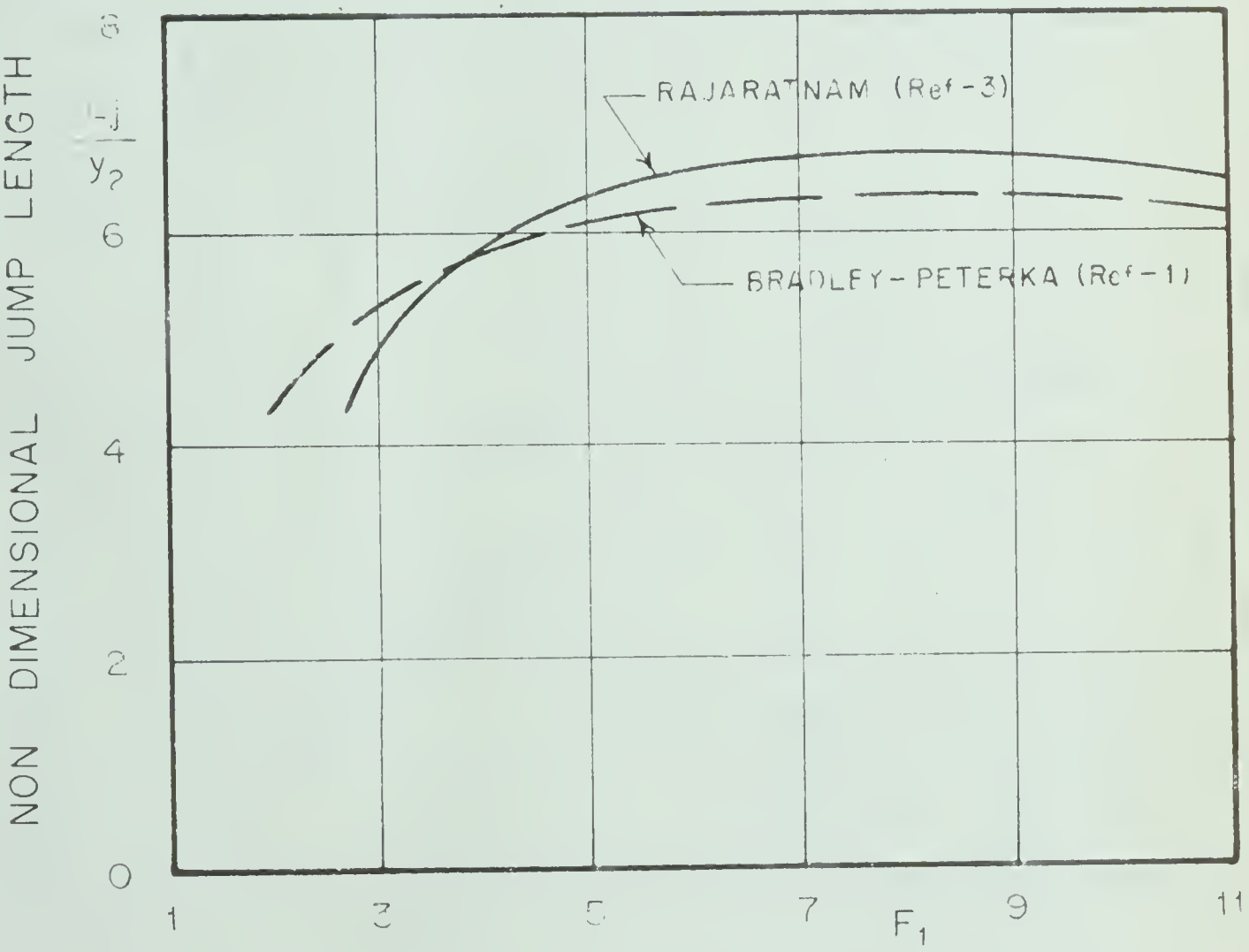

FICURE 1.3 LENGTH OF THE CLASSICAL JUMP

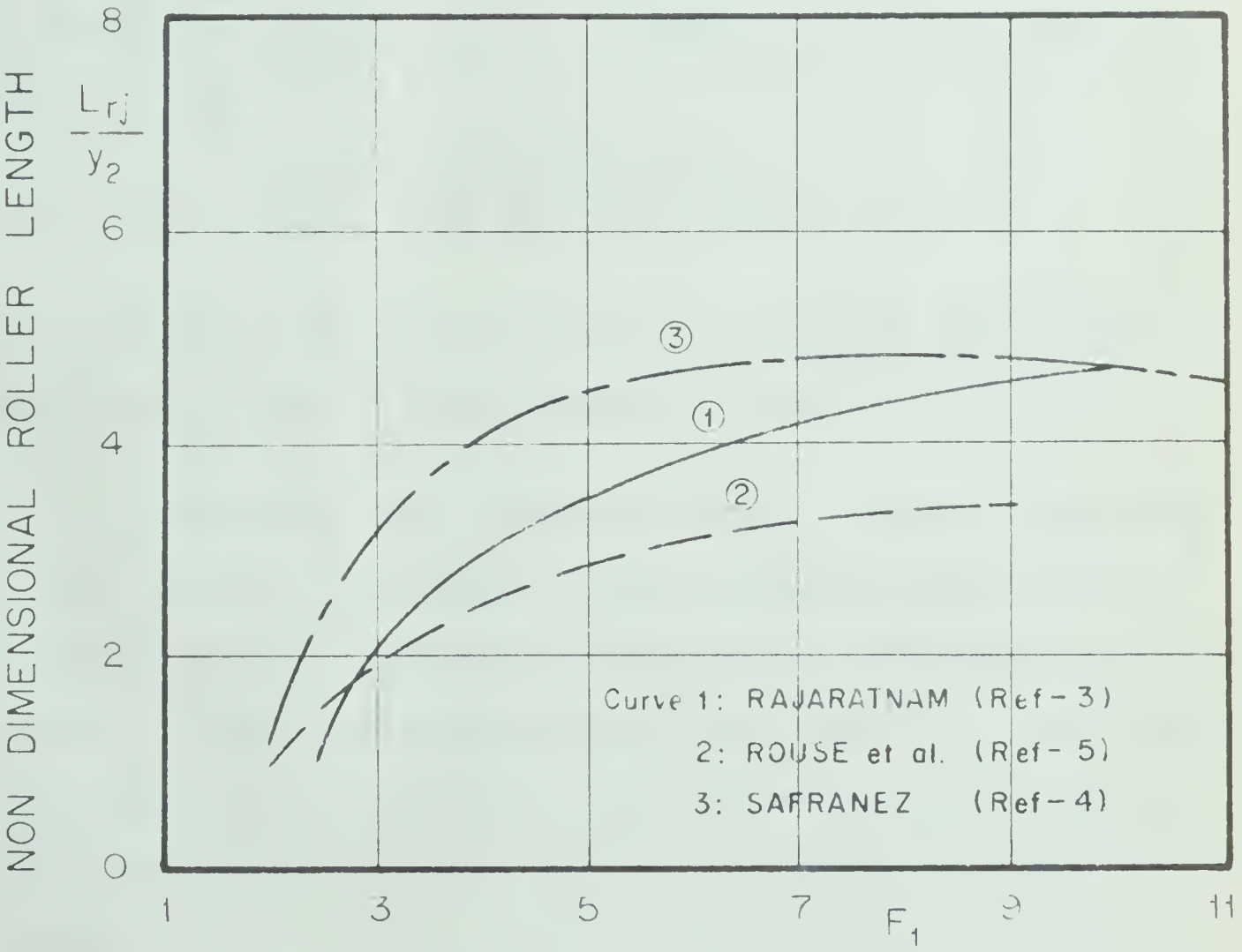

FIGURE 1.4 LENGTH OF THE ROLLER (CLASSICAL JUMP)

In the hydraulic jump, a considerable portion of the energy of the supercritical stream is first converted to turbulent energy, and then dissipated by viscous forces (5). If E_1 is the specific energy (defined as: The energy per pound of water at any section of a channel measured with respect to the channel bottom), of the supercritical stream before the jump, and if E_L is the specific energy lost in the jump, it can be shown (6) that $\frac{E_L}{E_1}$ is a function only of the supercritical Froude number F_1 written as:

$$\frac{E_L}{E_1} = \frac{1}{8} \frac{[\sqrt{1 + 8 F_1^2} - 3]^3}{[2 + F_1^2][\sqrt{1 + 8 F_1^2} - 1]}$$

For $F_1 = 20$, $\frac{E_L}{E_1}$ is as high as 0.86 (for dissipating 99.6% of initial energy, one would need a Froude number $F_1 = 1{,}000$!)

It is observed that a considerable amount of air is entrained in the jump. In 1962, Rajaratnam (7) made an extensive study of the air entrainment characteristics of the hydraulic jump, and showed that it is intimately related to the supercritical Froude number F_1. A more recent study by Rajaratnam (3) attempts to show the mechanism of the hydraulic jump by treating it as a plane turbulent wall jet, under adverse pressure gradient.

JUMP FORMATION IN SLOPING CHANNELS:

Sloping channels may be divided into two general cases. A channel which slopes downward in the direction of the flow is known as negatively sloping channel, or simply as a sloping channel, because of its frequent occurrence. Channels which slope upward in the direction of flow are said to have positive, reverse or adverse slope.

While a fairly good semi-empirical theory is available for jump formation in negatively sloping channels, very little is as yet known regarding jump formation on adverse slopes.

A brief review of jump formation on negative slopes will be presented in the next chapter, as a preliminary to developing the study of the jump formation on adverse slopes.

CHAPTER II

HYDRAULIC JUMP ON NEGATIVE SLOPES

INTRODUCTION:

Although, considerably more is known about jump formation in horizontal channels than in sloping channels, sloping channels are often preferred for energy dissipation purposes. Some of the important advantages of the jump on a sloping floor are: firstly, the longitudinal movements can be kept within relatively narrow limits for a wide variation of discharge and tail water levels. Secondly, if the provision of a level apron requires a large excavation, the sloping floor may be more economical. Finally, friction blocks and other stabilizing appurtenances are not generally required. Relatively few stilling basins are constructed with horizontal aprons, because the formation of the hydraulic jump on a horizontal apron is very sensitive to changes in discharge intensity and downstream water level.

While the case of the so called classical jump i.e., jump in a horizontal channel, neglecting friction, has been solved theoretically and verified experimentally, it has not been possible to develop a comparatively satisfactory solution for the jump in sloping channels. The main difficulty is that if the momentum equation is written in a direction parallel to the bed of the channel, the component of the weight

of the water in the body of the jump must be considered. On the other hand, if we write this equation in the horizontal direction, the horizontal component of the sloped floor pressure becomes a factor.

There is a lack of agreement among engineers and designers as to the amount of energy that is dissipated on a sloping floor. Thus the momentum formulas cannot be applied straight-forwardly to jumps on sloping floors. As will be shown in this chapter, however, the momentum principle can be used to derive an equation analogous to (Eq 1.01) which will contain an empirical function that has to be determined experimentally.

HISTORICAL REVIEW:

The first measurements and description of the hydraulic jump phenomenon were perhaps made by Bidone in 1818, in a small rectangular flume, with a slight slope. Bazin, in 1865, and later Beebe and Riegel (9) in 1917, experimented with jumps on sloping channels to determine depth relationships. In 1927, Ellms (10, 11) attempted a theoretical and experimental study using a small rectangular flume whose slope could be varied from approximately 9° to 17°. In 1934, Yarnell commenced an extensive research program with slopes of 1 on 6, 1 on 3, 1 on 2, and 1 on 1, to determine the apron floor pressure under the hydraulic jump. Unfortunately Yarnell's work was interrupted by his death in 1937.

In 1935, Rindlaub (12) conducted an experimental study on slopes of 8.2, 12.5, 24.2 and 30 degrees with the horizontal with many of his experiments being made on the 12.5° slope. In his analysis, Rindlaub compensated for the pressure component on the sloping floor by including a dimensionless term, which can be determined experimentally to account for any external forces. In 1938 Bakhmeteff and Matzke (13), published a careful analysis of this problem, with experimental data on very flat slopes. In order to compensate for the weight of the jump on a sloping floor, a dimensionless cubic equation was developed which was found to be dependent upon the shape of the jump.

The first rational and successful attempt to solve this problem was perhaps first made by Kindsvater (14) in 1944, who evaluated a pressure coefficient experimentally, for each channel slope and kinetic flow factor. Experimental results on a slope of 1 on 3 were added by Hickox (15) to Kindsvater's results on the 1 on 6 slope. In 1949, Dutta (16) developed design charts for a few slopes based on Kindsvater's equation.

An extensive study of this problem was made by Bradley and Peterka (17) at the U.S.B.R. in 1954 (Published in Journal of Hydraulic Division, A.S.C.E., October, 1957). Charts based on this study are useful in determining the length and the extra depth required for the hydraulic jump to form on a sloping apron compared to the length and the depth required for the jump to form on a horizontal apron. In 1954, Flores (18) attempted

to develop a general theory for jumps in sloping exponential channels. In 1958, Wigham (19) extended the work of Bradley and Peterka to steeper slopes of 1 on 1, and 1 on 3. Lin and Priest (20) conducted another investigation with slopes up to 15 degrees with the horizontal.

A theoretical and experimental analysis of the formation of hydraulic jumps in parabolic and triangular channels has been made by Argyropoulous (21, 22, 23) in Athens. This study included both horizontal and sloping flumes. Recently, Rajaratnam (24) has conducted a critical study of this problem and has presented two methods for the location of jump in sloping channels.

TYPES OF JUMP:

In developing simpler methods of solution, it is found convenient to classify the general case of jump formation on sloping beds into a number of types based on salient features. The following classification, shown in Figure 2.1, is due to Kindsvater (14). There are four basic types: A, B, C, and D. y_1 is the depth of the supercritical stream, measured normal to the slope, and y_2 is the vertical depth at the end of the jump. In sloping channels, the end of the jump is considered as being located at the end of the roller (15), which normally coincides with the section of maximum steady surface elevation for slopes steeper than 1 on 6.

Referring to Figure 2.1 again, if the tail water depth y_t is equal to the subcritical sequent depth y_2^* given by the Belanger equation, written as:

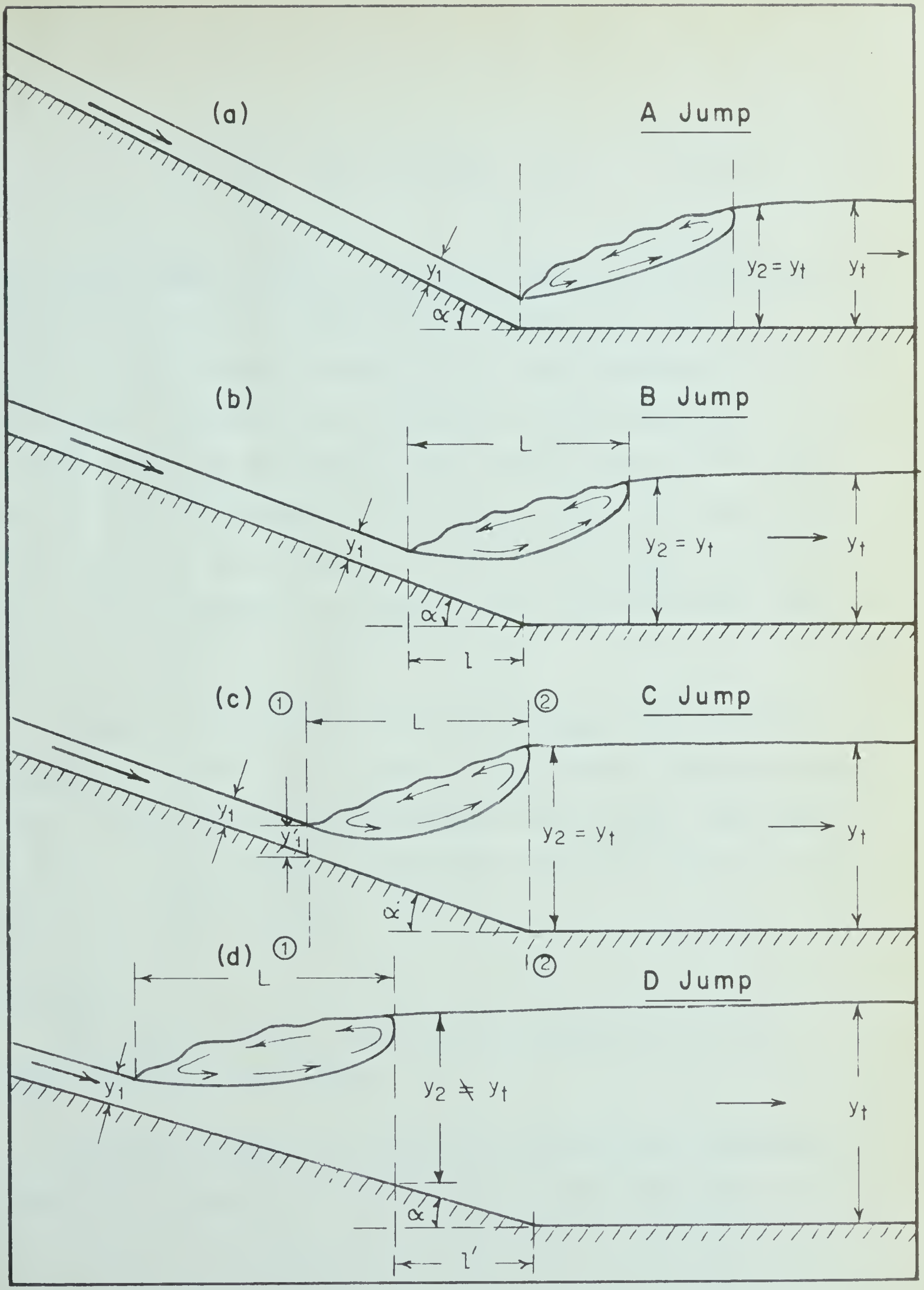

FIGURE 2.1 HYDRAULIC JUMP IN SLOPING CHANNELS

$$\frac{y_2}{y_1}^* = \tfrac{1}{2}\left(\sqrt{1 + 8 F_1^2} - 1 \right) \qquad (2.01)$$

then, an A-type jump is formed, in which the jump starts just below the junction. This is almost the same as the classical jump. If y_t is greater than y_2^*, the jump moves up the slope, and conversely, if y_t is less than y_2^*, the jump will move downstream to attain equilibrium. For $y_2 > y_2^*$, if the jump forms partly on the slope and partly on the level bed it is known as the B-jump. If the jump is formed on the slope, with the end located at the junction, it is known as the C-jump. If the tail water is increased beyond that required for the C-jump, the entire jump moves up the slope, and is termed the D-jump.

Figure 2.2 shows another jump (called E-jump), which is formed sometimes, on very flat channels and the F-jump, formed on adverse slopes. Figure 2.3 shows some other possible combinations of slopes, where jumps may occur. In each of these, the jump might form in any portion, and such cases are difficult to analyse.

TYPE C-JUMP:

The solution for the C-jump developed by Kindsvater (14), is briefly presented in this section.

Referring to Figure 2.1, based on the few but precise measurements of Bakhmeteff and Matzke (13), the horizontal external pressure P_1 at the

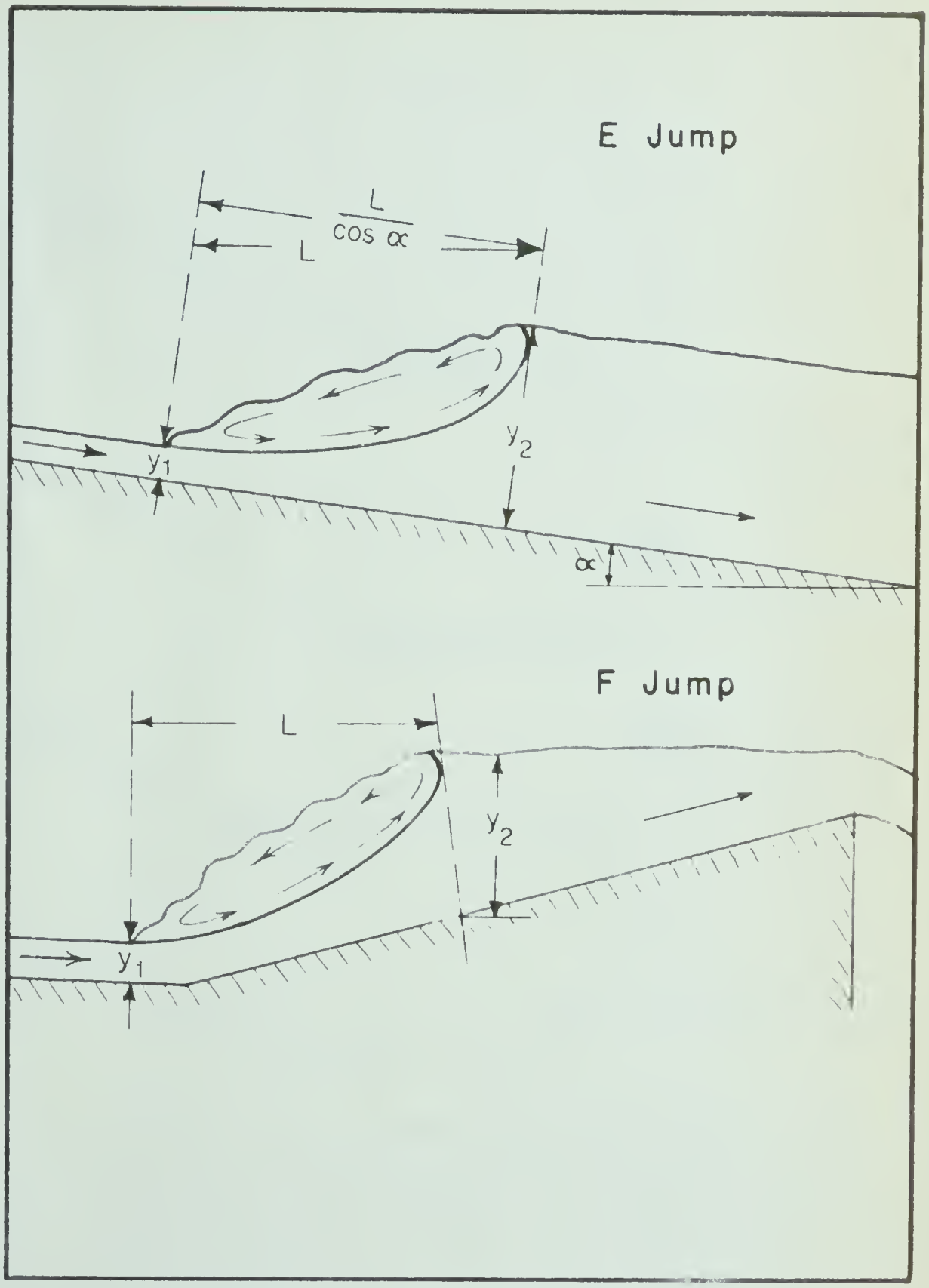

FIGURE 2.2 HYDRAULIC JUMP IN SLOPING CHANNELS

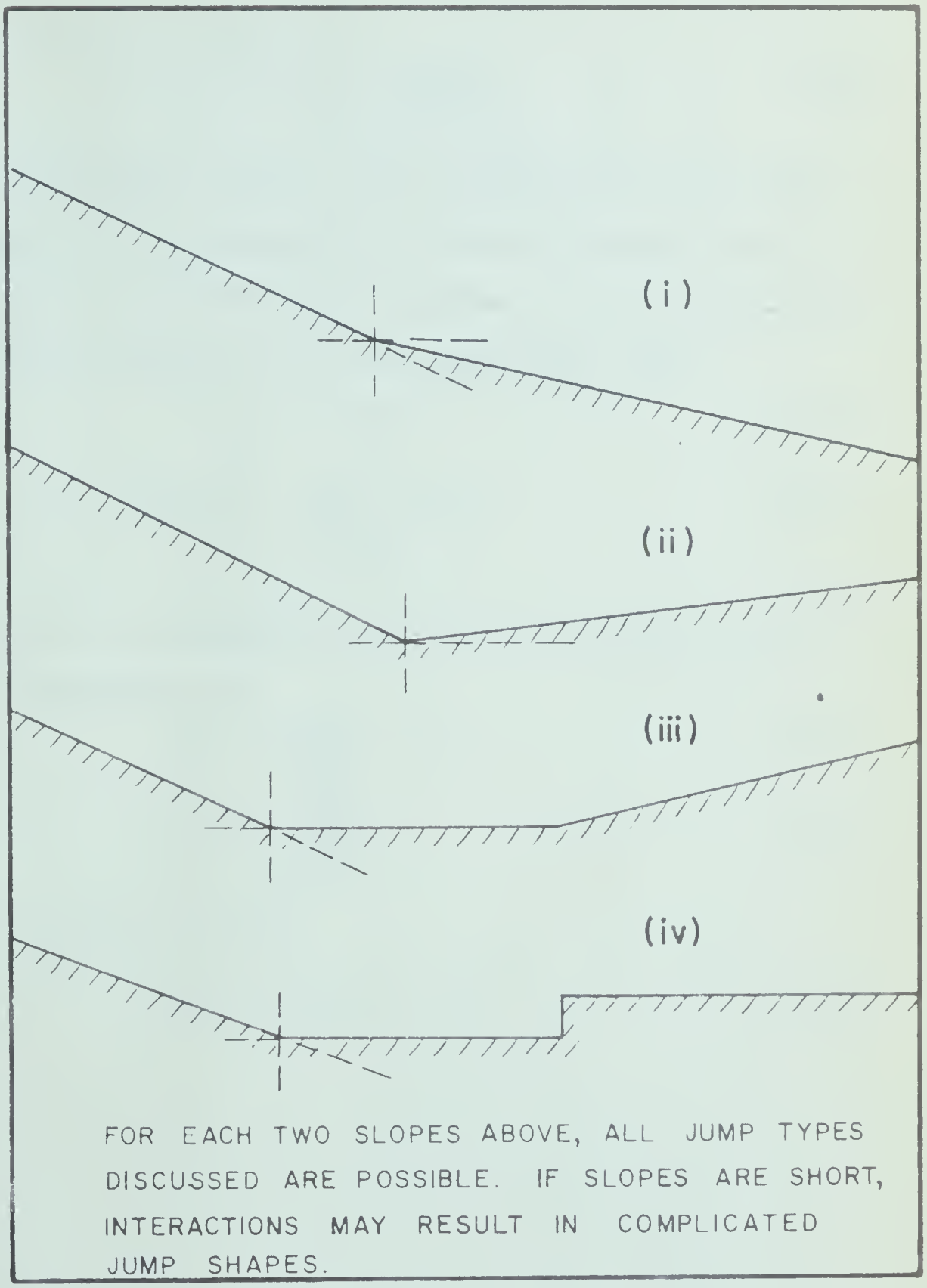

FIGURE 2.3 **HYDRAULIC JUMP IN SLOPING CHANNELS**

beginning of the jump can be written as:

$$P_1 = \tfrac{1}{2}\,\gamma\, y_1^2\, \frac{1}{\cos^2\alpha} \qquad (2.02)$$

where γ is the unit weight of water, and α is the slope of the channel with the horizontal. If P_2 represents the external horizontal force at the end of the jump, P is the horizontal component of the floor pressure, and K is an empirical parameter called the shape factor, then:

$$P_2 = \tfrac{1}{2}\,\gamma\, y_2^2 \qquad (2.03)$$

and

$$P = 2K\left[\frac{\gamma y_2^2}{2} - \frac{\gamma y_1^2}{2\cos^2\alpha}\right]\tan\alpha \qquad (2.04)$$

The momentum rates at the beginning and the end of the jump in the horizontal direction are written as:

$$M_1 = \frac{\gamma q^2}{g y_1}\cos\alpha \qquad (2.05)$$

$$M_2 = \frac{\gamma q^2}{g y_2} \qquad (2.06)$$

where q is the discharge intensity.

Now:

$$P_1 + P - P_2 = M_2 - M_1 \qquad (2.07)$$

Substituting equations (2.02) to (2.06) into equation (2.07), and simplifying,

$$\frac{y_2}{y_1} = \frac{1}{2 \cos \alpha} \left[\sqrt{1 + 8 F_1^2 \frac{\cos^3 \alpha}{1 - 2 K \tan \alpha}} - 1 \right] \qquad (2.08)$$

which is Kindsvater's original equation.

Using Bradley and Peterka's (17) observations showing that K is mainly a function of the slope α and could satisfactorily be considered to be independent of Froude number F_1, Rajaratnam (24) transformed Eq. (2.08) to

$$\frac{y_2}{y_1/\cos \alpha} = \frac{y_2}{y_1'} = \tfrac{1}{2} \left[\sqrt{1 + 8 G_1^2} - 1 \right] \qquad (2.09)$$

where y_1' is the vertical supercritical depth before the jump, and

$$G_1^2 = \Gamma_1^2 F_1^2 \qquad (2.10)$$

where

$$\Gamma_1^2 = \frac{\cos^3 \alpha}{1 - 2 K \tan \alpha} = f(\alpha) \qquad (2.11)$$

It was found that Γ_1 could also be given by a simpler expression:

$$\log_{10} \Gamma_1 = 0.027 \alpha \qquad (2.12)$$

with α in degrees, (24), and is also shown plotted in Figure 2.4.

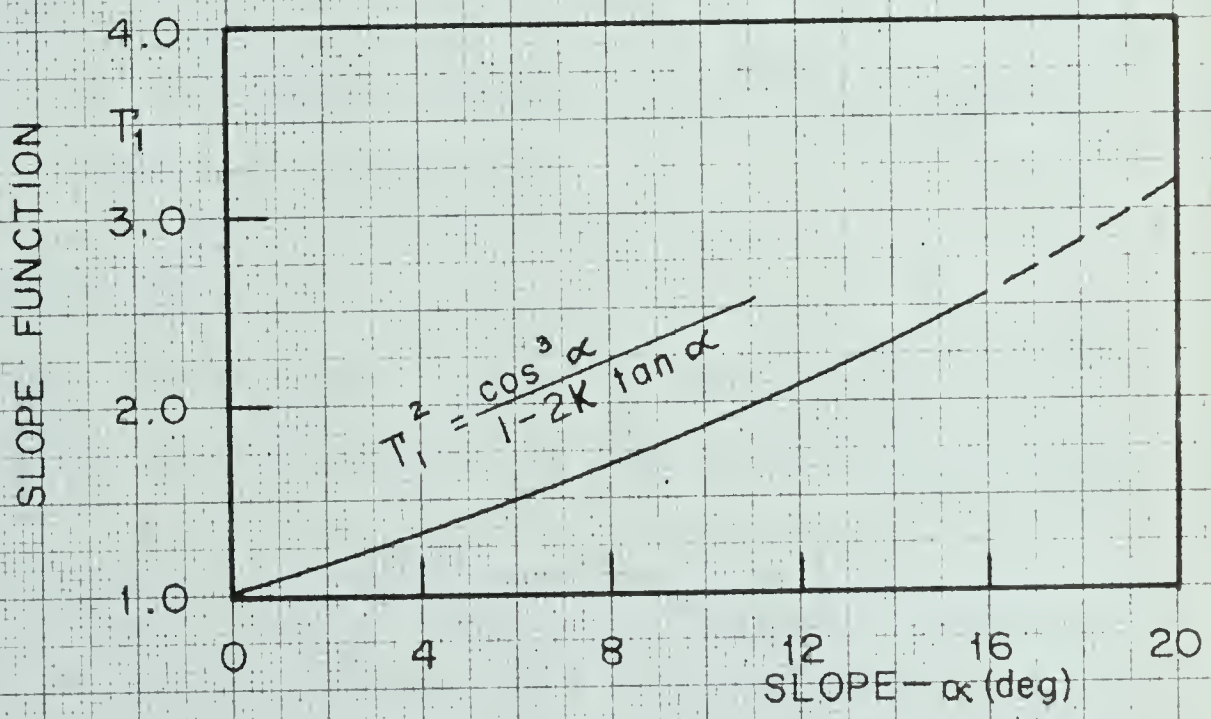

FIGURE 2.4 VARIATION OF T_1 WITH α

(Ref - 2.4)

Eq 2.09 is of the same form as the Belanger momentum equation, and hence the solution chart of the Belanger equation (i.e., $\frac{y_2}{y_1}$ versus F_1), given in most standard texts can be used for the calculation of the sloping channel jump.

For the C-jump, since $y_t = y_2$, Eq 2.09 can also be written as:

$$\frac{y_t}{y_1} = \tfrac{1}{2}[\sqrt{1 + 8\,G_1}^{\,2} - 1] \qquad (2.13)$$

Eq 2.09 has been found by Bradley and Peterka to be applicable to the D-type jumps also, with the only difference that $y_2 \neq y_t$. The length of C and D jumps as given by Bradley and Peterka is reproduced in Figure 2.5. For the B-jumps, a graphical solution has been proposed by Bradley and Peterka (17) which is reproduced in Figure 2.6, with two additional curves for tan $\alpha = 0.5$ and 1.0 from Wigham (19).

FIXING THE TYPE OF JUMP:

Rajaratnam has developed a chart, reproduced in Figure 2.7, of $\frac{y_t}{y_2^*}$ plotted against tan α. If y_1, F_1, y_t and tan α are known, using Eqs 2.09 and 2.12, y_2^* can be calculated. Hence $\frac{y_t}{y_2^*}$ is obtained. Then the given case is plotted in Figure 2.7. Depending upon the location of the plotted point, the type of jump is fixed. Rajaratnam (24) has also suggested two methods for locating the jump, after fixing its type, giving examples to illustrate these methods. The first method considers the case where the supercritical stream has attained terminal conditions,

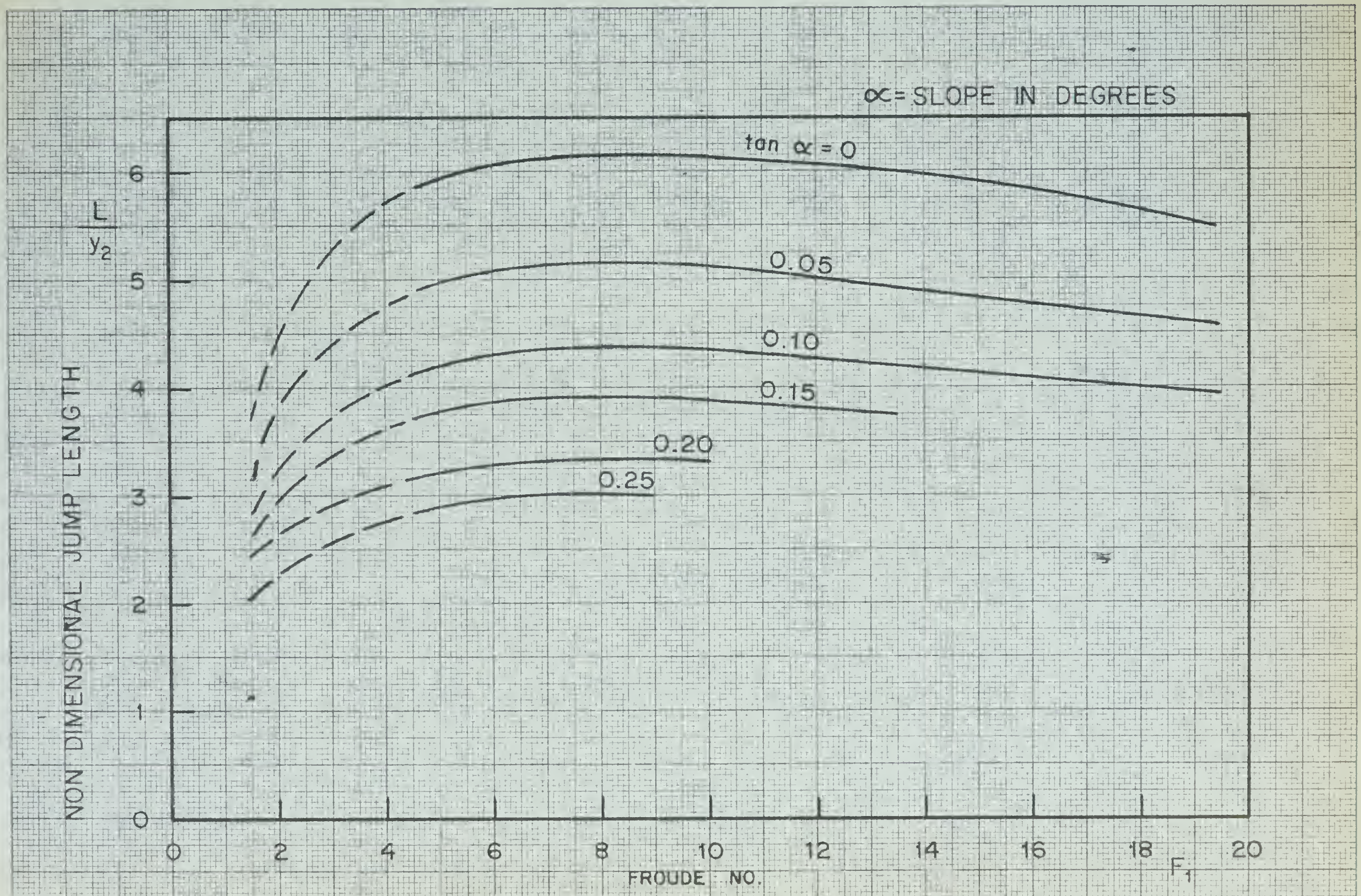

FIGURE 2.5 CHART FOR THE LENGTH OF C AND D JUMPS (Ref-1)

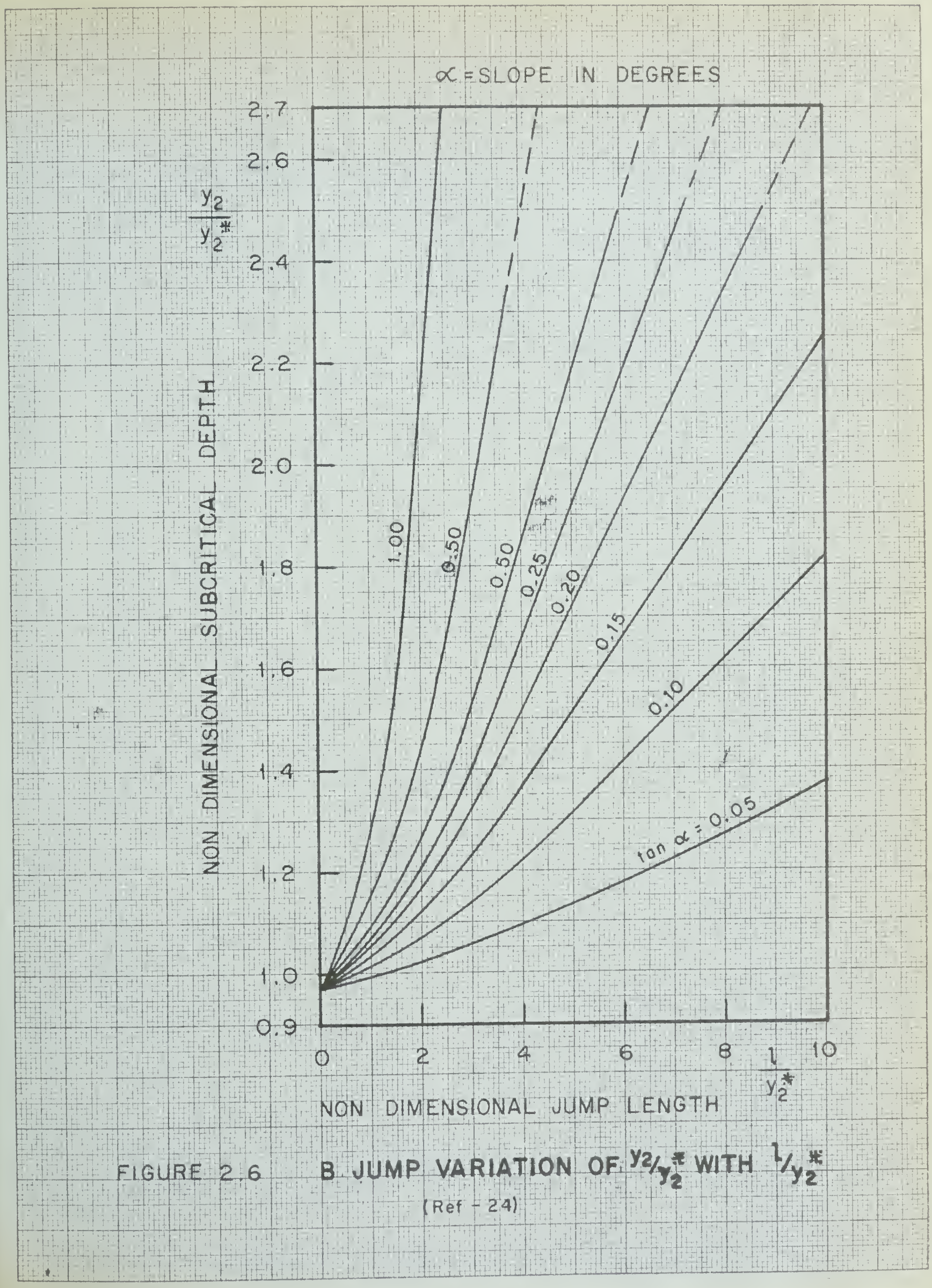

FIGURE 2.6 B JUMP VARIATION OF y_2/y_2^* WITH $1/y_2^*$

(Ref - 24)

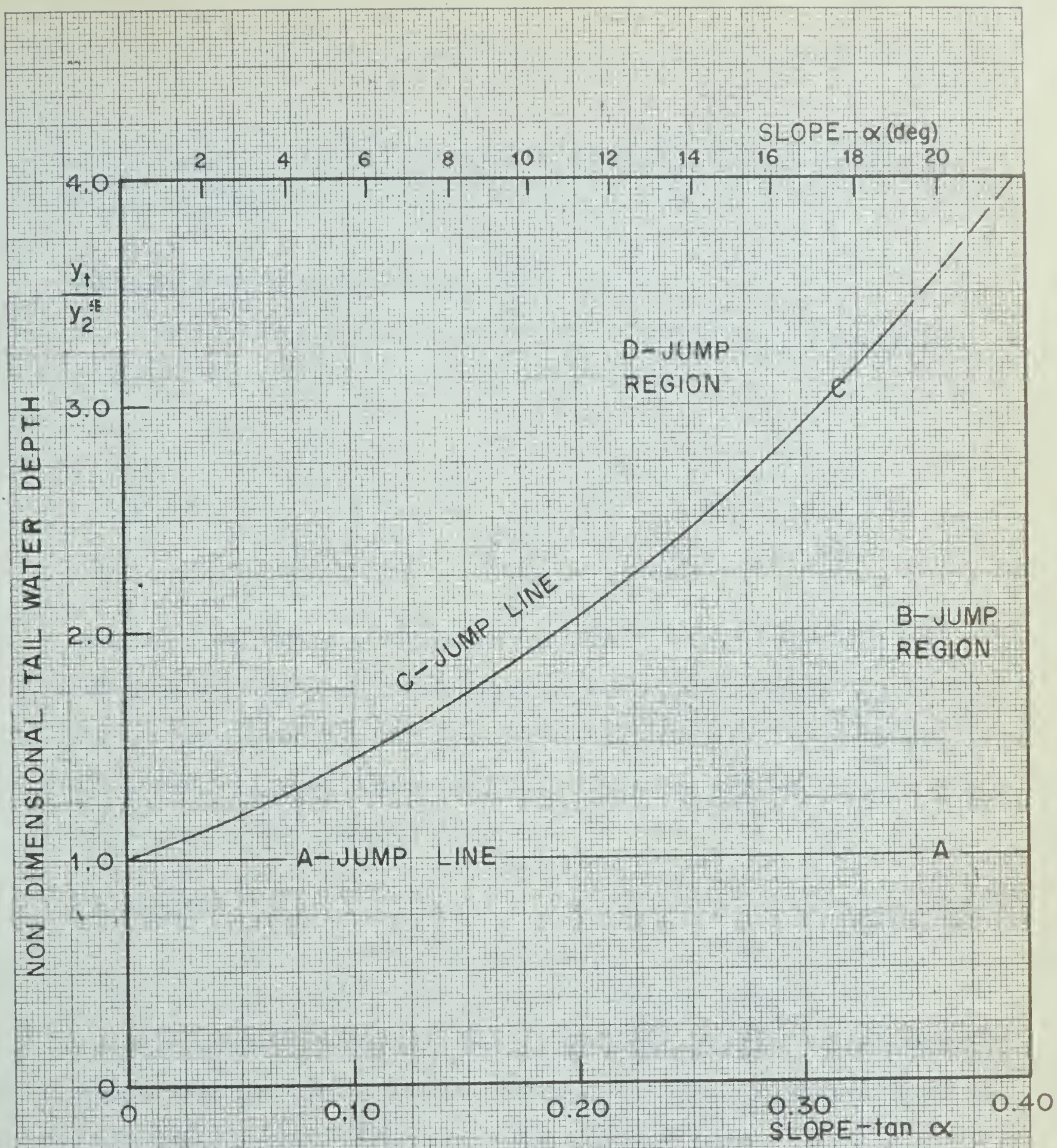

FIGURE 2.7 TYPE FIXING CHART FOR A, B, C and D JUMPS

(Ref - 24)

and the second method is suited for the case where it has not yet attained terminal conditions.

ENERGY LOSS IN THE SLOPING CHANNEL JUMP:

It has been shown (24) that the relative energy loss in the sloping channel (C or D) - jump is given by the expression:

$$\frac{E_L}{E_1} = \frac{\left[1 - \frac{y_2}{y_1}\right] + \frac{1}{2} F_1^2 \left[1 - \frac{1}{(y_2/y_1)^2}\right] + \tan\alpha \frac{L}{y_2} \cdot \frac{y_2}{y_1}}{1 + \frac{F_1^2}{2} + \tan\alpha \cdot \frac{L}{y_2} \cdot \frac{y_2}{y_1}}$$

$$= f(F_1, \tan\alpha) \qquad (2.14)$$

Eq 2.14, shown plotted in Figure 2.8 and also Figure 2.9 (reproduced from reference 17) shows that for any given Froude number F_1, the relative energy loss decreases, as the slope increases. Figure 2.10 shows similar curves for B-jump, and Figure 2.11 shows a method of locating the jump based on energy loss studies.

TYPE E-JUMP:

As has been mentioned earlier, Type E-jump is believed to occur in long and flat channels. Even though a theoretical equation, with empirical coefficients, has been repeatedly derived for this type of jump; satisfactory experimental data have not been published for evaluating the constants.

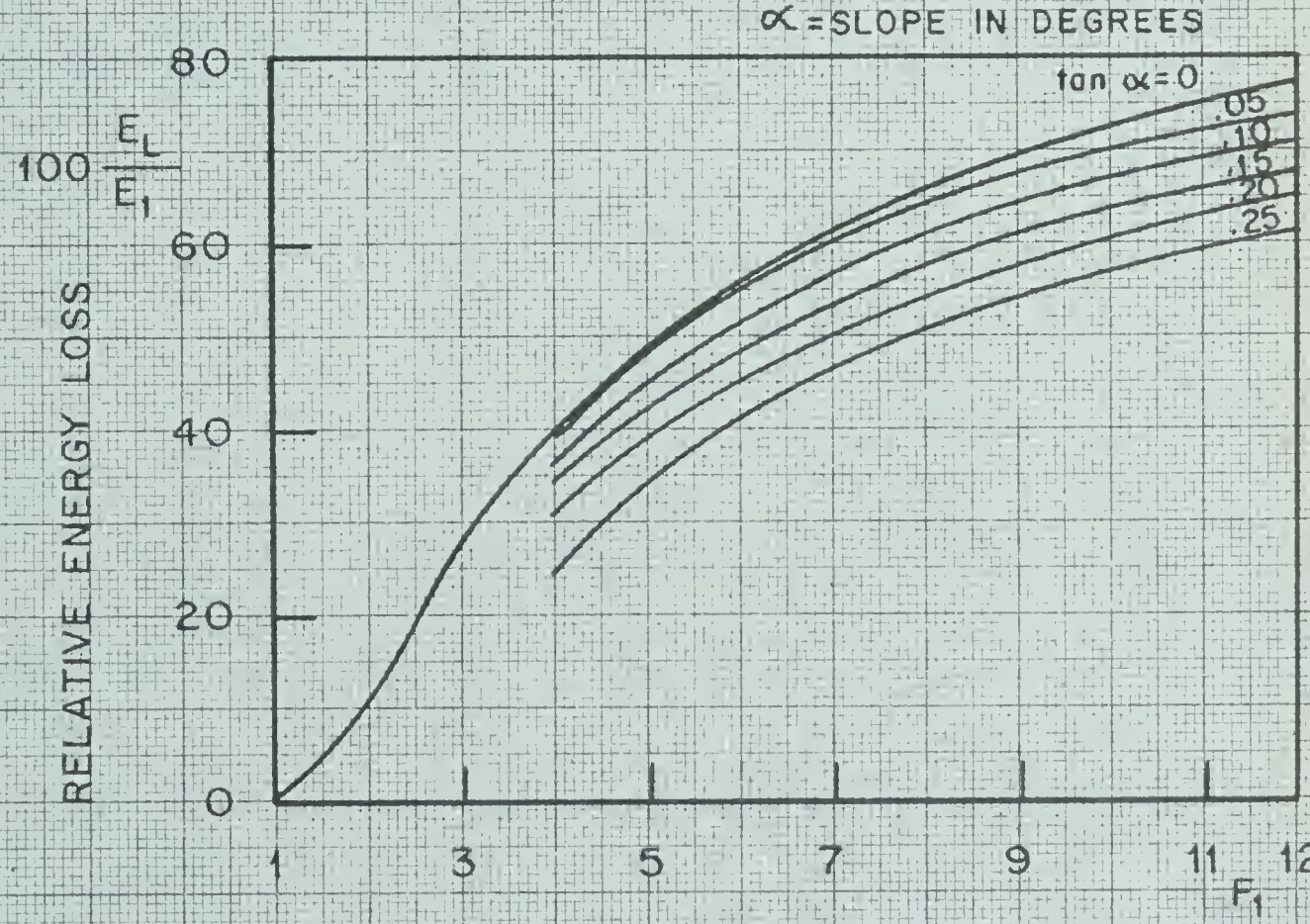

FIGURE 2.8 PLOT OF RELATIVE ENERGY LOSS

(Ref - 24)

$$\eta = \frac{\text{RELATIVE ENERGY LOSS – SLOPING FLOOR JUMP}}{\text{RELATIVE ENERGY LOSS – LEVEL FLOOR JUMP}}$$

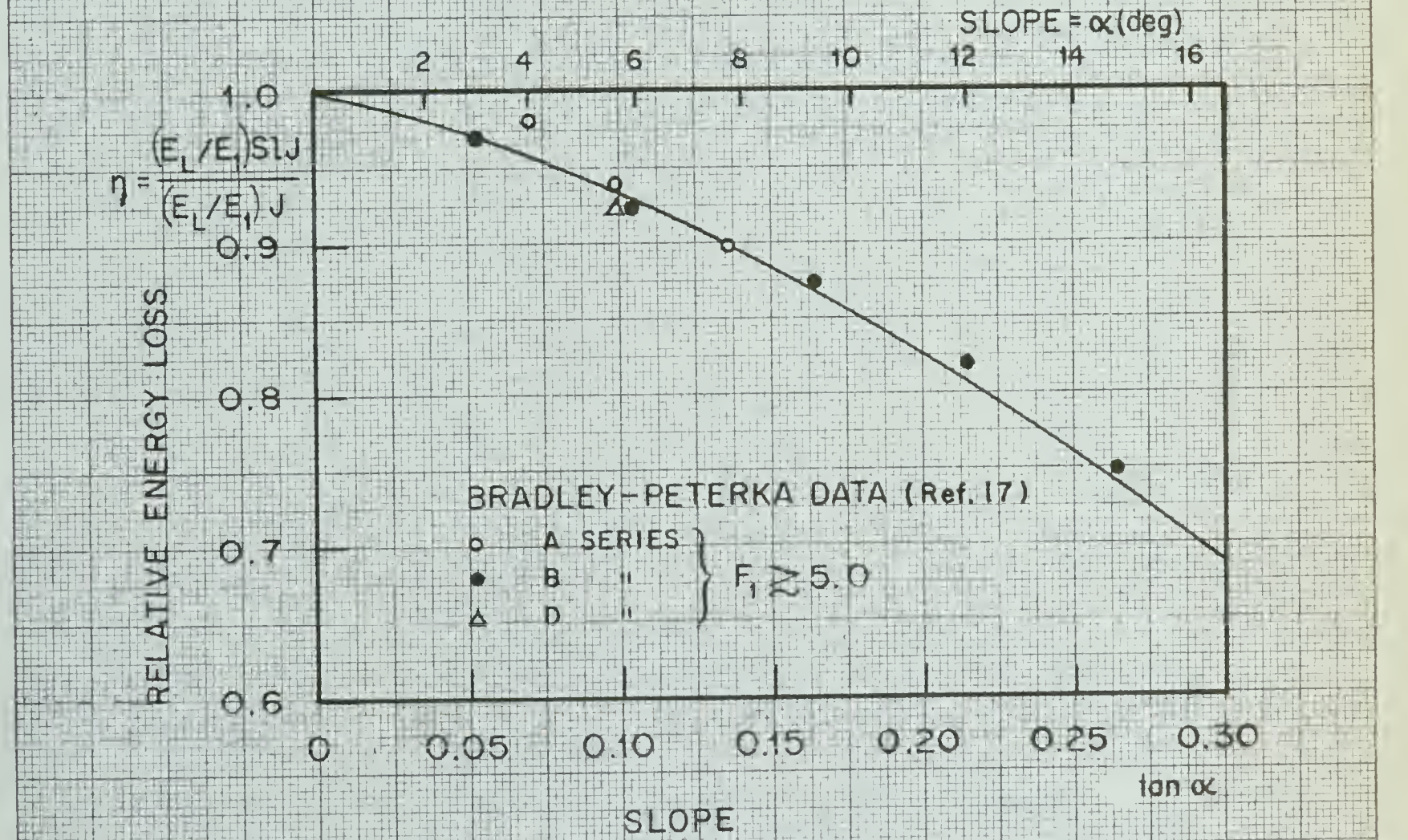

FIGURE 2.9 VARIATION OF η WITH tan α

(Ref. 24)

$$\epsilon = \frac{\text{RELATIVE ENERGY LOSS—B JUMP}}{\text{RELATIVE ENERGY LOSS—C JUMP}}$$

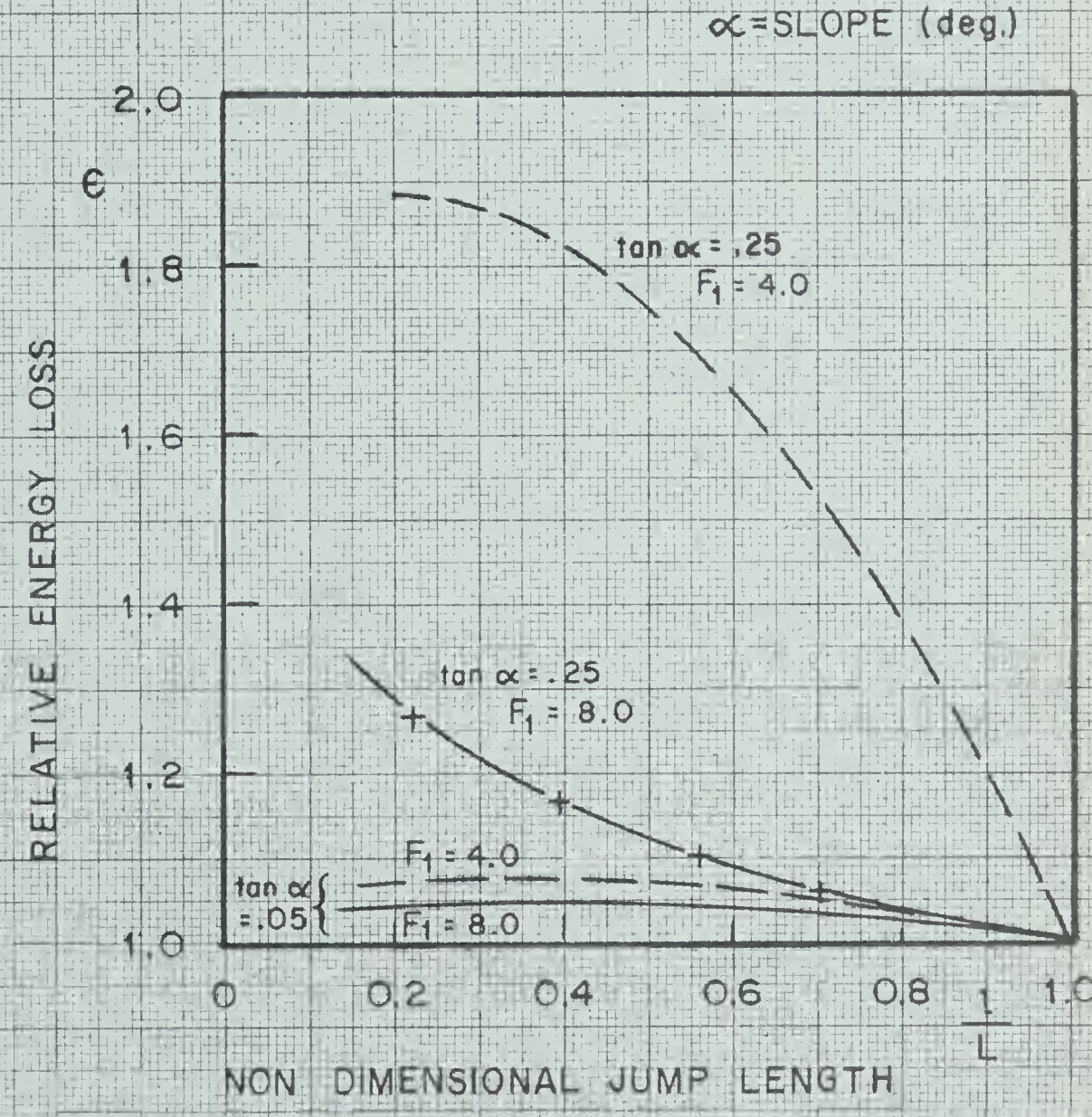

FIGURE 2.10 VARIATION OF ϵ WITH $\frac{l}{L}$ FOR B JUMP

(Ref. 24)

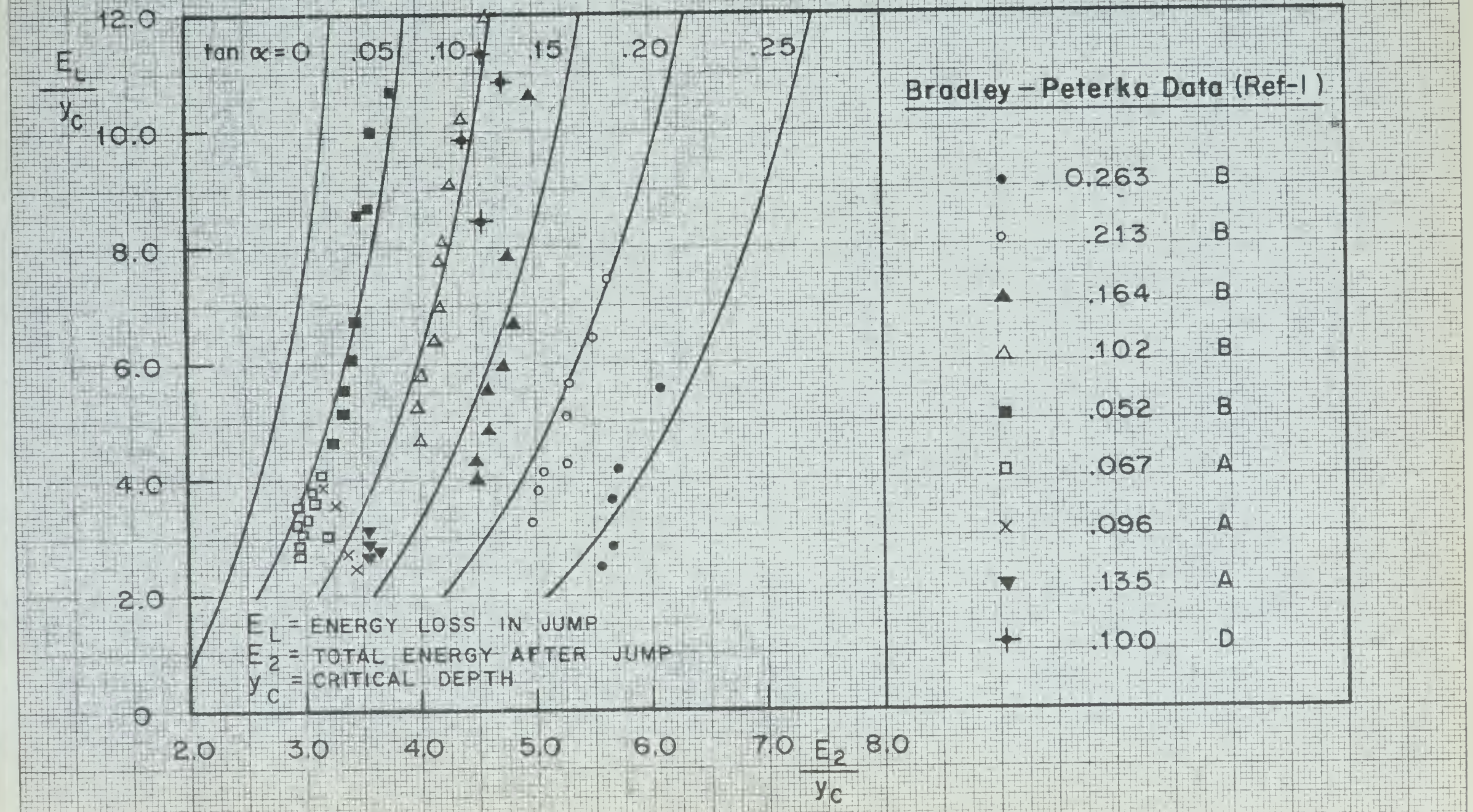

FIGURE 2.11 VARIATION OF $\frac{E_L}{y_c}$ WITH $\frac{E_2}{y_c}$ (Ref. 24)

With reference to Figure 2.2, it can be shown that the ratio of the (normal) sequent depths is given as:

$$\frac{y_2}{y_1} = \tfrac{1}{2}\left(\sqrt{1 + 8\,F_1^{\,2}\,\frac{1}{1 - K' \times \sin\alpha}} - 1\right) \qquad (2.15)$$

where

$$\frac{1}{x} = \frac{y_2 - y_1}{L/\cos\alpha} \qquad (2.16)$$

and K' is an empirical constant.

Eq 2.15 can be rewritten as:

$$\frac{y_2}{y_1} = \tfrac{1}{2}\left(\sqrt{1 + 8\,N_1^{\,2}} - 1\right) \qquad (2.17)$$

where $N_1 = F_1 \psi_1$ (2.18)

and $$\psi_1 = \frac{1}{\sqrt{1 - K' \times \sin\alpha}} \qquad (2.19)$$

The form of Eq 2.17 was probably first published by Kennison (25) in 1944, and later rederived by Chow (26) and Argyropoulous (23).

Assuming K' to be unity, the variation of ψ_1, with α and is studies in Figure 2.12. It is found that for small values of α the error in fixing x has only a very small effect on ψ_1. Experimental information is badly needed to evaluate precisely the coefficient in Eq 2.17 for the Type E-jump.

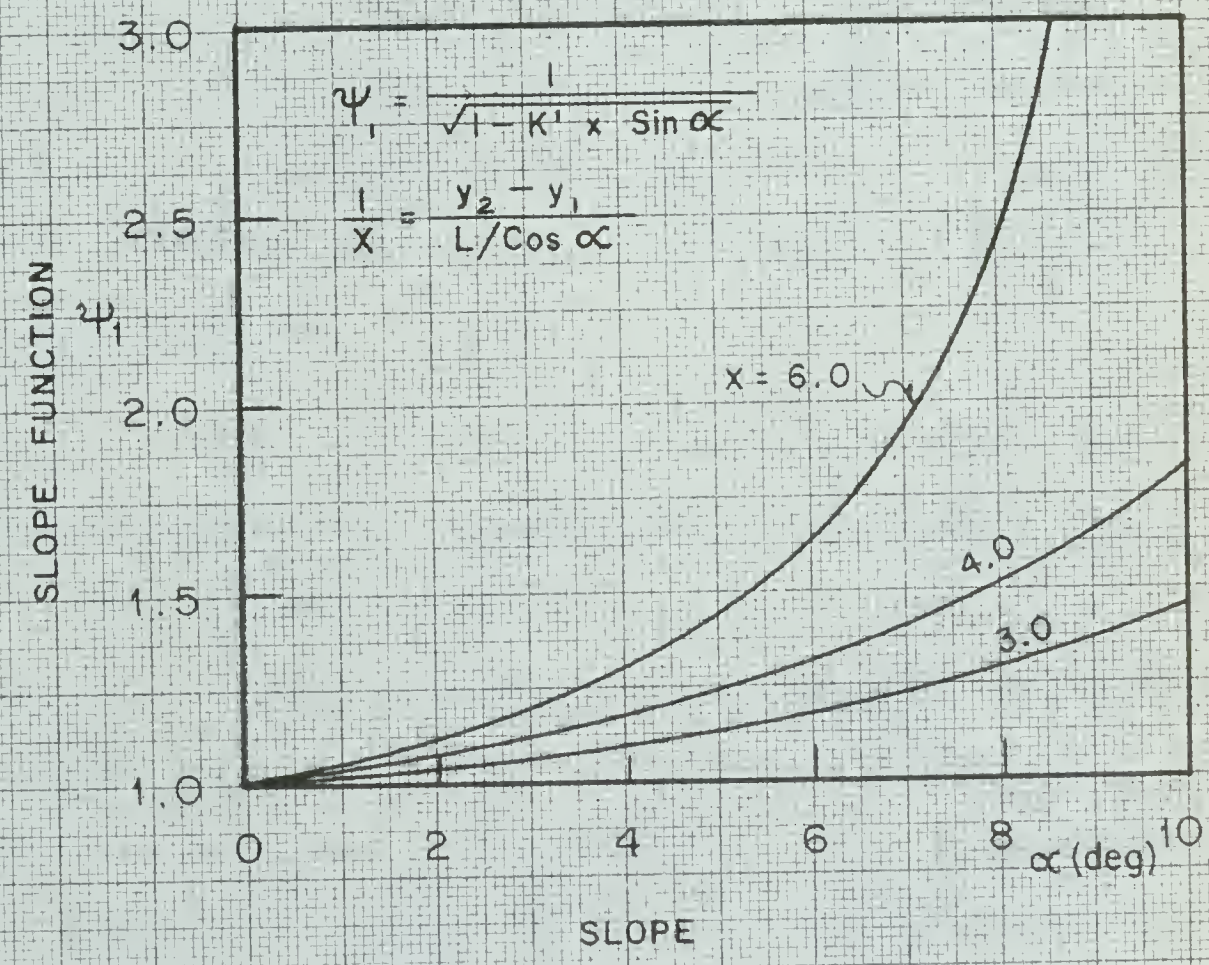

FIGURE 2.12 VARIATION OF Ψ_1 WITH α
(TYPE E JUMP)

CHAPTER III

HYDRAULIC JUMP ON POSITIVE (OR ADVERSE) SLOPES

THEORETICAL ANALYSIS

INTRODUCTION:

Only very little study appears to have been made on the jump formation on adverse slopes. In his work on "Open Channel Hydraulics", (published in 1959), while referring to this type of jump, Chow has written that "this is a rare type of jump, and no adequate experimental data are available at the present moment". The author has been unable to find any other publication, dealing with an experimental study specifically involving this problem.

In 1944, J.C. Stevens (27), while discussing Kindsvater's paper on the theory of jump formation on negative slopes, developed an approximate method to predict the sequent depths on adverse slopes. (This will be referred to later on, in this chapter). Rajaratnam (24), as a result of his experimental work on an 1 on 10 adverse slope has mentioned that he has found it almost impossible to form a stable jump. In this chapter, a theoretical solution is developed for two types of jumps formed on adverse slopes.

TYPES OF JUMP:

Two types of jump are considered, as shown in Figure 3.1, and are referred to as A-1 and A-2. A-1 jump is formed completely on the reverse slope. A-2 jump begins on the level, and ends on the reverse slope. In this work, the end of the surface roller, because of the difficulty in determining exactly the end of the jump, will be assumed to be itself the end of the jump.

A-1 JUMP: GENERAL SOLUTION

Referring to Figure 3.1, let y_1 and y_2 be the vertical depths at the beginning and the end of the jump; q, the discharge intensity; and α, the slope of the channel with the horizontal.

Writing the momentum equation for the free body of the jump in a direction parallel to the bed,

$$P_1 - P_2 - W \sin \alpha = M_2 - M_1 \qquad (3.01)$$

where P_1 and P_2 are the external forces at the beginning and the end of the jump, W is the weight of the water in the body of the jump, and M_1 and M_2 are the respective momentum rates. The bed and side shear has been neglected in this equation.

As in the case of the jump on negative slopes, assuming hydrostatic pressure distribution (as an approximation) in the vertical direction,

$$P_1 = \tfrac{1}{2} \gamma \, y_1^2 \cos\alpha \qquad (3.02)$$

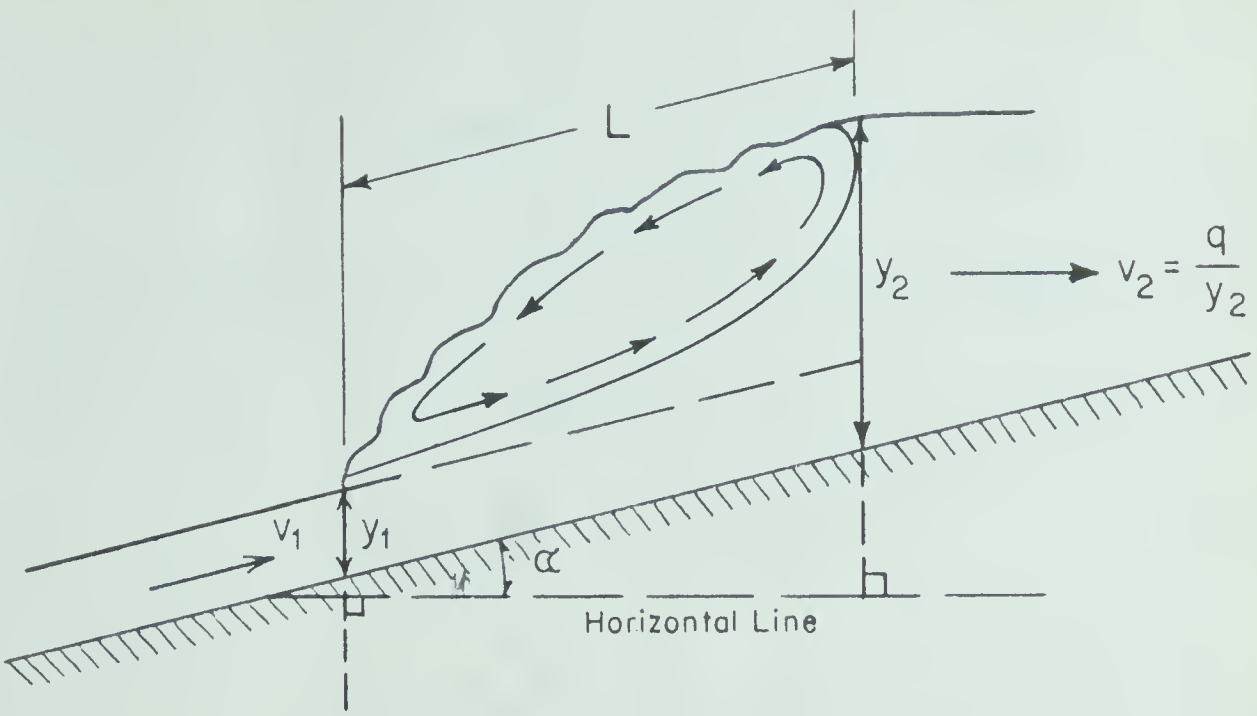

FIGURE 3.1(a) A – 1 JUMP

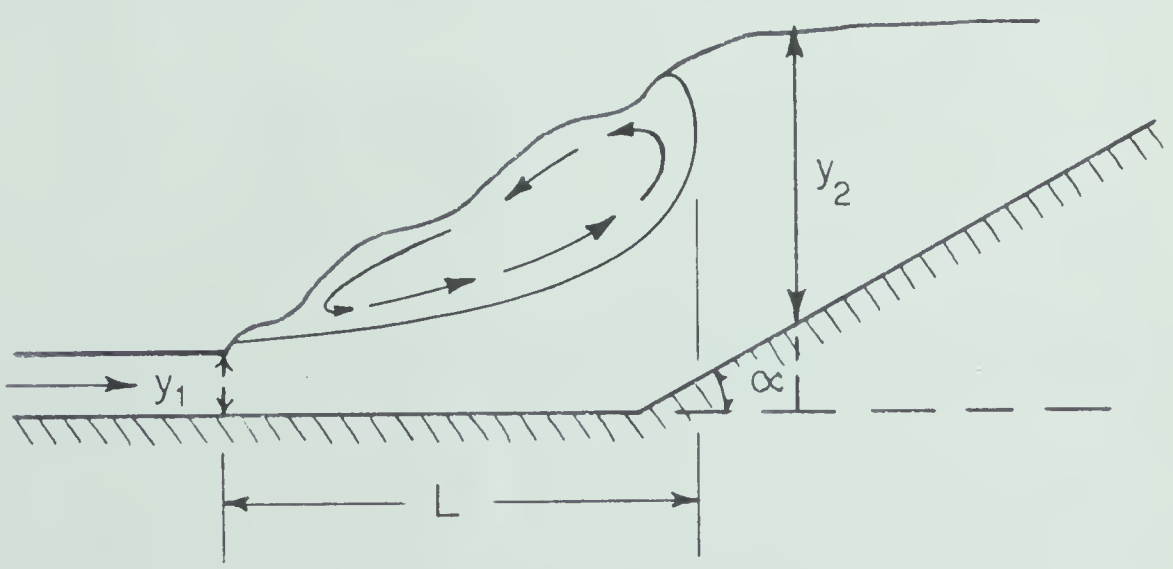

FIGURE 3.1(b) A – 2 JUMP

$$P_2 = \tfrac{1}{2} \gamma y_2^2 \cos \alpha \qquad (3.03)$$

Assuming a linear surface profile for the jump, with

$$L = n (y_2 - y_1) \qquad (3.04)$$

where L is the length of the jump parallel to the bed, and n is the surface slope factor,

$$W = \frac{\gamma n}{2} (y_2^2 - y_1^2) \qquad (3.05)$$

Also

$$M_1 = \frac{\gamma q^2}{g} \cdot \frac{1}{y_1 \cos \alpha} \qquad (3.06)$$

and

$$M_2 = \frac{\gamma q^2}{g} \cdot \frac{1}{y_2} \cos \alpha \qquad (3.07)$$

assuming that the mean velocity V_2 at the end of the jump is essentially horizontal.

Substituting Eqs 3.02 to 3.07 into 3.01

$$\tfrac{1}{2} \gamma y_1^2 \cos \alpha - \tfrac{1}{2} \gamma y_2^2 \cos \alpha - \frac{\gamma}{2} n (y_2^2 - y_1^2) \sin \alpha \qquad (3.08)$$

$$= \frac{\gamma q^2}{g} \left[\frac{\cos \alpha}{y_2} - \frac{1}{y_1 \cos \alpha} \right]$$

i.e.

$$1 - \frac{y_2^2}{y_1^2} - n \left[\left(\frac{y_2^2}{y_1^2}\right) - 1 \right] \tan \alpha = \frac{2 q^2}{g y_1^2 \cos \alpha \cdot y_1 \cos \alpha} \left[\frac{\cos \alpha}{y_2 \frac{1}{y_1 \cos \alpha} - 1} \right] \qquad (3.09)$$

$$= \frac{2 q^2}{g y_1^3 \cos^3 \alpha} \cdot \cos \alpha \left[\cos^2 \alpha \cdot \frac{y_1}{y_2} - 1 \right] \qquad (3.10)$$

$$= 2 F_1^2 \cos \alpha \left[\cos^2 \alpha \frac{y_1}{y_2} - 1 \right] \quad (3.11)$$

If $\frac{y_2}{y_1} = \psi$; Eq. 3.11 can be written as

$$1 - \psi^2 - n (\psi^2 - 1) \tan \alpha = 2 F_1^2 \cos \alpha \left[\frac{\cos^2 \alpha}{\psi} - 1 \right] \quad (3.12)$$

Eq. 3.12 can be reduced to

$$(1 - \psi^2) \psi \left[1 + n \tan \alpha \right] = 2 F_1^2 \cos \alpha \left[\cos^2 \alpha - \psi \right] \quad (3.13)$$

i.e. $$2 F_1^2 = \frac{(1 - \psi^2) \psi \left[1 + n \tan \alpha \right]}{\cos \alpha \left(\cos^2 \alpha - \psi \right)} \quad (3.14)$$

At this stage, for convenience, the $\cos^2 \alpha$ term, inside the bracket in the denominator may be replaced by unity (to get an idea of the size of the error involved, for $\alpha = 15^\circ$, $\cos^2 \alpha = 0.95$).

With this approximation,

Eq 3.14 becomes

$$2 F_1^2 = \frac{(1 - \psi^2) \psi (1 + n \tan \alpha)}{\cos \alpha (1 - \psi)} \quad (3.15)$$

$$= (1 + \psi) \psi \left[\frac{1 + n \tan \alpha}{\cos \alpha} \right] \quad (3.16)$$

i.e. $$= (1 + \psi) \psi = 2 F_1^2 \frac{\cos \alpha}{1 + n \tan \alpha} \quad (3.17)$$

or $$(1 + \psi) \psi = 2 J^2 \quad (3.18)$$

where $$J^2 = F_1^2 \frac{\cos \alpha}{1 + n \tan \alpha} \quad (3.19)$$

i.e. $$J = F_1 \sqrt{\frac{\cos \alpha}{1 + n \tan \alpha}} \qquad (3.20)$$

The variation of $\sqrt{\frac{\cos \alpha}{1 + n \tan \alpha}}$ with α is studied in Figure 3.2 for n = 5, 6 and 7. In further work n is assumed to be equal to 6, based on the results for the horizontal channel. It should be noted here that from observations, the jumps on adverse slopes are seen to be longer than those on negative slopes, and comparable to those on level channels for corresponding Froude numbers.

In Figure 3.2, the ordinate can be seen to equal J/F_1 and decreases with increase in slope. The solution of Eq 2.18 can be written as:

$$\psi = \tfrac{1}{2} \left[\sqrt{1 + 8 J^2} - 1 \right] \qquad (3.21)$$

which is of the same form as Belanger's well known momentum equation.

Eq 3.21 has been evaluated for F_1 from 2 to 20, and tan α = 0.0 to 0.25, and shown in Figure 3.3. It is found that for any given supercritical Froude number, the sequent depth ratio decreases as the slope increases and thus the corresponding curves for the negative slopes will be below the line for level channel.

In Figure 3.4, the present result is compared with that of Stevens (27) for two values of tan α . In developing his method, Stevens calculated the volume of the jump using the empirical formula of Ivanchenko. It is seen that for any given value of F_1 higher than about 7, and tan α ,

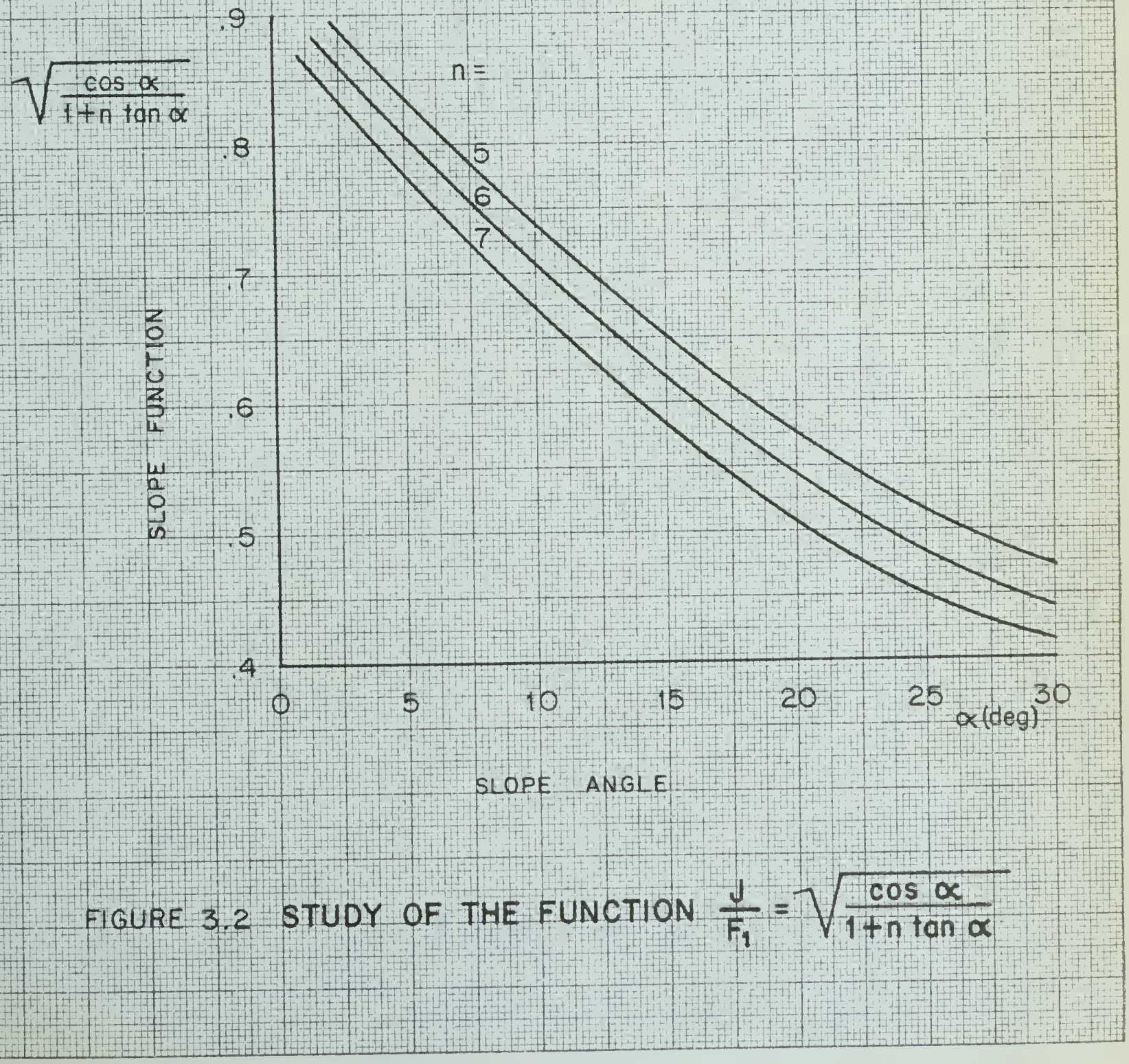

FIGURE 3.2 STUDY OF THE FUNCTION $\frac{J}{F_1} = \sqrt{\frac{\cos \alpha}{1+n \tan \alpha}}$

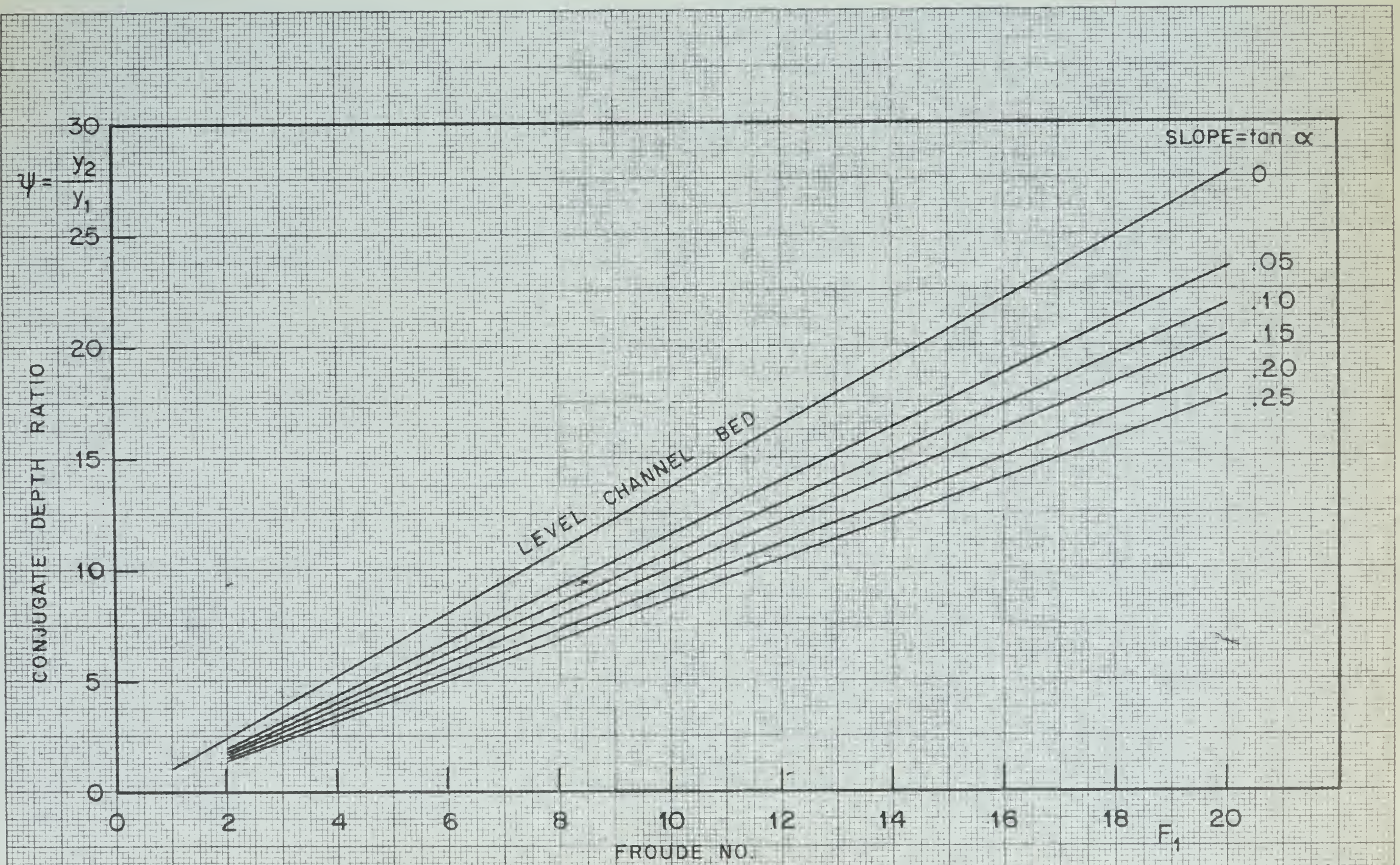

FIGURE 3.3 STUDY OF EQ. 3.21: $\psi = \left[\sqrt{1+8J} - 1\right]$

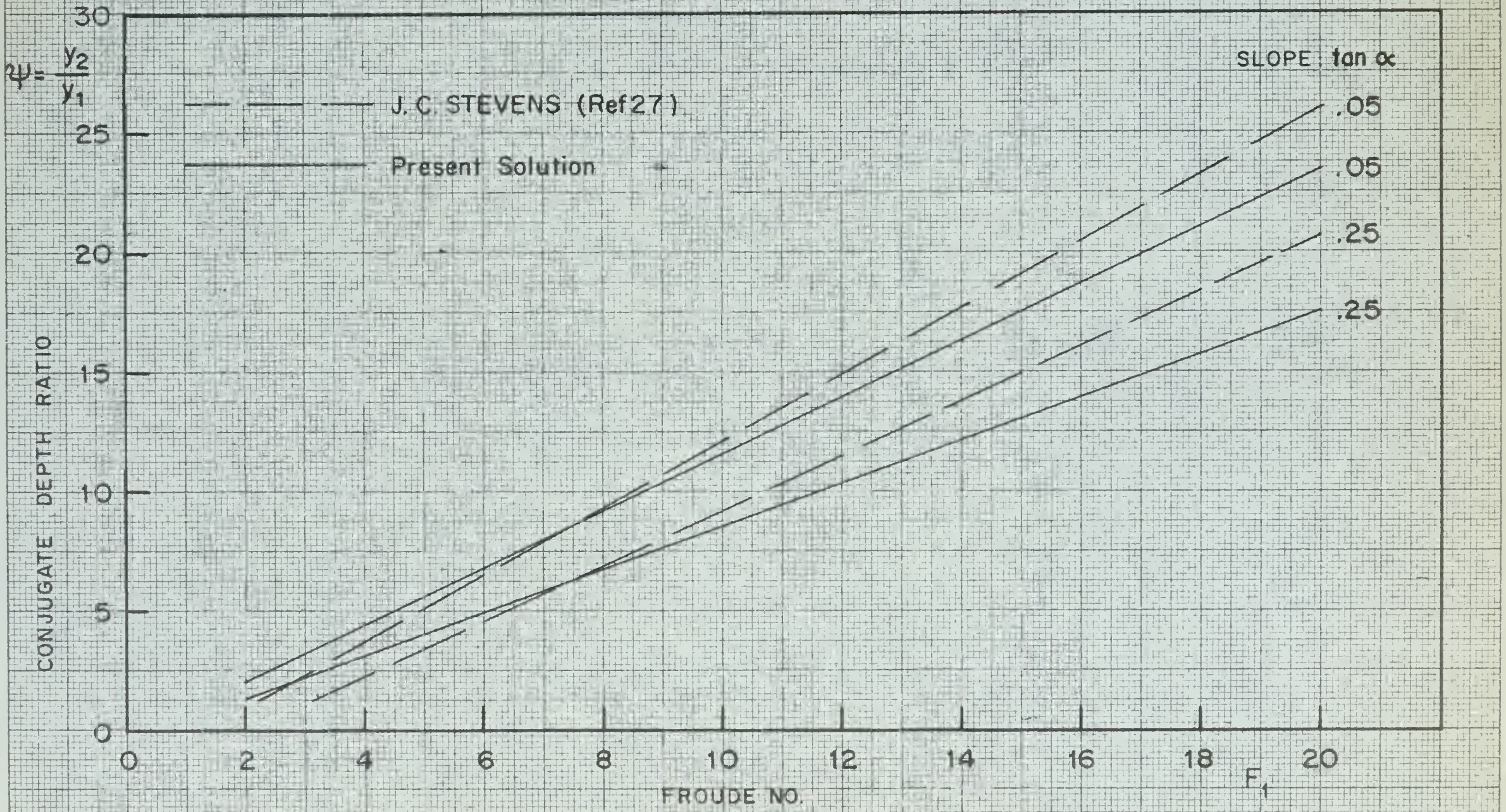

FIGURE 3.4 COMPARISON OF PRESENT SOLUTION WITH STEVENS' SOLUTION

Stevens' method indicates a higher value of the sequent depth ratio, and this trend is reversed for $F_1 \leq 7.0$.

APPROXIMATE SOLUTION FOR SMALL ADVERSE SLOPES:

When the adverse slope is small (i.e., tan α less than 1 on 10 i.e., $\alpha \simeq 6$ degrees), the depth normal to the floor can be replaced by the vertical depth as a good approximation, and the solution becomes much simpler.

In a direction parallel to the bed

$$P_1 = \tfrac{1}{2} \gamma y_1^2 \qquad (3.22)$$

$$P_2 = \tfrac{1}{2} \gamma y_2^2 \qquad (3.23)$$

$$W = \frac{\gamma}{2} n (y_2^2 - y_1^2) \qquad (3.24)$$

$$M_1 = \frac{\gamma q^2}{g} \cdot \frac{1}{y_1} \qquad (3.25)$$

$$M_2 = \frac{\gamma q^2}{g} \cdot \frac{1}{y_2} \qquad (3.26)$$

Substituting Eqs 3.22 to 3.26 into the basic momentum equation, it can be shown that

$$1 - \left(\frac{y_2}{y_1}\right)^2 - n \left[\left(\frac{y_2}{y_1}\right)^2 - 1 \right] \sin\alpha = \frac{2 q^2}{g y_1^3} \left[\frac{y_1}{y_2} - 1\right] \qquad (3.27)$$

$$= 2 F_1^2 \left[\frac{y_1}{y_2} - 1\right] \qquad (3.28)$$

Letting $\psi = \frac{y_2}{y_1}$, Eq. 3.28 can be reduced to:

$$2 F_1^2 = \psi (1 + \psi) (1 + n \sin \alpha) \qquad (3.29)$$

$$= \psi (1 + \psi) (1 + 6 \sin \alpha) \qquad (3.30)$$

i.e. $$\psi^2 + \psi - \frac{2 F_1^2}{1 + 6 \sin \alpha} = 0 \qquad (3.31)$$

Let $$\frac{F_1^2}{1 + 6 \sin \alpha} = H_1^2 \qquad (3.32)$$

Then Eq. 3.31 becomes $$\psi^2 + \psi - 2 H_1^2 = 0 \qquad (3.33)$$

solving $$\psi = \tfrac{1}{2} \left[\sqrt{1 + 8 H_1^2} - 1\right] \qquad (3.34)$$

This is of the same form as the well known Belanger equation for the classical jump.

Eq. 3.34 has been evaluated and shown in Figure 3.5 for tan α = 0.05, 0.10, 0.15, 0.20 and 0.25. On comparison with figure 3.3, it is seen that there is only a slight difference between the two.

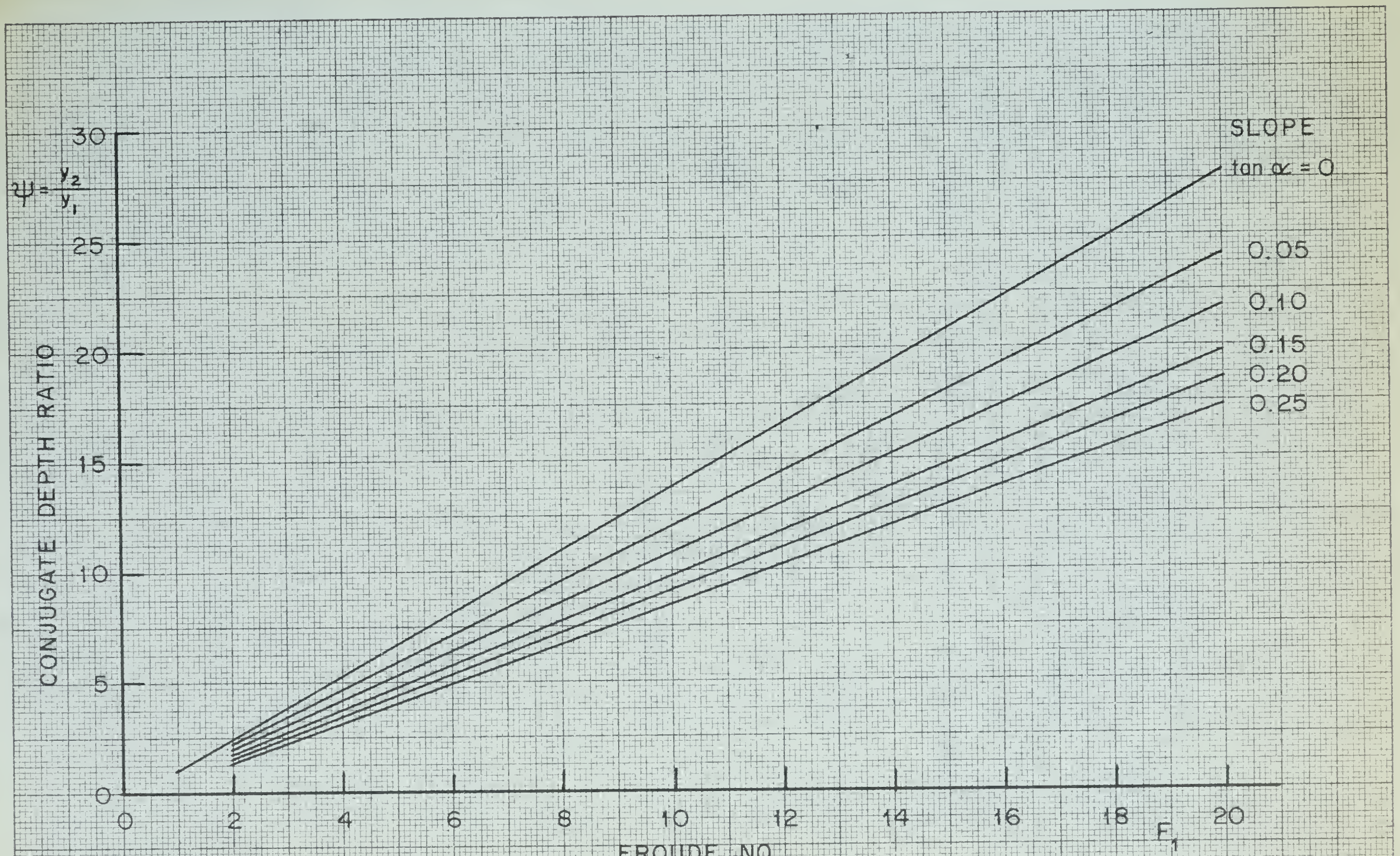

FIGURE 3.5 SOLUTION FOR CHANNELS OF SMALL ADVERSE SLOPE

A-2 JUMP:

Referring to Figure 3.1 (b), an elaborate analysis was developed for this jump, but was found to contain too many unknown factors, and hence is not presented here. It is believed that in analogy with the B-jump on negative slopes discussed in Chapter III it might be possible to develop a solution experimentally, indicating the relationship between $\frac{y_2}{y_2^*}$, $\frac{l}{L}$ and α, believed to be independent of Froude Number F_1.

CHAPTER IV

THE EXPERIMENT, TEST PROCEDURE AND ANALYSIS

GENERAL AIMS OF THE EXPERIMENT

The aims of the experiments were:

a) To create A-1 jumps on slopes with tan α from 0.05 to about 0.33, and to experimentally check the theoretical equations 3.21 and 3.34, derived in Chapter III.

b) To obtain a basic experimental equation for A-2 jump.

c) To study experimentally, the stability of jump formation on adverse slopes.

d) To study the length characteristics of the A-1 and A-2 jumps.

e) To study the velocity profile at the end of the roller to determine its agreement with the similarity profile of the plane turbulent wall jet.

f) To study the validity of a number of equations evolved recently by Rajaratnam (3), treating the hydraulic jump as a wall jet under adverse pressure gradient.

EXPERIMENTAL ARRANGEMENT:

The experiments were conducted in the Hydraulics Laboratory of the Northern Alberta Institute of Technology at Edmonton, Alberta. The experimental arrangement is shown in Figures 4.1 and 4.2. The flume used is a rectangular channel, 18 inches wide, 24 inches high, with a smooth brass bottom, and glass side walls. The reverse slope was formed by means of a 3/4" fir plywood plank, fastened firmly to the bed of the flume by means of a steel plate with a finely machined, knife edge, at the front end.

The water enters the channel from a constant head tank under a sluice gate, working on a closed circuit system. The discharge was measured by means of a calibrated orifice meter located in the line, and was checked by using the sluice gate as a flow measuring device. The water depth was controlled by means of a tailgate.

The surface profile measurements was made photographically. Figure 4.3 is a typical photograph for surface profile recording for Run A-1. (Photographs of the remaining 24 runs made are shown in Appendix A). To make measurements from the photographs, a measuring grid placed on the flume, was also photographed with the camera at the same location (see Figure 4.4). Measurements for the depth of flow at any point, and the length of the jump, were then made simply by superimposing the grid on top of the photographic recordings, and reading off from the grid.

The author was fortunate in having been able to obtain assistance from the Photographic Technology Laboratories at the Northern Alberta Institute of Technology. The camera used was a Calumet 4" x 5" view

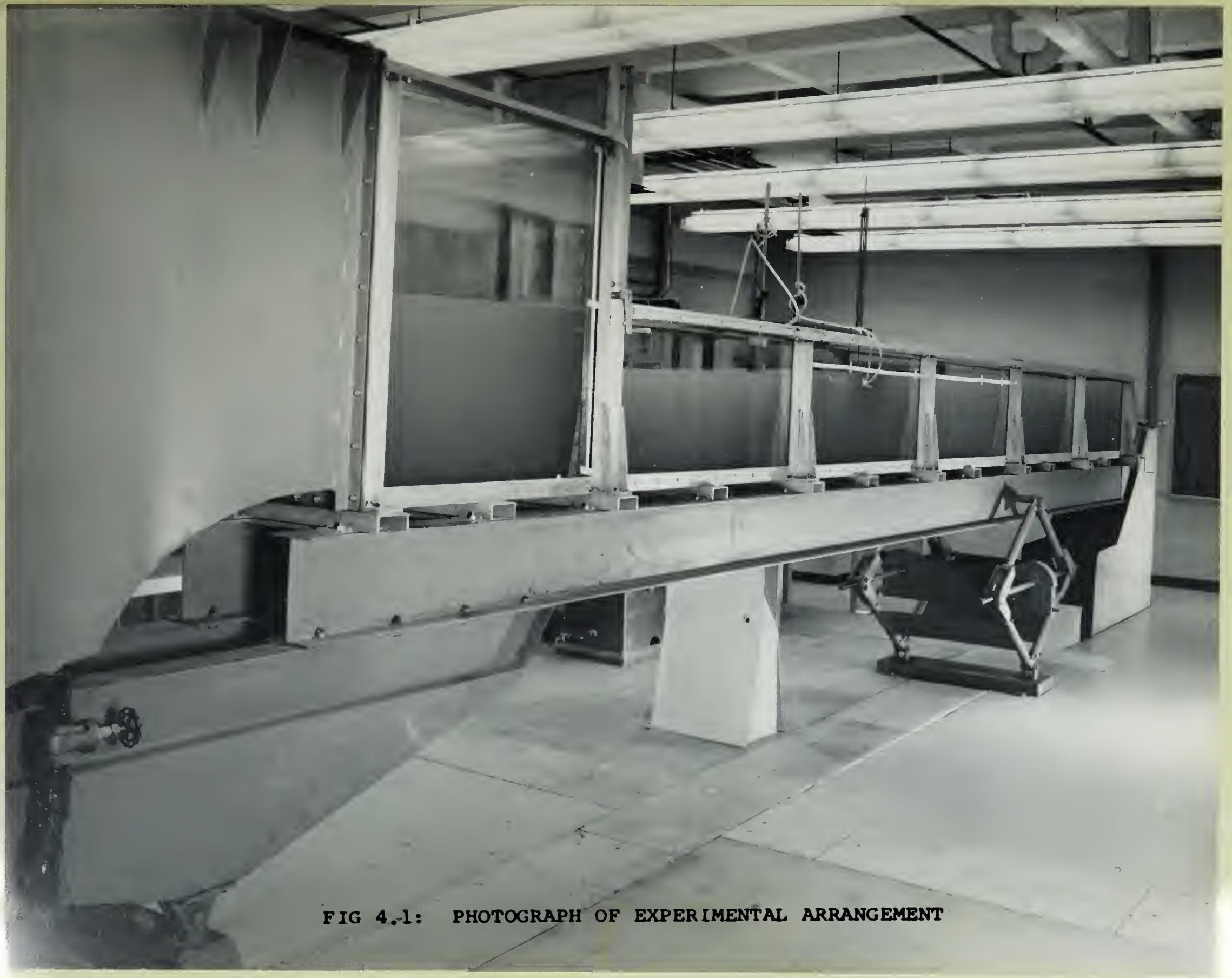

FIG 4.1: PHOTOGRAPH OF EXPERIMENTAL ARRANGEMENT

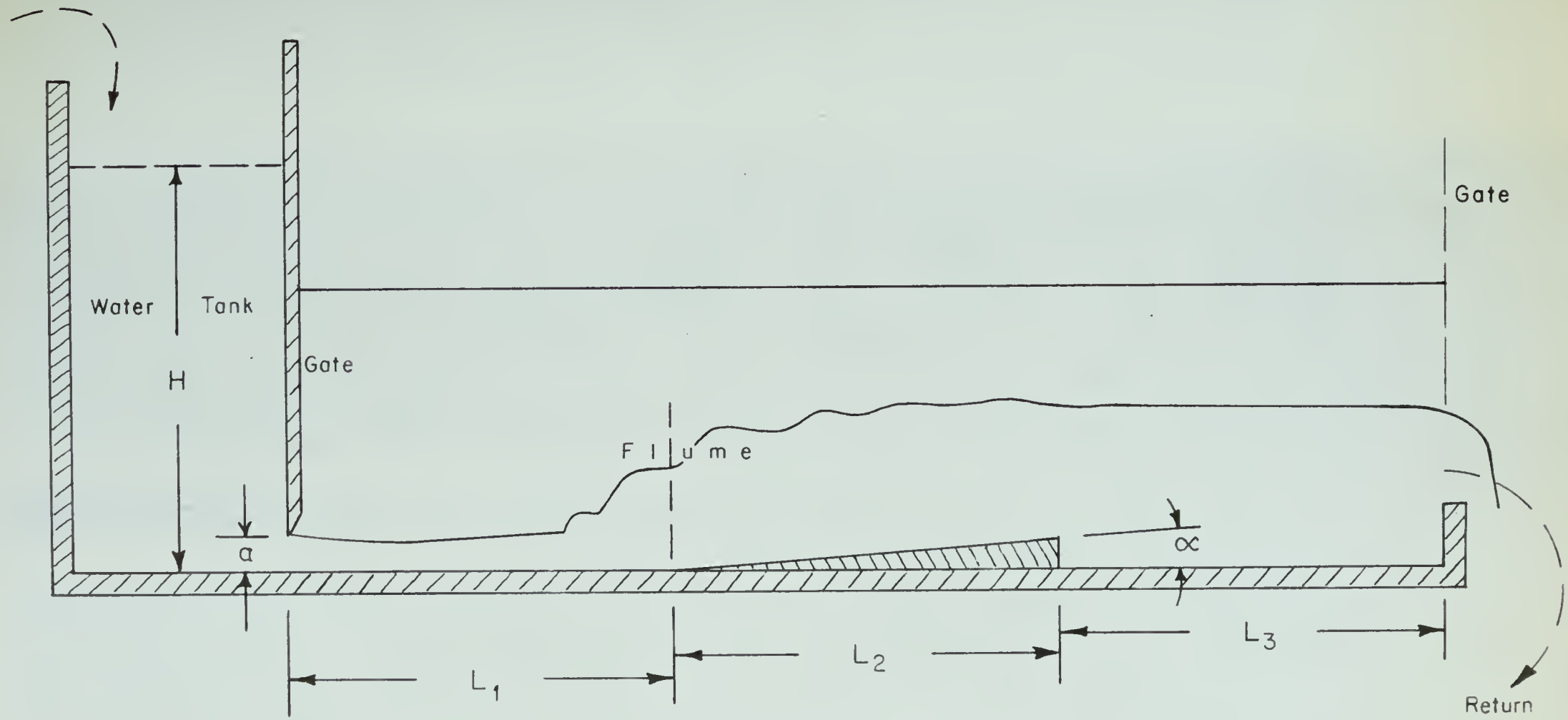

FIGURE 4.2 SCHEMATIC LINE DIAGRAM OF THE REVERSE SLOPE

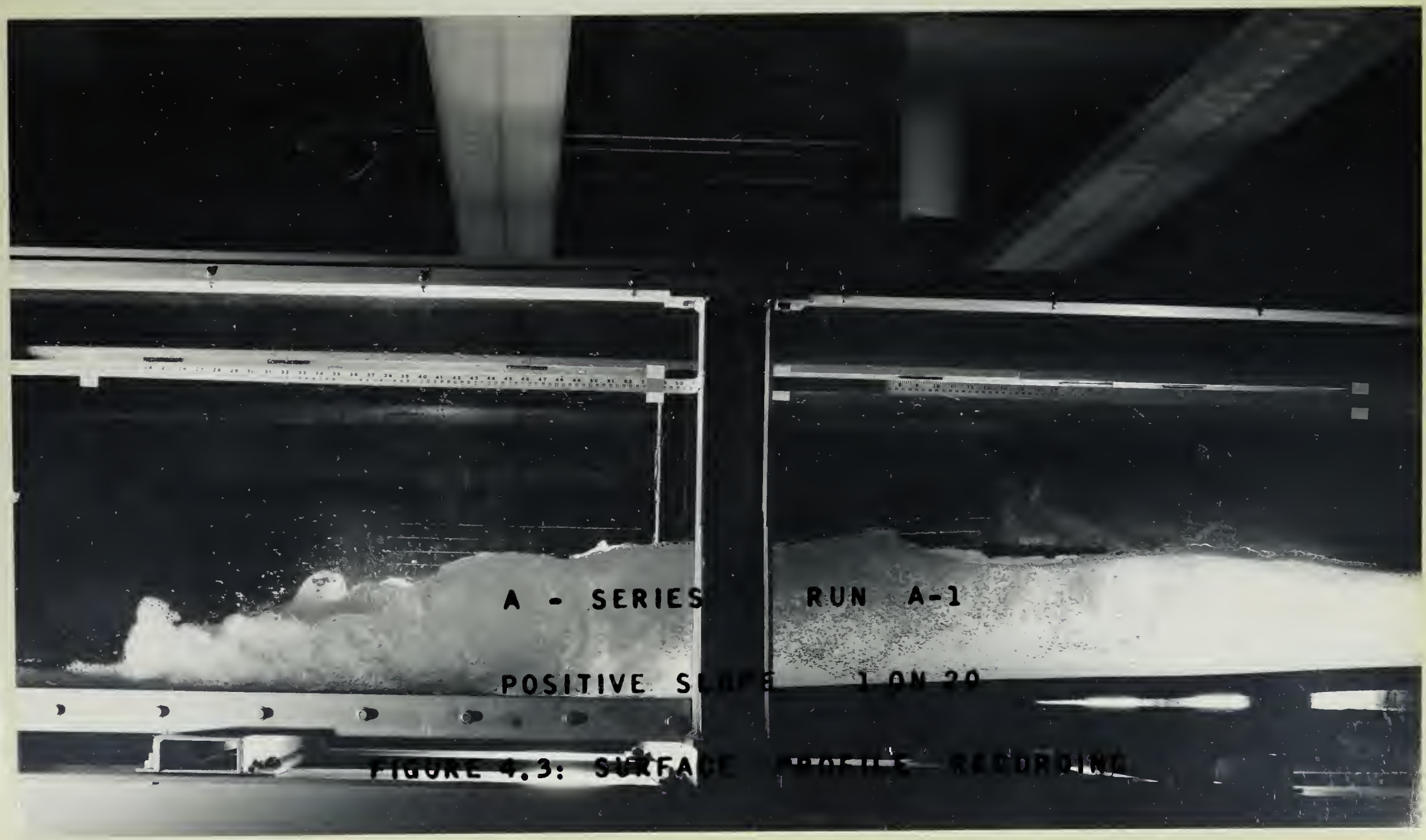

FIGURE 4.3: SURFACE PROFILE RECORDING

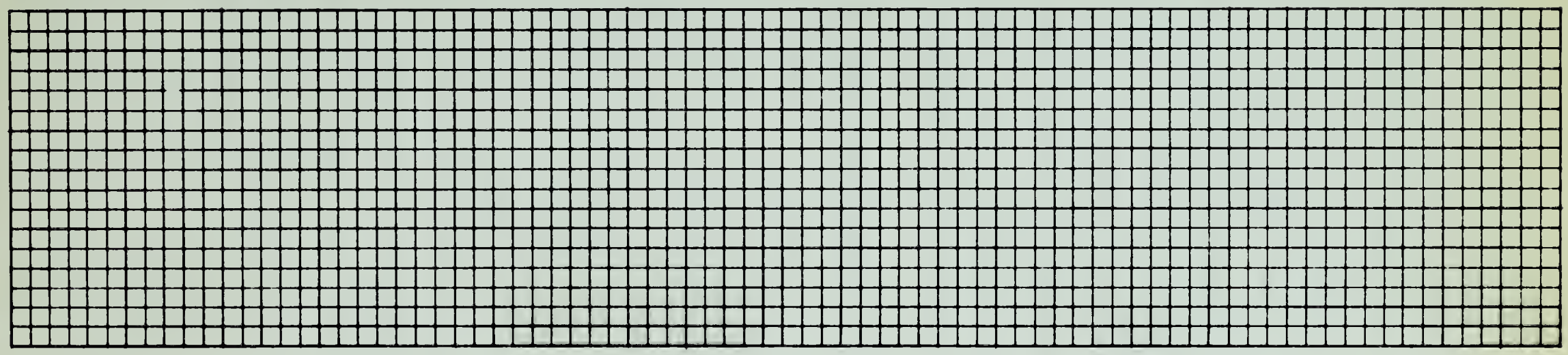

FIGURE 4.4 MEASURING GRID

camera, equipped with an 8 1/2" 210 mm F 4.5 Schneider Symmar Lens, large format Majestic tripod, Brockway incident light meter, Ascor and Photogenic Studio Electronic Flash Units. The black and white film used was Versapan. A polaroid 4" x 5" back with Type P-N film was used extensively during trial runs, until the photographic techniques could be refined, and following this, the experimental runs were recorded. In case of two runs, surface profile measurements were made by means of a precision point gage, and this showed satisfactory correlation with readings obtained by the photographic method. Hence, in all the runs, the photographs were used for obtaining all the geometrical properties of the jump.

In every case, the end of the surface roller, was found by colour injection from the top, using an eye dropper, and a velocity traverse was taken at the end of the roller. To develop a technique of visually distinguishing separation point of the boundary layer on the bed accurately, fluorescene dye was used, in conjunction with ultra-violet light sources. (This provided satisfactory discrimination).

STABILITY OF THE JUMP ON ADVERSE SLOPE:

It was soon discovered that it was impossible to form a stable jump of the A-1 type. Starting from an A-2 jump to attain an A-1 jump, the moment the tail water was lowered to move the jump a little on the slope, it became unstable, and slowly moved up the slope. Figure 4.5 shows a sequence of this phemonena.

FIG. 4.5(a) to (c) : SEQUENTIAL PHOTOGRAPHS OF UNSTABLE JUMP :

a

54

q

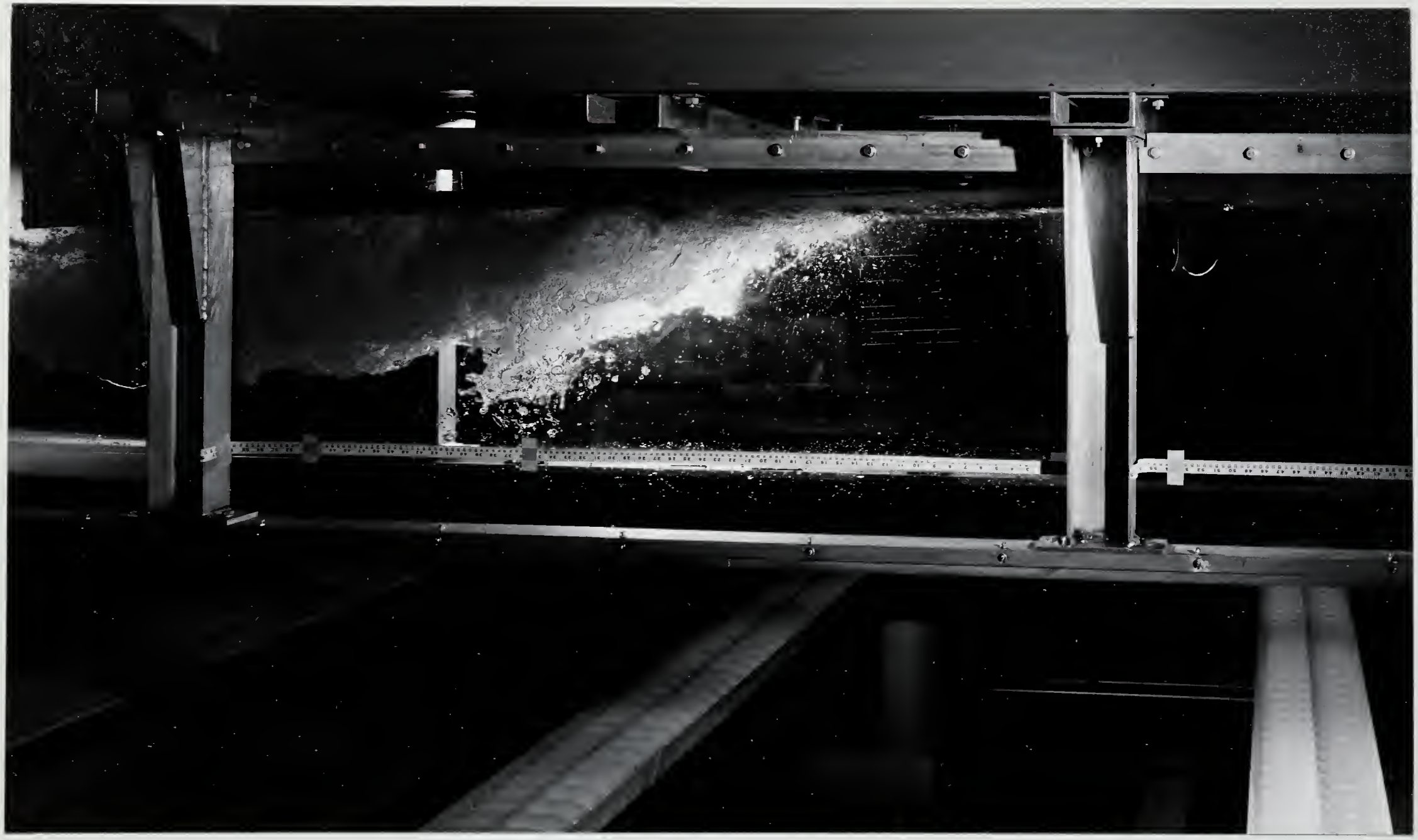

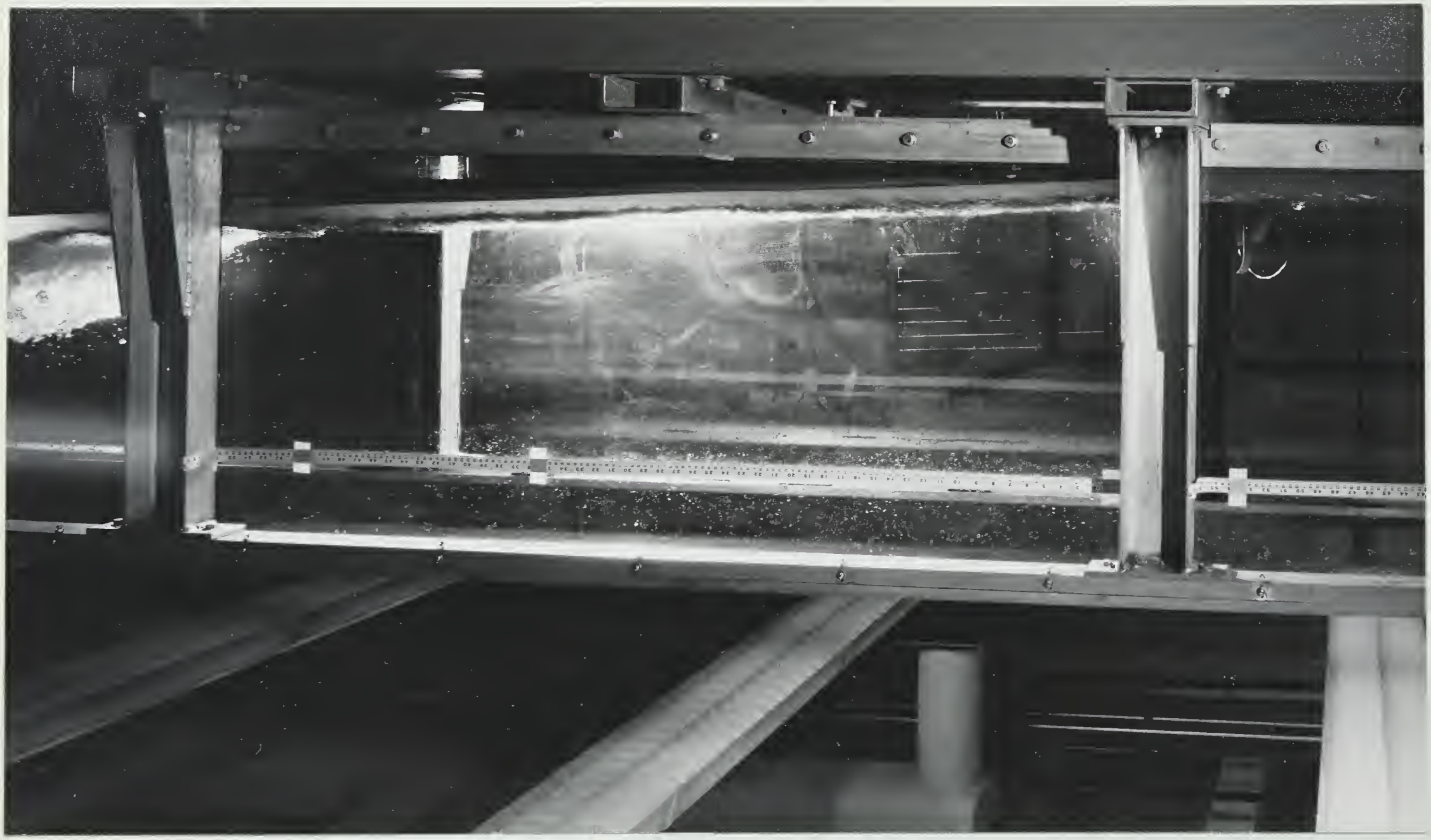

Extreme care was taken in attempting to maintain the jump on the slope. It was repeated on slopes of 1 on 20, 1 on 15, and 1 on 10, but it was not possible to get the A-1 jump. Even when the A-2 jump was formed the portion of the jump up to the end of the roller had to be on the level channel.

The author can find no logical explanation for this strange behaviour. In this connection, it should be pointed out that Rajaratnam (24) had reported earlier that he had encountered similar difficulty with a 1 on 10 adverse slope.

EXPERIMENTAL DETAILS:

Because of the difficulties mentioned in the preceding sections, it was not possible to study the A-1 jump in greater detail than described above. Only A-2 jump could be formed. Five slopes were studied and for each slope, runs were made with 5 different supercritical Froude numbers varying between 5.72 to about 12.0. Tan α was varied from 0.05 to 0.33. Table I gives a summary of some of the test results of the experiment.

LENGTH OF A-2 JUMP:

From a study of the Photographs (Figures 4.3 and Appendix A) it was found that the end of the roller could be taken as the effective end of the jump. In most cases, this was also the point of maximum mean elevation. The surface profile became almost level at this point. In several runs, there was a further surface rise after this section. In comparison with negative slopes, the end of the roller was taken as the end of the

TABLE I

EXPERIMENTAL DATA

Runs	$F_1 = \frac{U_1}{\sqrt{g\ y_1}}$	y_1 ft	y_r ft	y_r/y_1	L_{rj} ft	Slope ($\tan\alpha$)	U_1 (ft/sec)
A-1	11.70	.059	.625	10.60	2.08	.05	12.90
A-2	11.45	.067	.750	11.20	2.25	.05	14.20
A-3	9.64	.076	1.042	13.70	3.33	.05	15.20
A-4	9.21	.088	.667	7.60	2.75	.05	15.60
A-5	8.15	.103	.792	7.72	2.77	.05	14.85
B-1	9.20	.068	.667	9.80	2.67	.067	15.40
B-2	10.80	.077	.583	7.60	2.50	.067	12.60
B-3	9.55	.086	.792	9.20	2.75	.067	13.25
B-4	8.80	.089	.833	9.37	2.83	.067	14.85
B-5	-----	1.094	.930	9.86	2.75	.067	-----
C-1	7.62	.065	.540	8.30	2.54	.100	11.00
C-2	8.00	.074	----	----	----	.100	12.30
C-3	6.30	.095	.770	8.10	2.75	.100	11.00
C-4	6.56	.105	.750	7.15	1.83	.100	12.10
C-5	7.25	.107	.750	7.00	2.33	.100	13.40
D-1	9.14	.060	.540	9.00	2.29	.200	12.70
D-2	8.70	.075	.550	7.35	3.63	.200	13.60
D-3	6.96	.090	.920	10.20	3.46	.200	11.85
D-4	7.62	.097	.750	7.75	3.25	.200	13.35
D-5	7.00	.109	.960	8.80	3.29	.200	13.10
E-1	7.14	.069	.650	9.40	2.50	.330	10.6
E-2	6.65	.081	.750	9.25	3.25	.330	10.7
E-3	5.72	.109	.820	7.50	3.08	.330	10.7
E-4	6.87	.104	.710	6.85	2.75	.330	12.5
E-5	7.85	.107	.867	8.10	3.43	.330	14.5

jump, as being the only quantity that could be fixed with some confidence.

The length of the roller L_{rj} of the A-2 jump is compared with the results for the classical jump in Figure 4.6 to observe whether the reverse slope has any effect on the length of the jump formed upstream.

From Figure 4.6, it is found that for the steeper slopes, there is very little effect on the jump, but in case of the flat adverse slopes, the jumps are somewhat shorter. If Y_r is the depth of flow at the end of the roller, the variation of the ratio $\frac{y_r}{y_1}$ with F_1 is studied in Figure 4.7, which also presents two curves for the classical jump. It is seen that the A-2 jumps on the flat adverse slopes give lower value of $\frac{y_r}{y_1}$ than the classical jump for the corresponding supercritical Froude numbers.

VELOCITY DISTRIBUTION IN THE BOUNDARY LAYER PORTION:

The velocity distribution measurements made at the end of the roller shown in Figure 4.8 and Appendix B, show clearly that there is a boundary layer with a free mixing region over it. This is in good agreement with Rajaratnam's method of treating the jump as a plane turbulent wall jet. No correction for air entrainment was made to the velocity measurements. The error is believed to be small because the mean air concentration is low at the end of the roller, (7).

The consistent results of Figure 4.8 in the $\frac{U}{U_m}$ boundary layer portion are plotted non-dimensionally in Figure 4.9 to see whether a similar velocity profile is present. From Figure 4.9 it is found that when $\frac{U}{U_m}$ is plotted against $\frac{y}{\delta}$ where U is the velocity at y above the bed, U_m is the

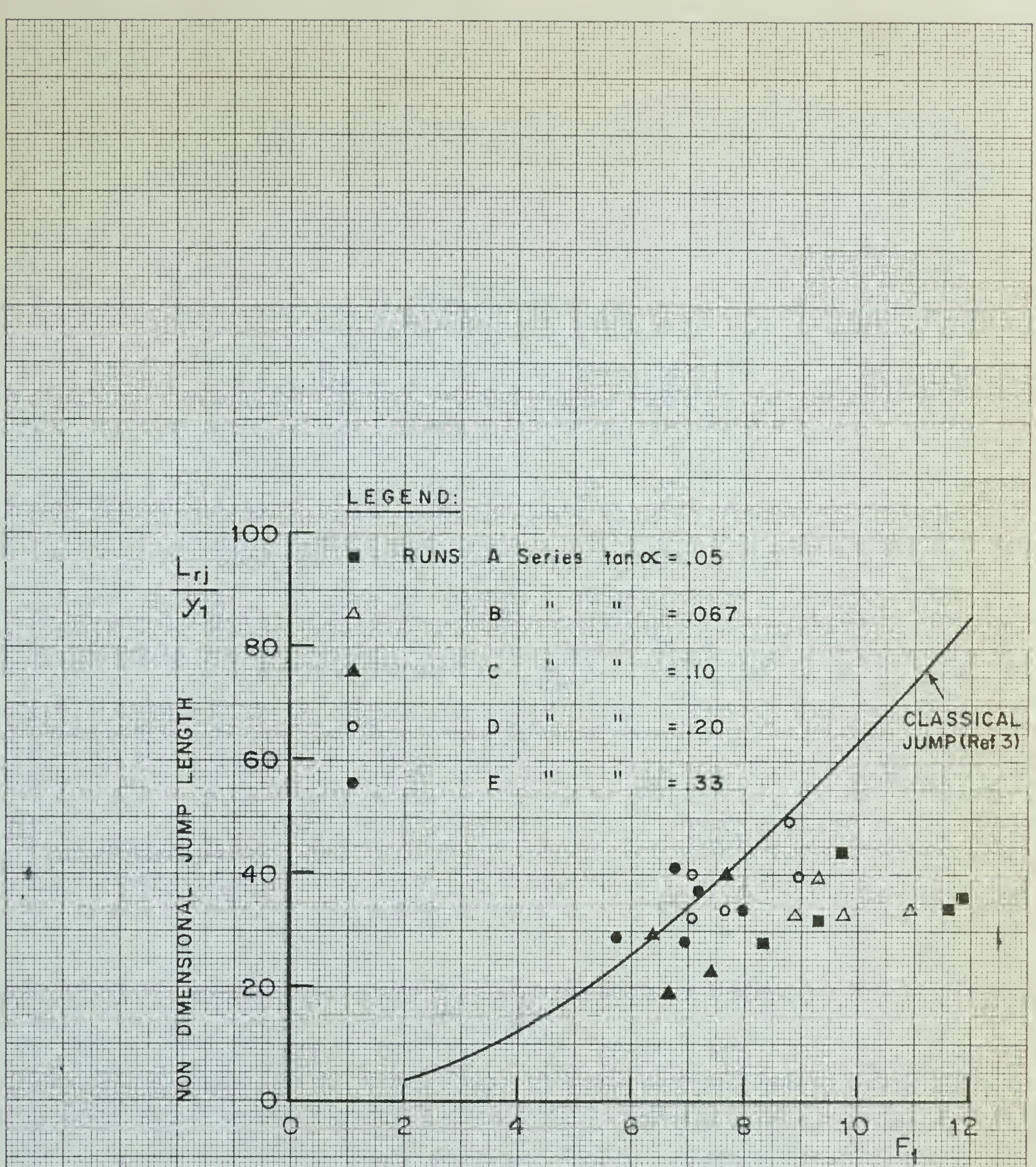

FIGURE 4.6 VARIATION OF $\frac{L_{rj}}{y_1}$ WITH F_1

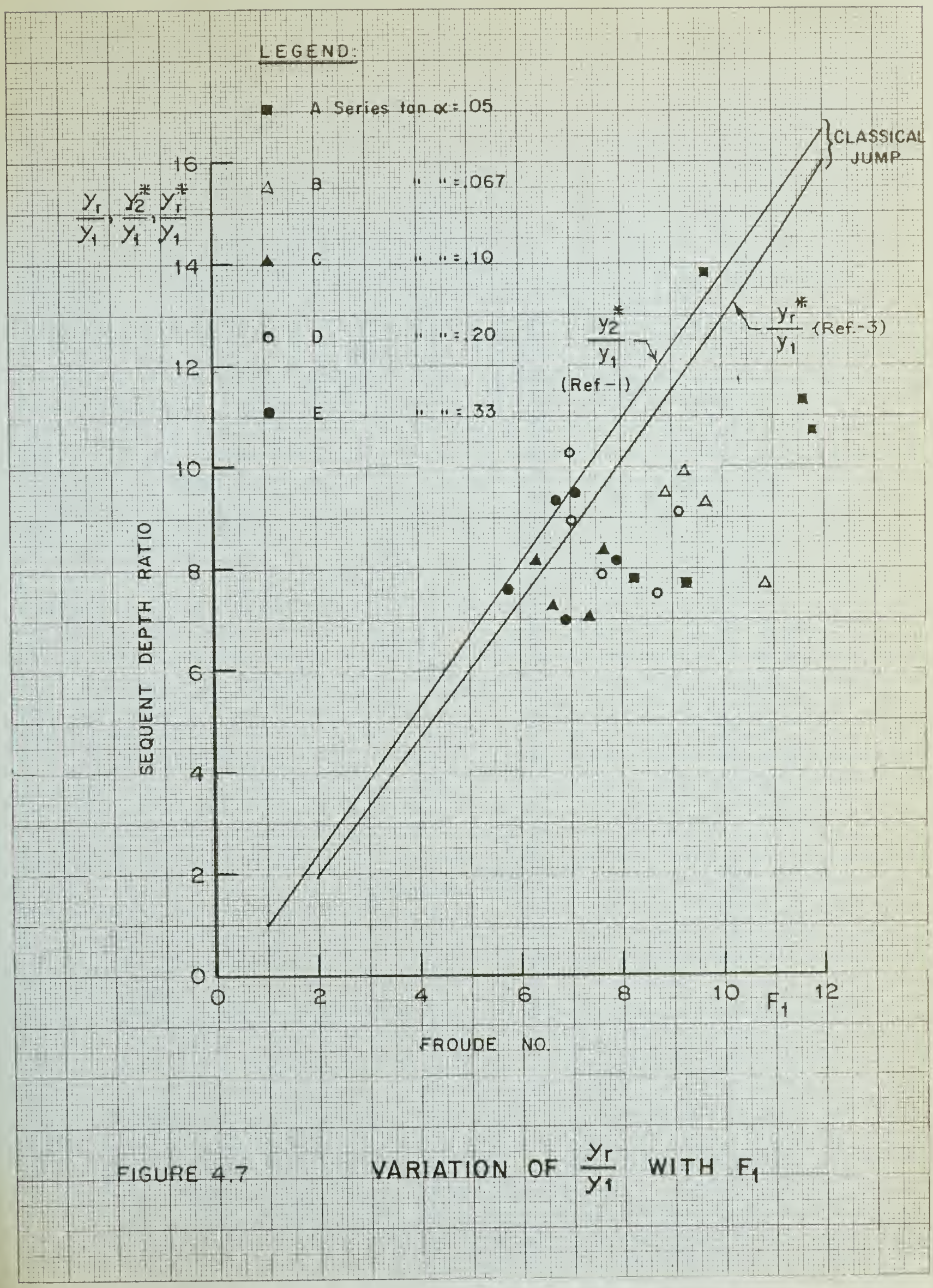

FIGURE 4.7 VARIATION OF $\frac{y_r}{y_1}$ WITH F_1

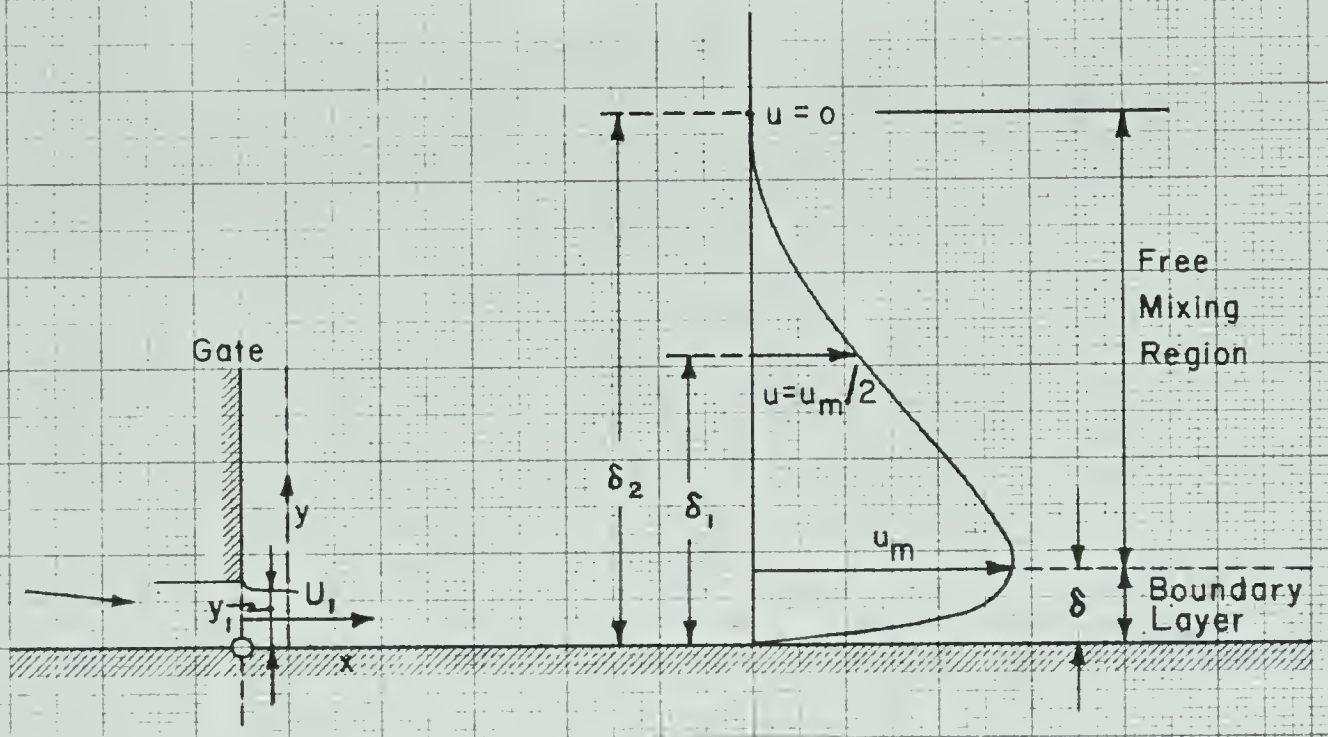

Fig. 4.8 VELOCITY DISTRIBUTION PLOT

(IDEALISED SKETCH OF WALL JET TO DEFINE SYMBOLS)

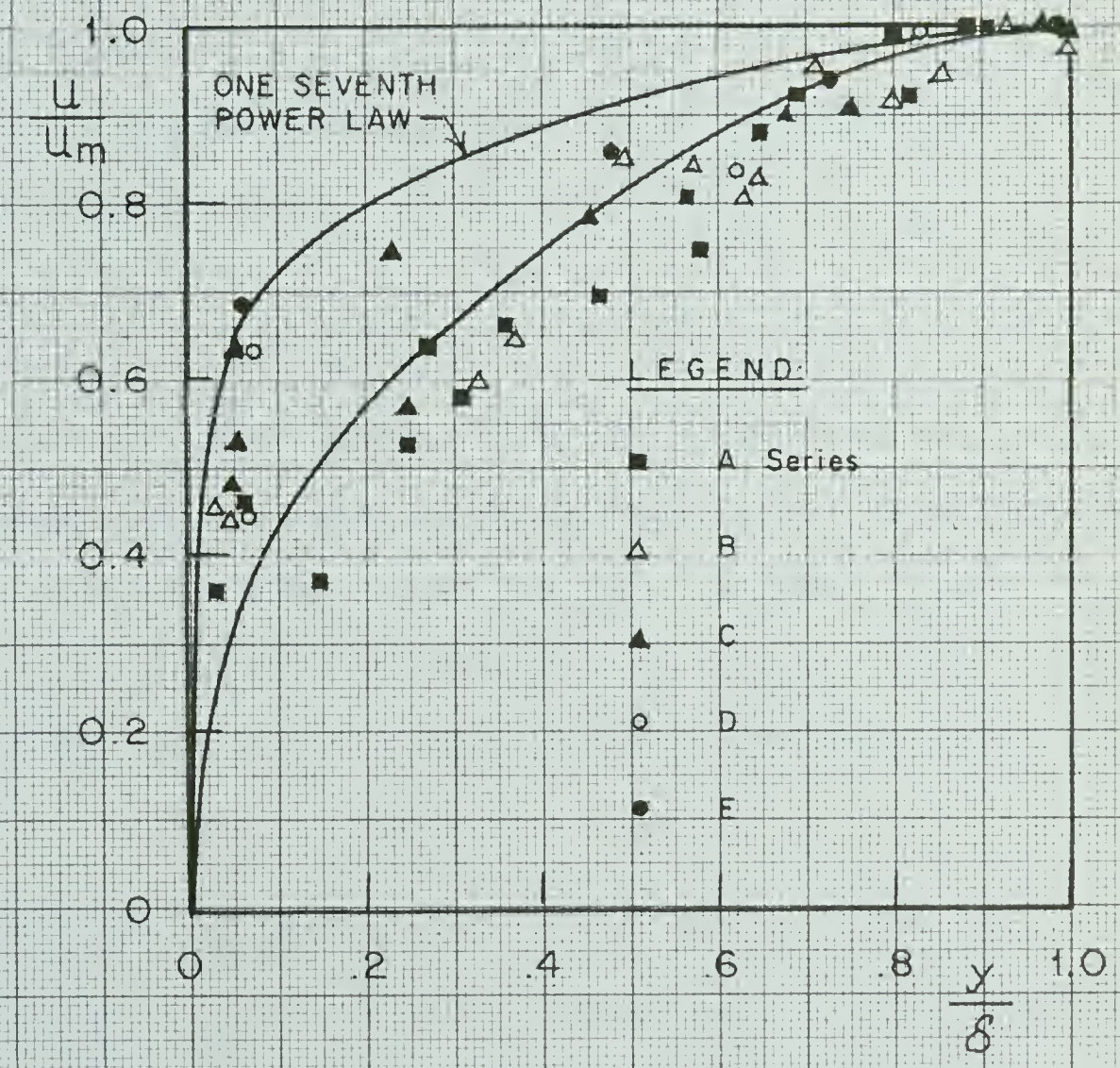

FIGURE 4.9 **VELOCITY DISTRIBUTION (BOUNDARY LAYER PORTION)**

maximum velocity, and δ is the boundary layer thickness, as an approximation, one single curve can be drawn. In the same figure, the well known one seventh power law is also shown.

On a close observation of Figure 4.9, it is seen that the velocity field is much retarded, and is probably approaching separation. In fact separation of the boundary layer was observed in many cases, a short distance after the end of the roller.

FREE MIXING REGION:

In Figure 4.10, which is reproduced from Ref. 3, the velocity distribution curve of the free mixing region for the plane turbulent wall jet under zero pressure gradient is shown by plotting

$$\eta' = \frac{y - \delta}{\delta_1 - \delta} \quad \text{vs} \quad U = \frac{U_m}{2}$$

where δ_1 is the depth at which $U = \frac{U_m}{2}$. The experimental results of the present study are also shown plotted in Figure 4.10. It is found that even though there is some scatter, the classical wall jet curve appears to be a good fitting curve for the data. Thus it is seen that the velocity distribution in the forward flow of the end of the roller is essentially similar.

VARIATION OF THE PARAMETER δ_1/y_1:

Having studied the similarity of the velocity distribution at the end of the roller, the variation of the scale factor $\frac{\delta_1}{y_1}$ (δ_1 is the value of y, where $U = U_m/2$ and du/dy is negative), at the roller end with the non-dimensional longitudinal distance $\frac{x}{y_1}$ ($= \frac{L_{rj}}{y_1}$) is studied in Figure 4.11. The solid curve shown is for the classical jump as given

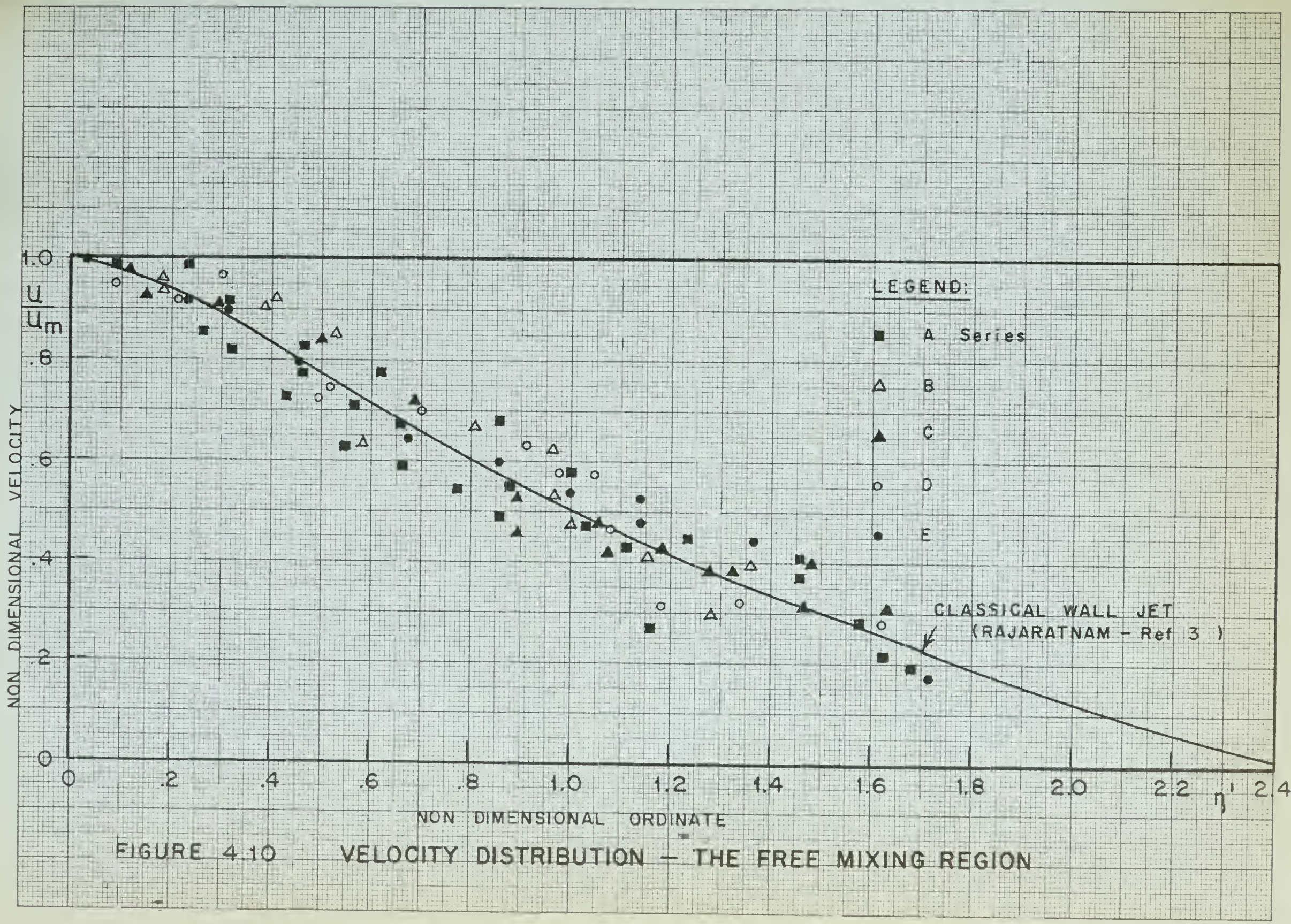

FIGURE 4.10 VELOCITY DISTRIBUTION — THE FREE MIXING REGION

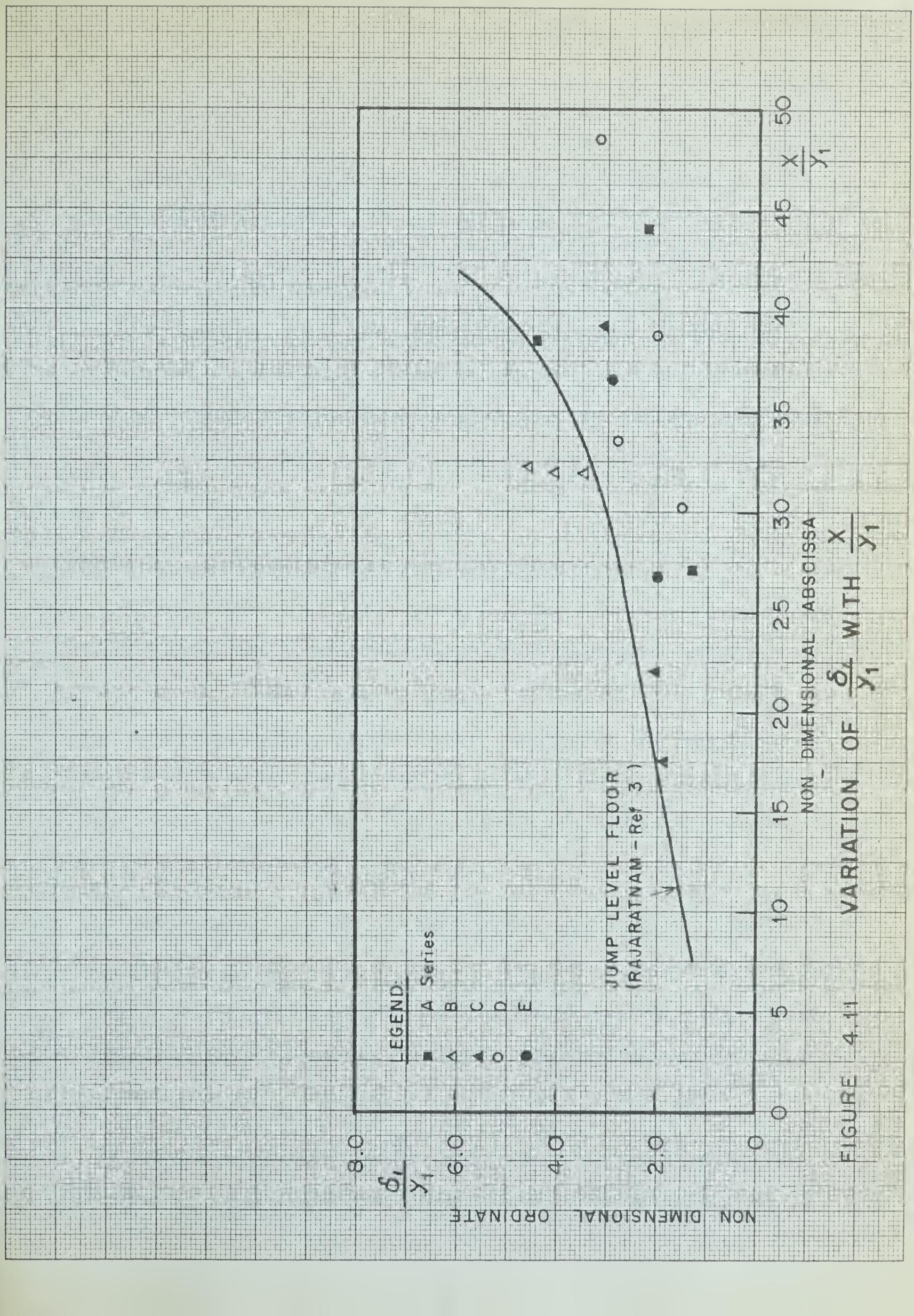

FIGURE 4.11 VARIATION OF $\frac{\delta_1}{y_1}$ WITH $\frac{X}{y_1}$

by Rajaratnam (3). The present results are at least of the same order of magnitude as those of Rajaratnam. The cause of the difference might be explained by the presence of the reverse slope.

DECAY OF THE MAXIMUM VELOCITY:

In Figure 4.12, the solid curve from Rajaratnam (3) describes the decay of the non-dimensional maximum velocity with x/y_1 for the classical jump. The present results generally agree with the classical jump curve. It is seen that the value of $\frac{U_m}{U_1}$ at the end of the roller is roughly about 0.2 to 0.4.

MOMENTUM AND ENERGY COEFFICIENTS AT THE END OF THE ROLLER:

If the end of the jump is normally taken as the end of the roller, then it is necessary to get an estimate of the Boussinesq momentum correction factor β and Coriolis' energy correction factor α' at that section. Since the velocity distribution is essentially the same as the similar profile of the classical wall jet, with some difference in the boundary layer portion only, β and α' should be roughly the same as those for the classical wall jet.

To calculate β and α' for the classical wall jet, its velocity distribution is reproduced in Figure 4.13 from Reference 28. As mentioned earlier δ_1 is the normal distance from the boundary at which the velocity U is equal to half the maximum velocity U_m, and the velocity gradient $\frac{du}{dy}$ is negative.

If $\frac{y}{\delta_1}$ is written as η and $\frac{U}{U_m}$ as $f(\eta)$, in Figure 4.13, the region where $f(\eta)$ increases from zero to unity is the boundary layer, and

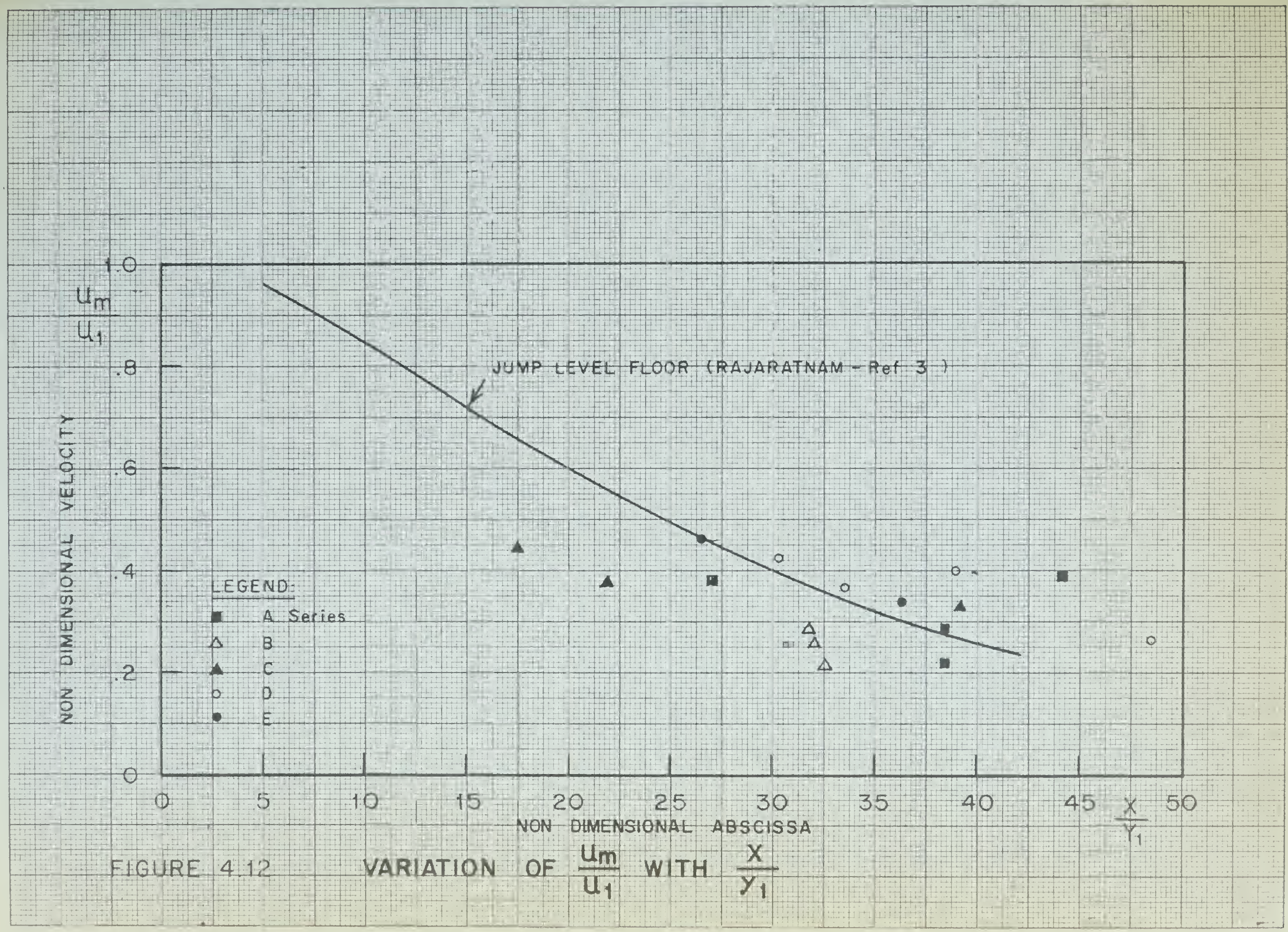

FIGURE 4.12 VARIATION OF $\frac{U_m}{U_1}$ WITH $\frac{X}{Y_1}$

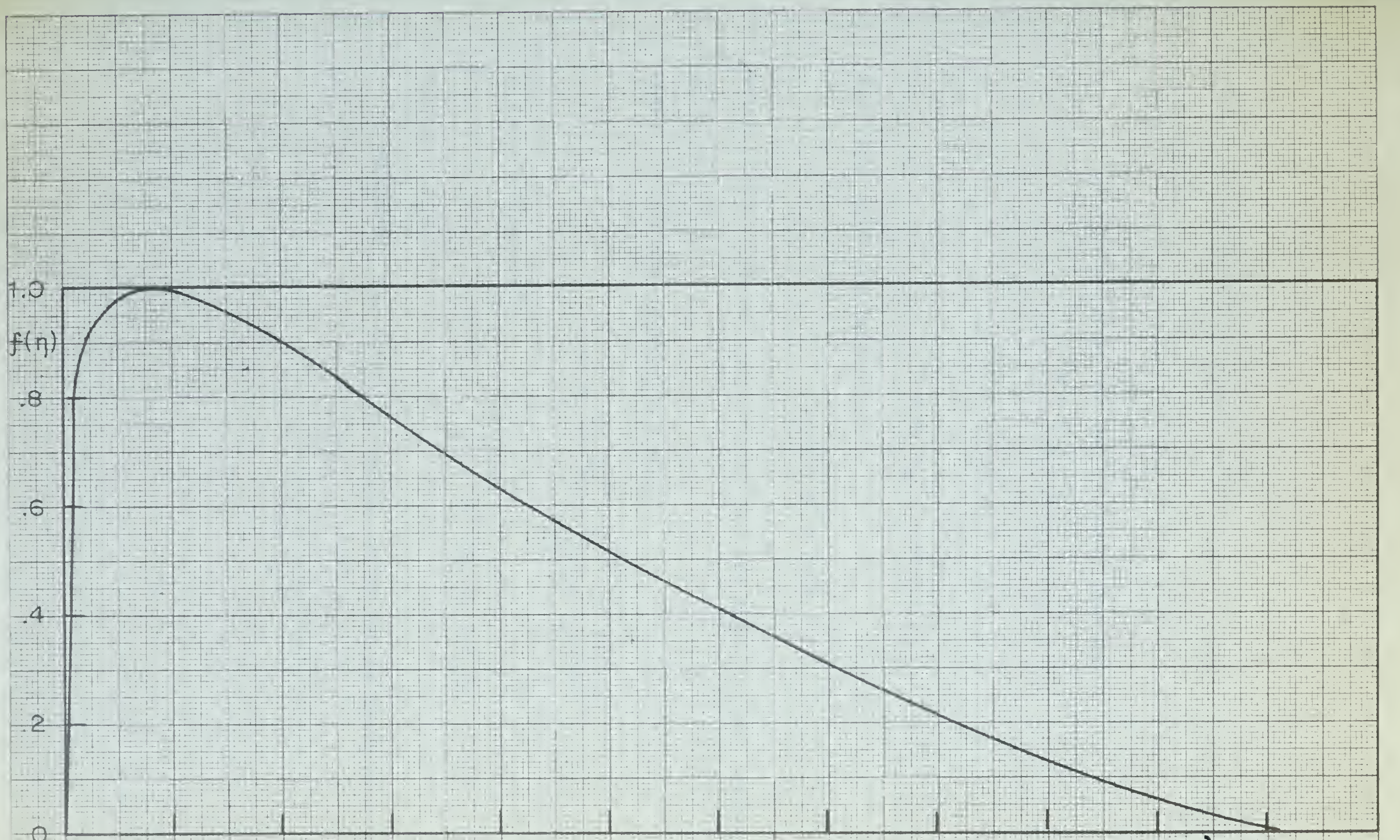

FIGURE 4.13 VELOCITY DISTRIBUTION IN THE CLASSICAL WALL JET (From Ref. 3)

the region where f (η) decreases from unity to zero is the free mixing region.

The momentum M at any section is written as:

$$M = \int \rho u \, dy.u \tag{4.01}$$

$$= \rho \int u^2 \, dy \tag{4.02}$$

$$= \rho \, \delta_1 \, U_m^2 \int_0^{2.25} f^2 (\eta) \, d\eta \tag{4.03}$$

This must equal the expression:

$$\beta \rho \, V^2 \times 2.25 \, \delta_1 \tag{4.04}$$

which is the momentum using uniform velocity distribution, corrected with coefficient β,

where V is the mean velocity of flow,

$$\beta = \frac{\delta_1 U_m^2 \int_0^{2.25} f^2 (\eta) \, d\eta}{2.25 \, V^2 \, \delta_1} \tag{4.05}$$

It can be shown that

$$\int_0^{2.25} f^2 (\eta) \, d = 0.67 \tag{4.06}$$

Hence $\beta = 1.31$ (4.07)

Similarly, the energy correction factor can be shown to be given as

$$\alpha' = \frac{U_m^3 \, \delta_1 \int_0^{2.25} f^2 (\eta) \, d\eta}{2.25 \, \delta_1 \, V^3} \tag{4.08}$$

It can be shown that

$$\int_0^{2.25} f^3(\eta)\, d\eta = 0.495 \qquad (4.09)$$

Hence $\alpha' = 2.06$

Thus it is seen that the two correction factors β and α' are much greater than unity and careful consideration should be given to this aspect in a more accurate analysis.

CHAPTER V

CONCLUSIONS AND RECOMMENDATIONS

CONCLUSIONS:

The results and conclusions of the investigation are dealt with in this chapter.

1. Theoretical analysis for A-1 jumps is developed in Chapter III for the general case as well as for small adverse slopes. The general solution for A-1 jump has been compared with the calculations of Stevens, as shown in Fig. 3.4.

2. A form of solution has been suggested for the A-2 jump.

3. It has been found that the A-1 jump is very unstable. This is in agreement with the earlier finding of Rajaratnam on a 1 on 10 adverse slope.

4. A-2 jump is stable so long as the portion of the jump up to the end of the roller is on the level apron. The moment the end of the surface roller is moved on to the adverse slope, the jump becomes unstable, and slowly moves out of the reverse slope.

5. Figure 4.3 shows the surface profile in most of the runs.

6. With the exception of the relatively flat slopes, the variation in $\frac{L_{rj}}{y_1}$ with F_1 is essentially the same as that of the classical jump.

7. The variation in $\frac{y_r}{y_1}$ with F_1 is essentially the same as that of the classical jump, with the exception of the relatively flatter slopes.

8. It has been found that the velocity distribution in the boundary layer at the end of the surface roller is somewhat similar to the case of the classical jump, and shows the effect of the adverse pressure gradient, and that it is heading towards eventual separation.

9. The velocity distribution in the free mixing region is similar and follows the curve of the classical wall jet.

10. The variation in the scale factor $\frac{\delta_1}{y_1}$ with x/y_1 is mostly the same as that of the classical hydraulic jump.

11. The decay of the maximum velocity $\frac{U_m}{U_1}$ with x/y_1 has the same trend as the curve of the classical jump.

RECOMMENDATIONS FOR FUTURE RESEARCH:

1. Further studies are suggested to investigate the reasons for the apparent instability of the jump on an adverse slope. The effect of sills and friction blocks to improve the stability could also be studied.

2. Photography, both still and motion pictures, can prove to be extremely helpful in obtaining instantaneous relationships within the jump. Refinements in techniques of ultraviolet photography, and high speed motion photography, can be valuable in any future studies involving the hydraulic jump.

3. The effects of the momentum correction factor β, and the energy correction factor α', have been neglected in the analysis of this study. However, as shown in Chapter IV, the magnitude of these factors is sufficiently large to warrant a more detailed analysis taking these factors into account.

BIBLIOGRAPHY

1. Bradley, J.N. and Peterka, A.J., (1957). "The Hydraulic Design of Stilling Basin: Hydraulic Jump on a Horizontal Apron (Basin I)"; Proceedings ASCE J. Hyd. Division (October).

2. Harleman, D.R.F., (1959). "Discussion of Turbulence Characteristics of the Hydraulic Jump by Rouse, H., Siao, T.T. and Nargaratnam, S", Trans ASCE.

3. Rajaratnam, N., (1965). "The Hydraulic Jump as a Plane Turbulent Wall Jet Under Adverse Pressure Gradient", Proc. ASCE; J. Hyd. Division.(September).

4. Safranez, K., (1929). "Research Relating to the Hydraulic Jump" Bauinginiur, Heft 37 and 38; translated by D.P. Barnes, USBR, Denver, 1934.

5. Rouse, H; Siao, T.T. and Nagaratnam, S., (1959). "Turbulence Characteristics of the Hydraulics Jump", Trans. ASCE.

6. Elevatorski, E.A., (1959). "Hydraulic Energy Dissipators", McGraw-Hill Book Company Inc., p-68.

7. Rajaratnam, N., (1962). "Air Entrainment Characteristics of the Hydraulic Jump", J. of the Institution of Engineers, India, (March).

8. Chow, V.T., (1959). "Open Channel Hydraulics". McGraw-Hill Book Company Inc., N.Y. P. 425.

9. Beebe, J.C., and Riegel, R.M., (1917). "The Hydraulic Jump as a Means of Dissipating Energy". Miami Conservancy District, Technical Report, Part III.

10. Ellms, R.W., (1927-28). "Computation of the Tail Water Depth of the Hydraulic Jump in Sloping Flumes". Trans ASME, Paper HYD 50-5.

11. Ellms, R.W. (1932). "Hydraulic Jump in Sloping and Horizontal Flumes". Trans. ASME, Vol. 54, Paper HYD 54-6.

12. Rindlaub, B.D., (1935). "The Hydraulic Jump in Sloping Channels", MS. Thesis, University of California.

13. Bakhemeteff, B.A. and Matzke, A.E., (1938). "The Hydraulic Jump in Sloped Channels", Trans ASME, HYD-60.

14. Kindsvater, C.E., (1944). "The Hydraulic Jump in Sloping Channels", Trans ASCE.

15. Hickox, G.H., (1944). Discussion of Ref. 14, Trans ASCE.

16. Dutta, D.N., (1949). "Curves for the Determination of the Variables of the Hydraulic Jump in Sloping Channels", M.S. Thesis, University of Colorado.

17. Bradley, J.N. and Peterka, A.J., (1957). "Hydraulic Design of Stilling Basins; Stilling Basin with Sloping Apron (Basin V);" Proc. ASCE, J. Hyd. Division, (October).

18. Flores De Mello, J.O., (1954). "Le Ressaut", La Houille Blanche, pp. 811-822, No. 6, (December).

19. Wigham, J.M., (1958). "An Experimental Study of the Fluid Pressures Exerted on Spillway Floors", M.Sc. Thesis, University of Alberta, Edmonton, Alberta.

20. Lin, K. and Priest, M.S., (1958). "The Hydraulic Jump over an Inclined Bottom". Bull No. 30, (April); Engrg. Expt. Stn., Alabama Ploytechnic Institute, Auburn, Alabama.

21. Argyropoulos, P.A., (1957). "Theoretical and Experimental Analysis of the Hydraulic Jump in a Sloping Parabolic Flume", Proc. I.A.H.R., Vol. II.

22. Argyropoulos, P.A., (1961). "The Hydraulic Jump and the Effect of Turbulence on Hydraulic Structures; Contribution to the Research of the Phenomenon", Proc. I.A.H.R.

23. Argyropoulos, P.A., (1962). "General Solution of the Hydraulic Jump in Sloping Channels", Proc. ASCE. J. Hyd. Division, (July).

24. Rajaratnam, N., (1965). "The Hydraulic Jump in Sloping Channels", J., C.B.I. and P., New Delhi, (October).

25. Kennison, K.R., (1944). Discussion of Ref. 14, Trans, ASCE.

26. Chow, V.T., (1959). "Open Channel Hydraulics", McGraw-Hill Book Company Inc., N.Y. p.-426.

27. Stevens, J.C., (1944). Discussion of Ref. 14, Trans ASCE.

28. Rajaratnam, N., (1965). "On the Submerged Hydraulic Jump as a Wall Jet", Proc. ASCE, J. Hyd. Division, (July).

APPENDIX A

SURFACE PROFILE RECORDINGS

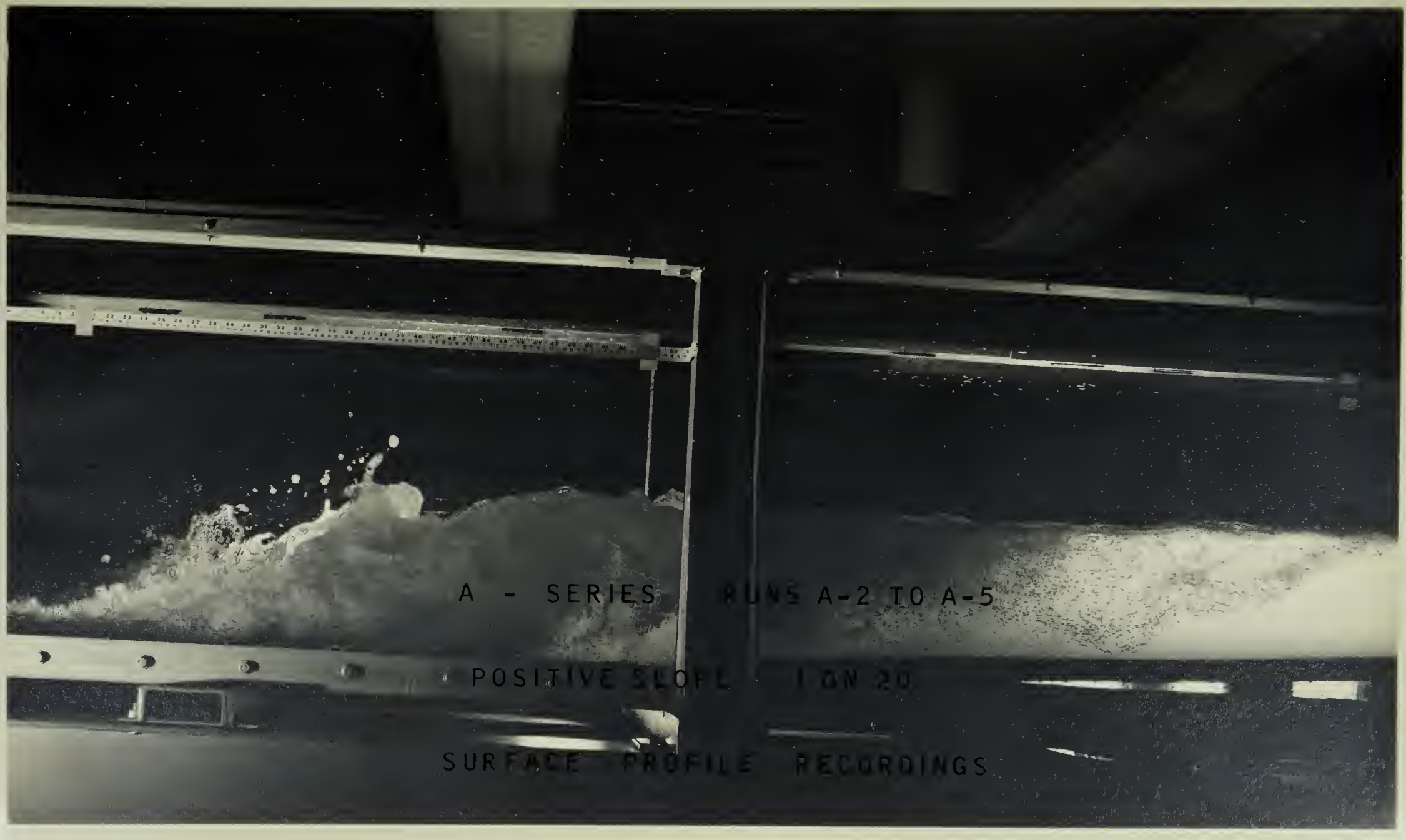
A - SERIES RUNS A-2 TO A-5
POSITIVE SLOPE 1 ON 20
SURFACE PROFILE RECORDINGS

A 2

A 3

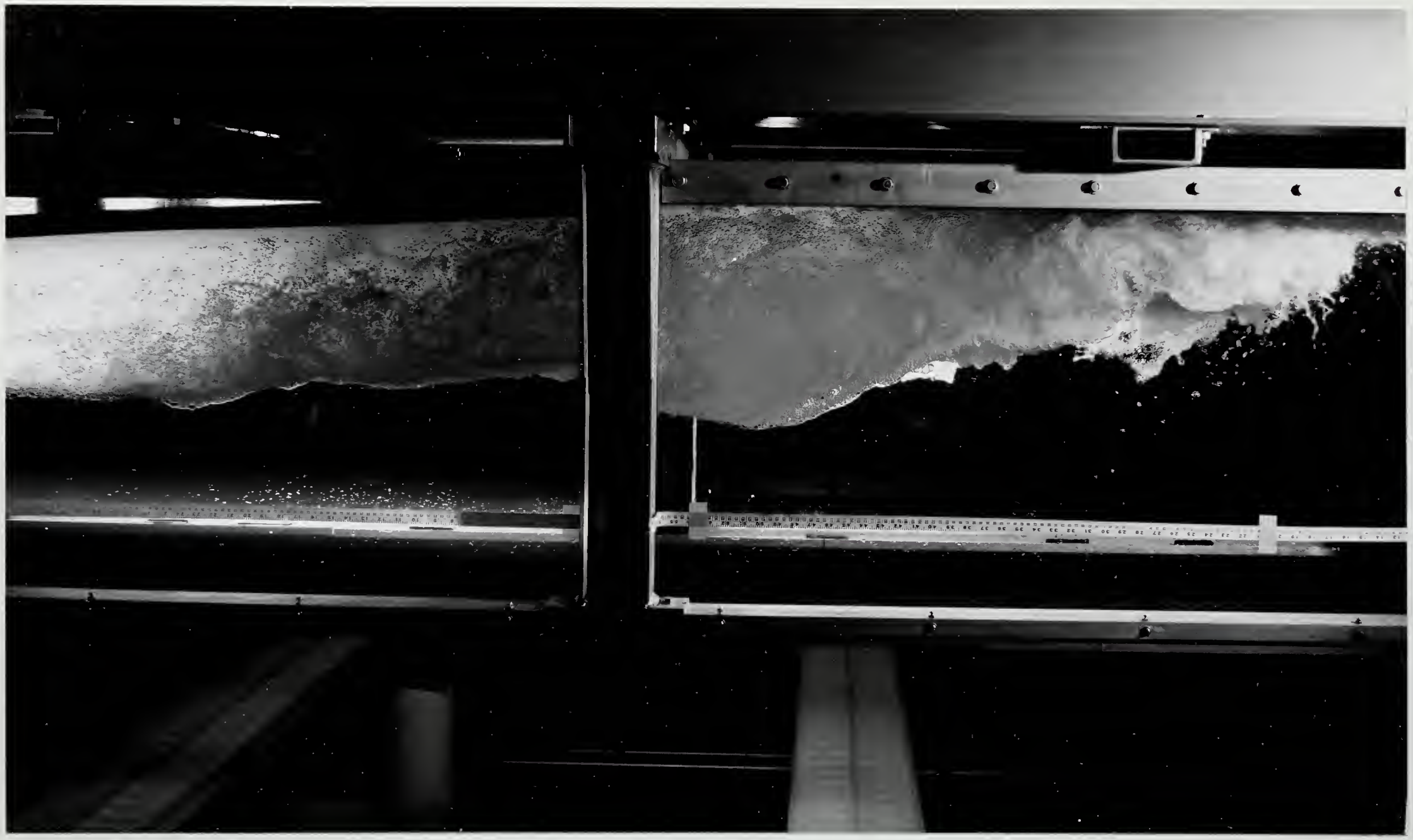

A 4

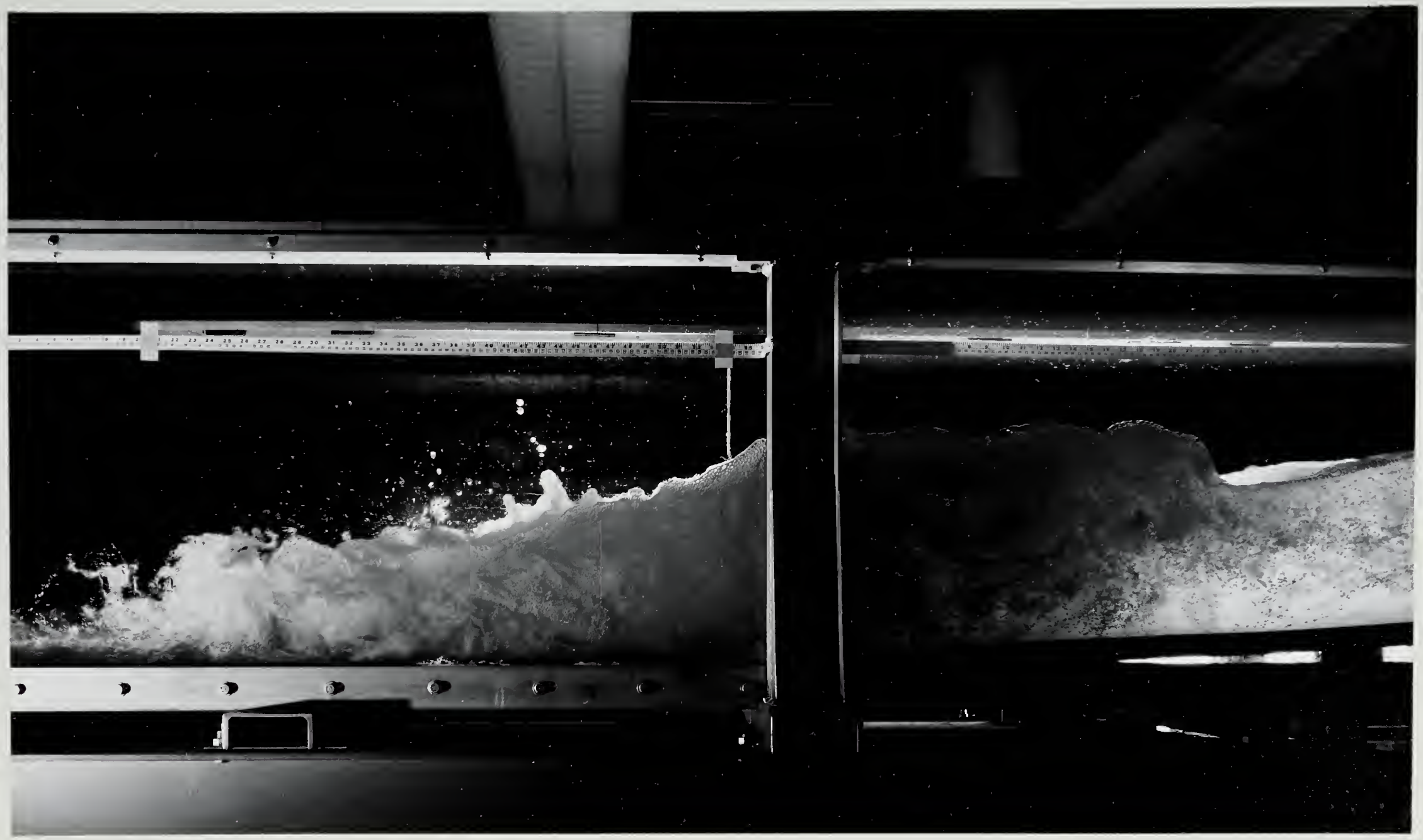

A 5

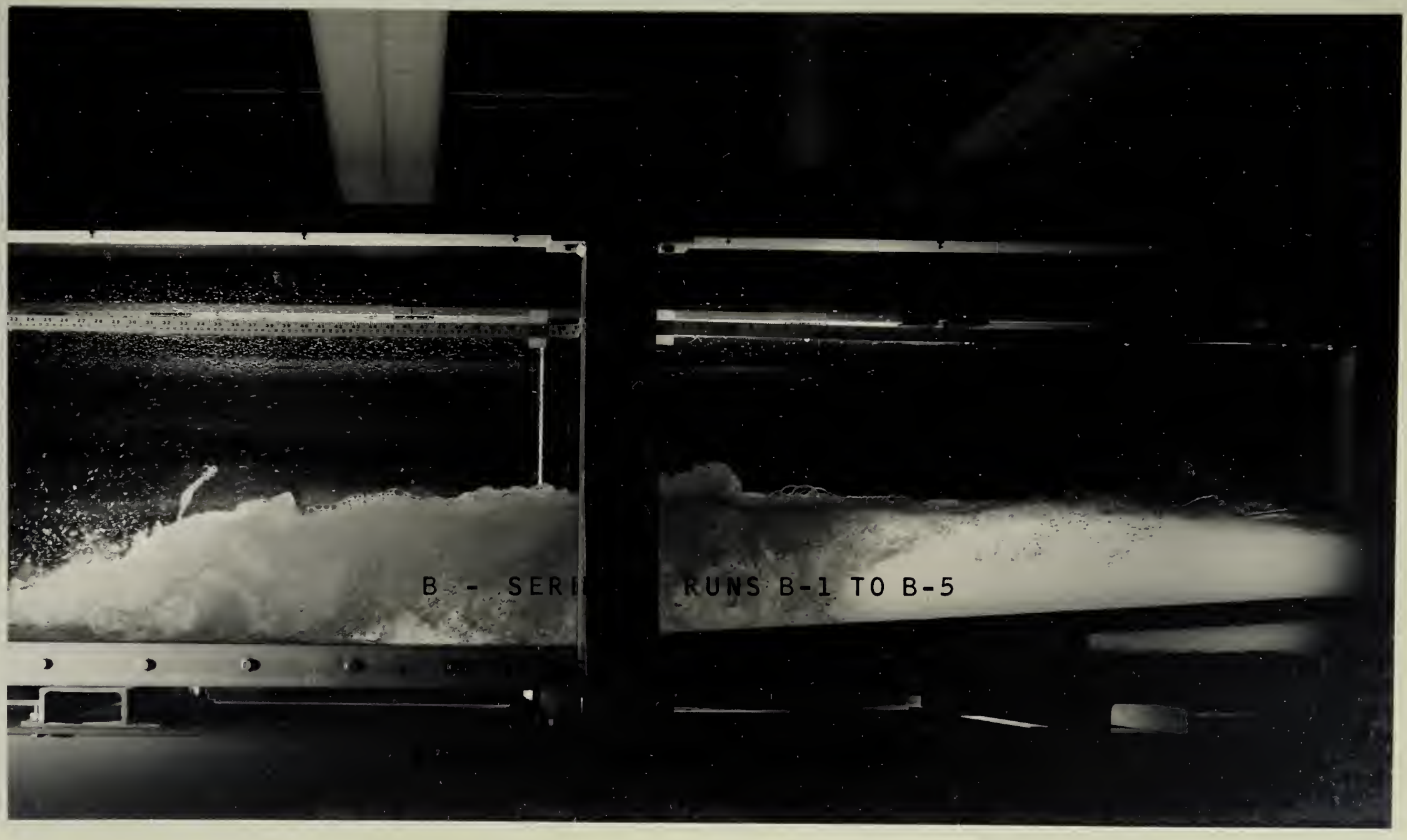

B 1

81

B 2

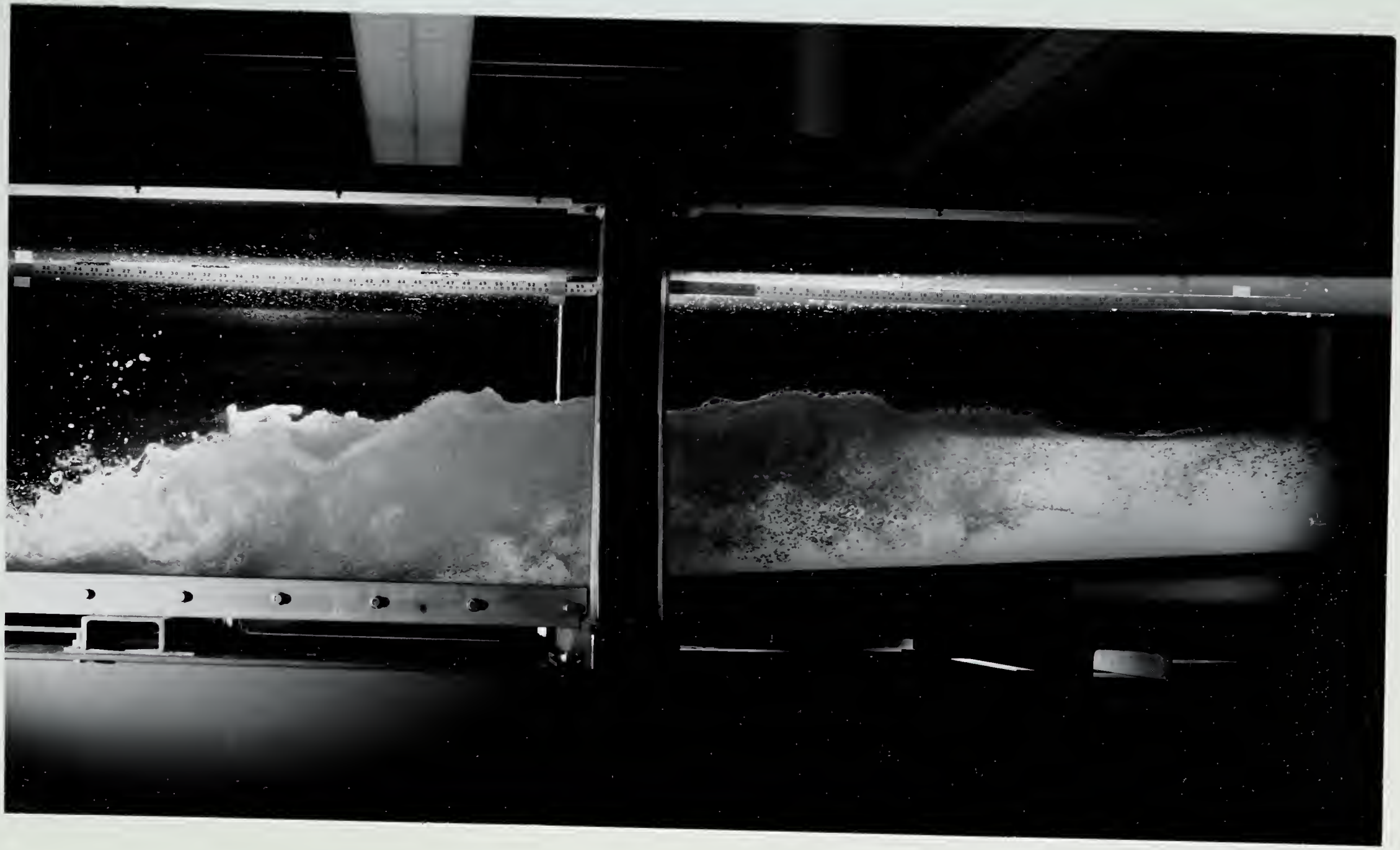

B 3

B 4

B 5

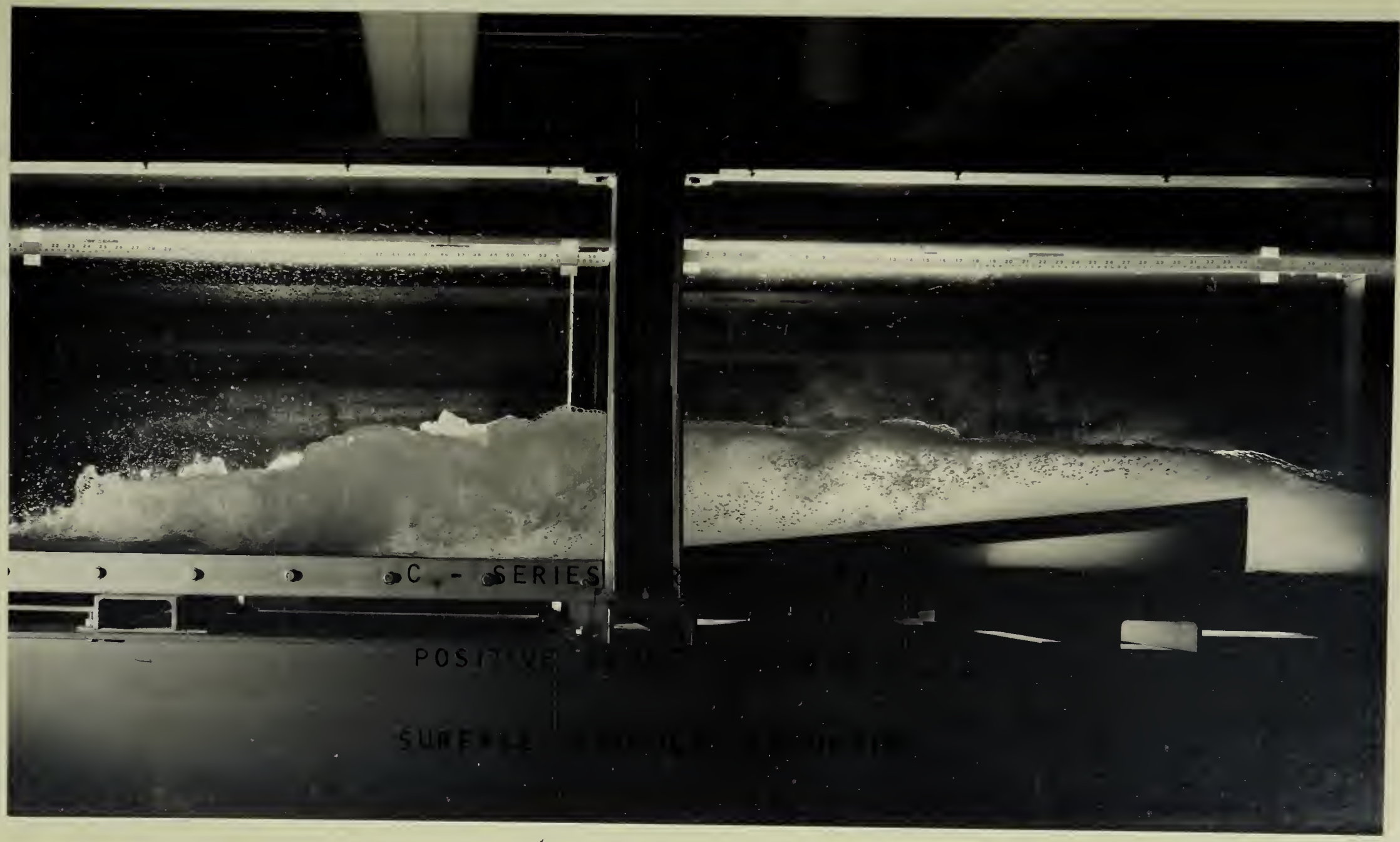

C 1

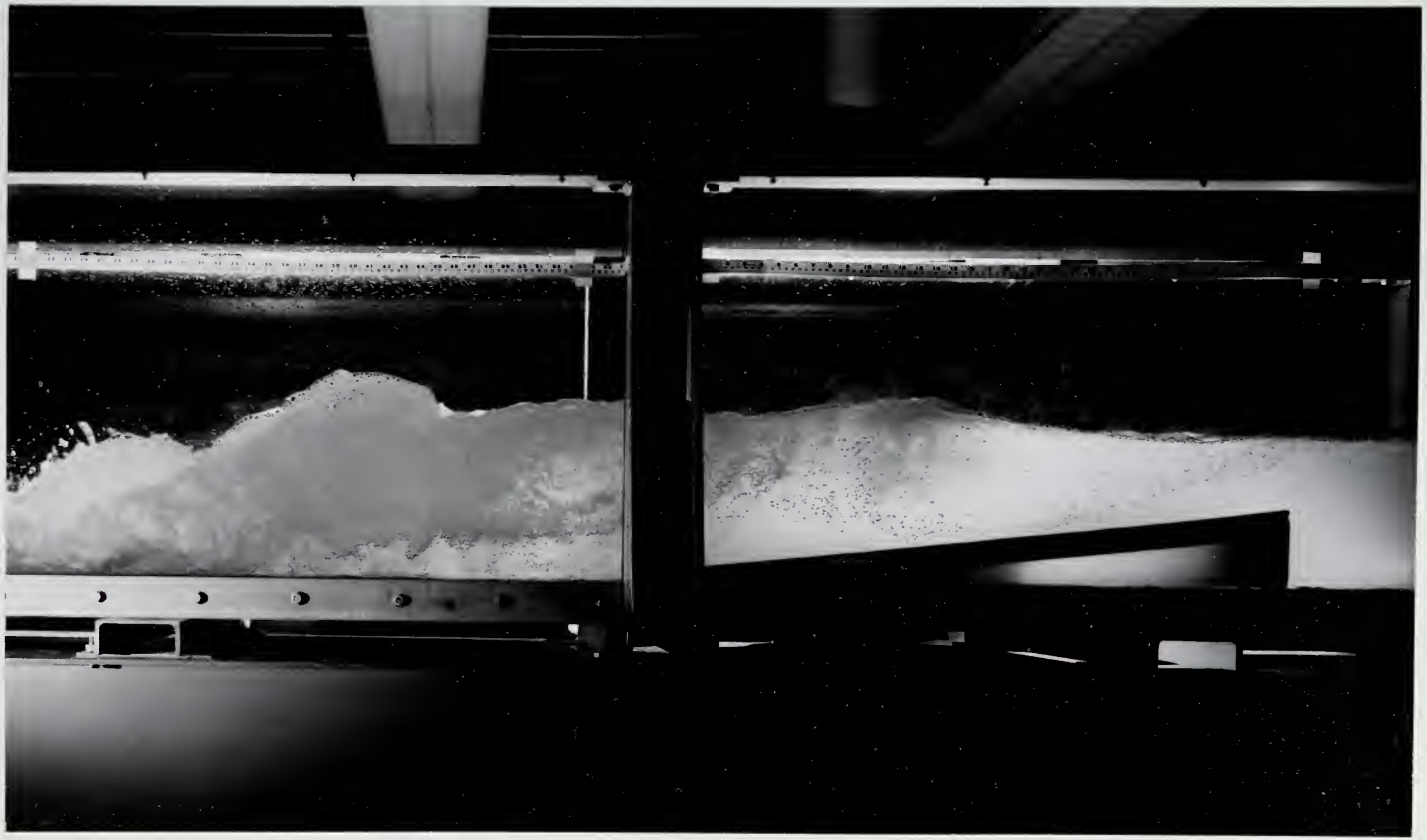

C 2

C 3

C 4

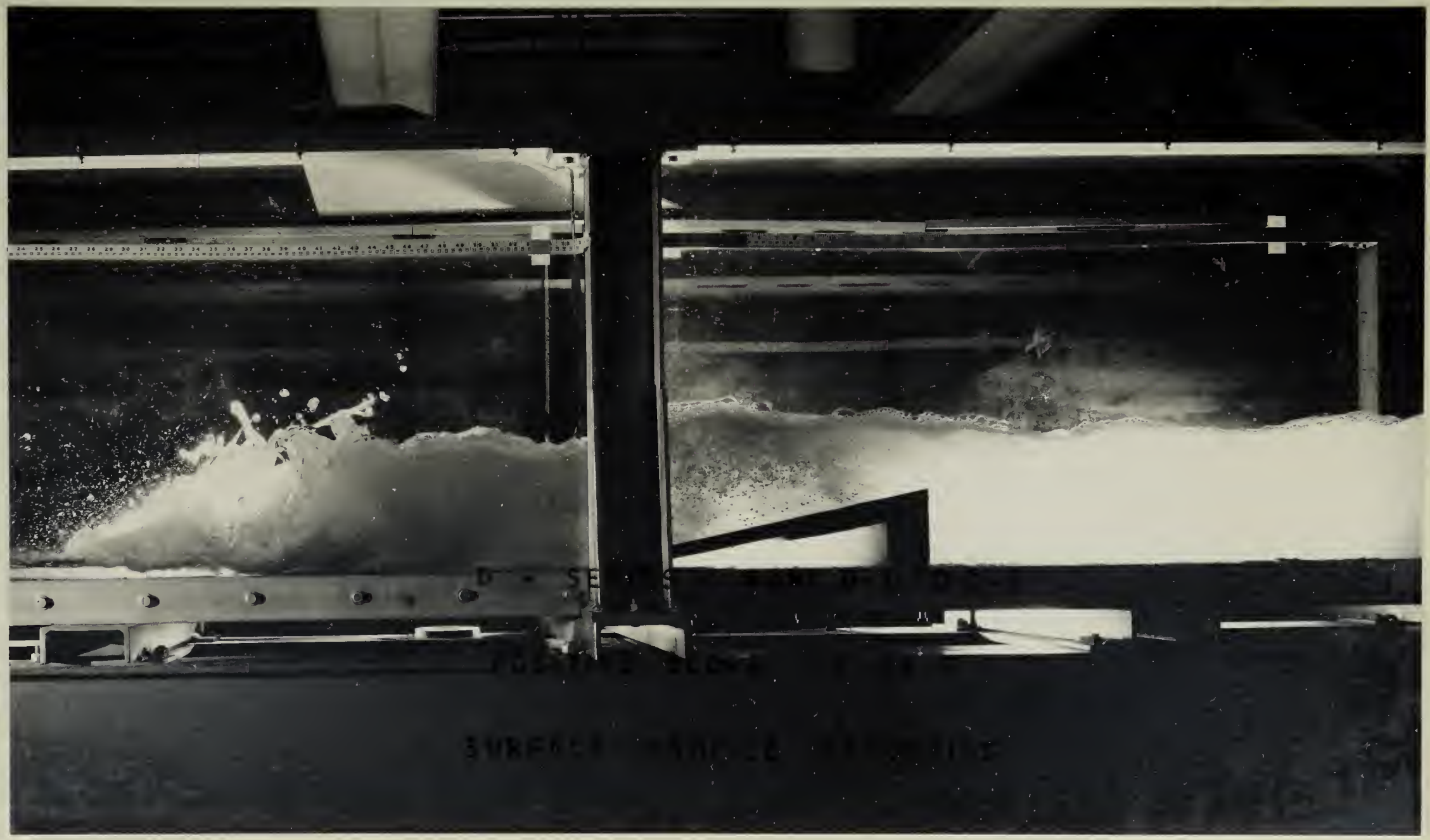

D 1

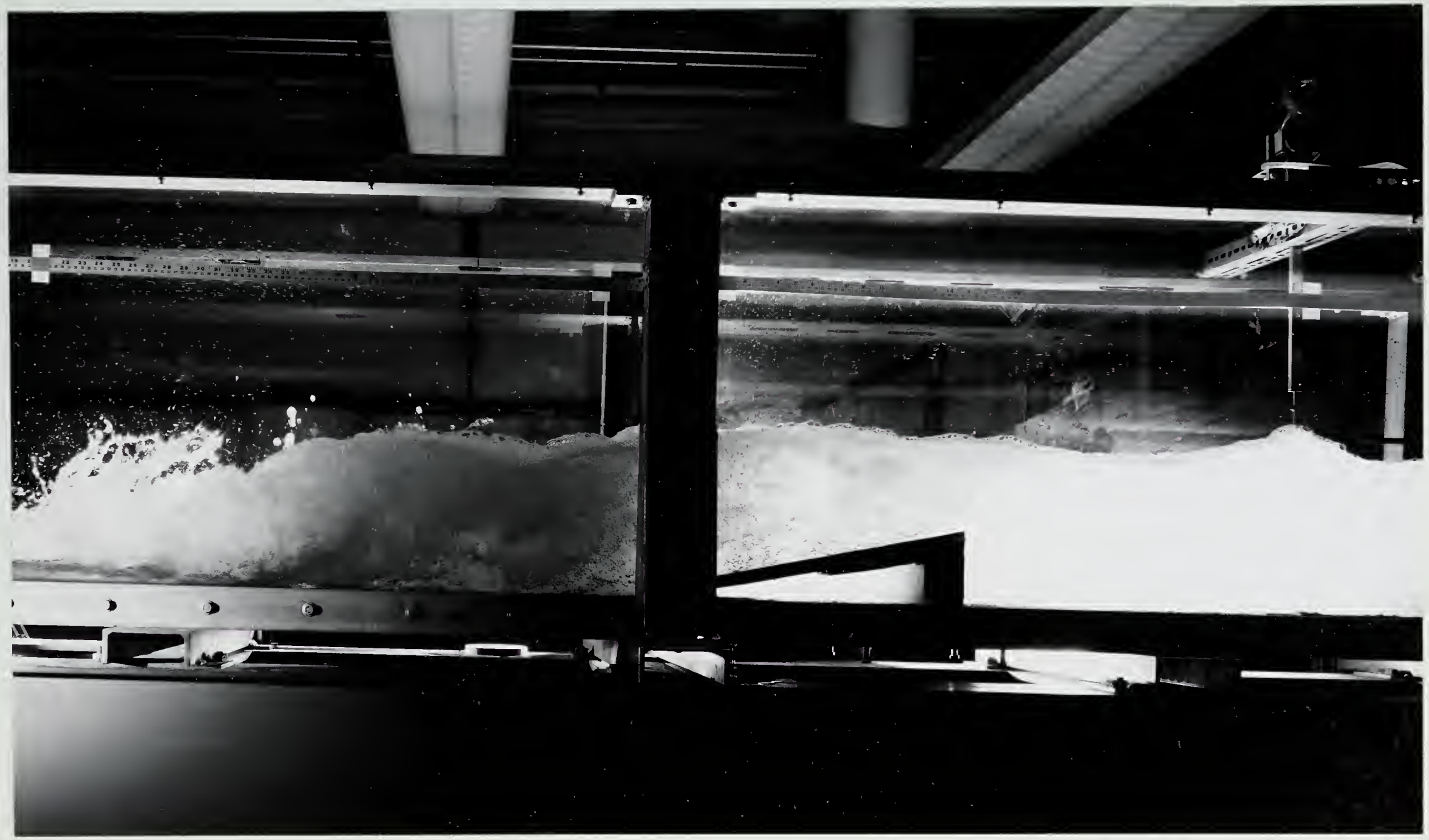

D 2

D 3

D 4

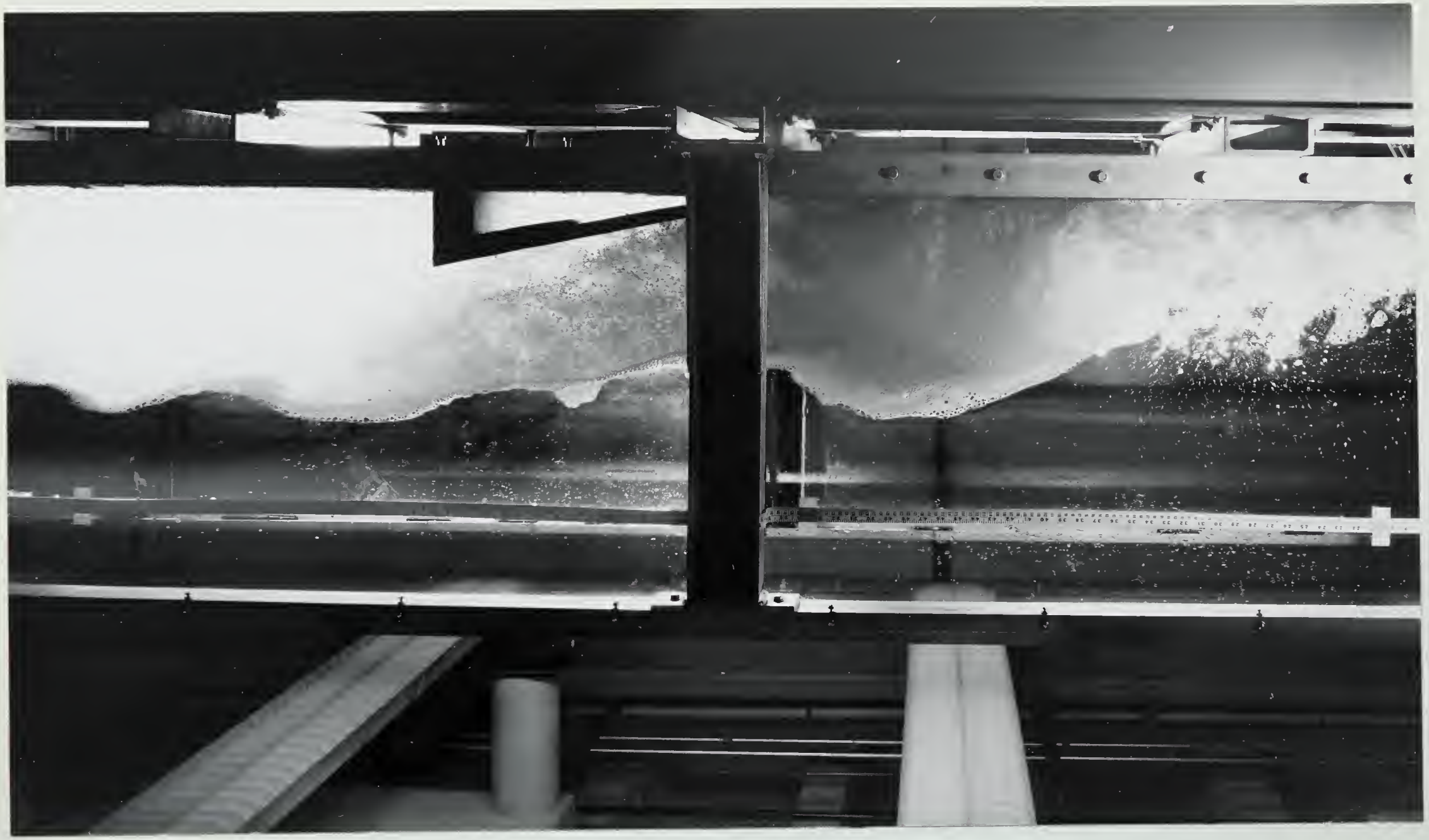

D 5

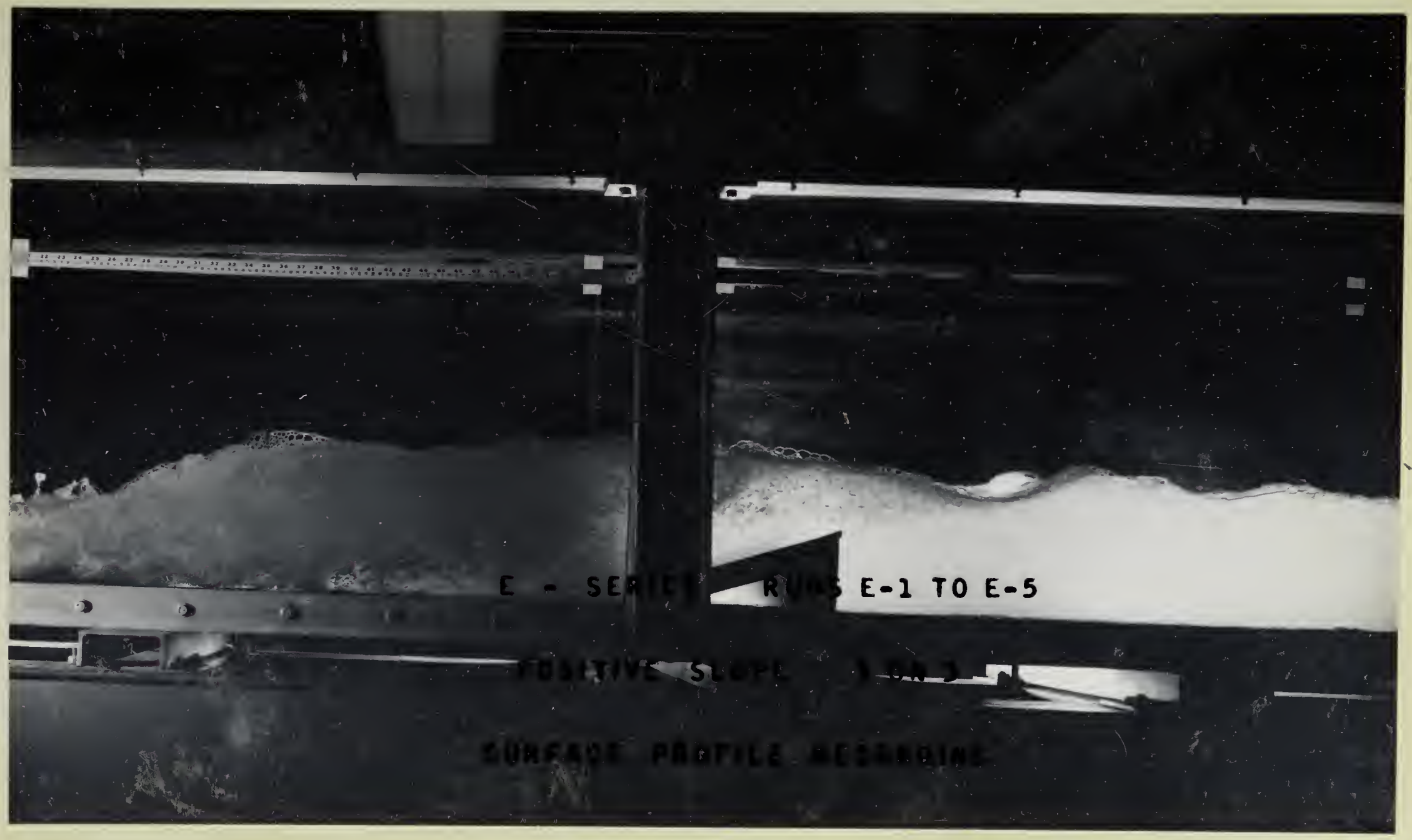
E - SERIES RUNS E-1 TO E-5
POSITIVE SLOPE
SURFACE PROFILE RECORDING

E 1

E 2

E 4

97

APPENDIX B

VELOCITY DISTRIBUTION PLOTS

(At The Roller End)

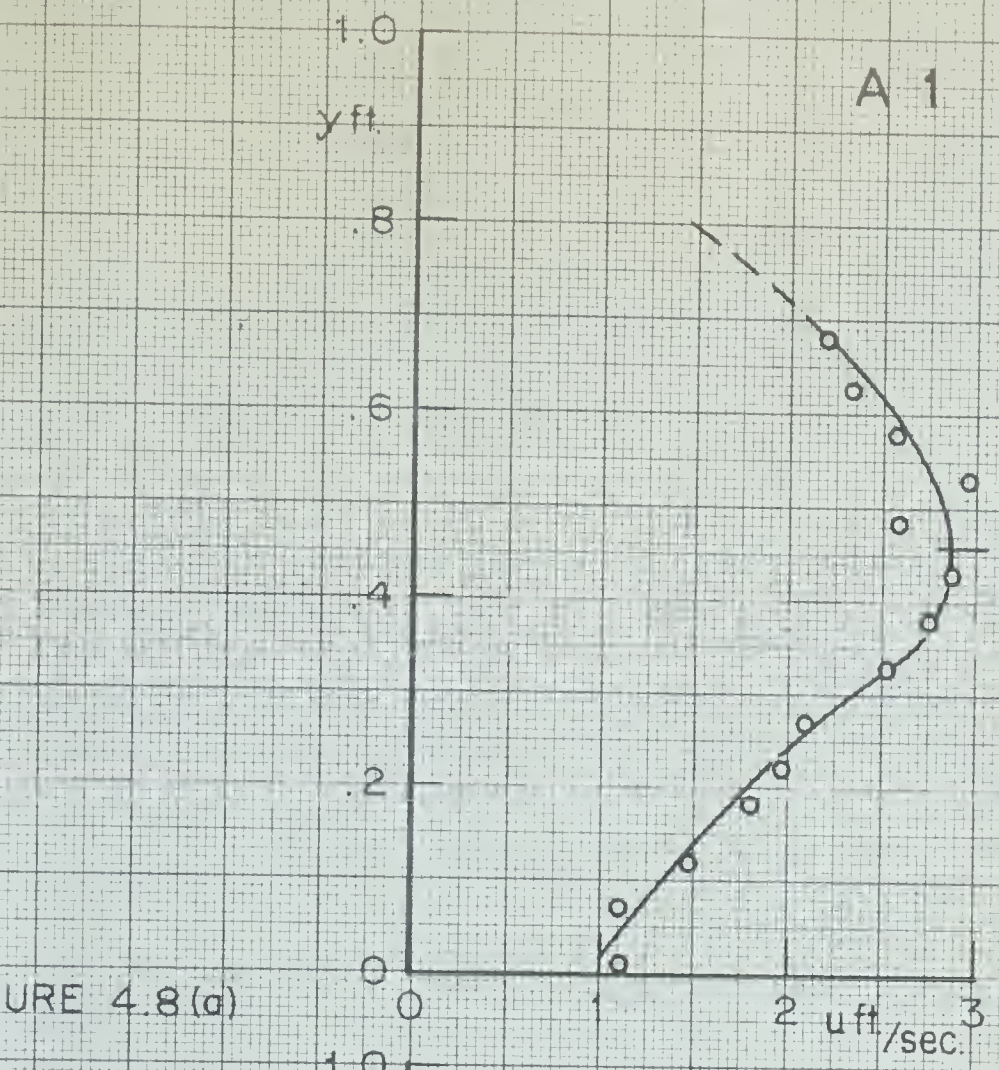

FIGURE 4.8(a)

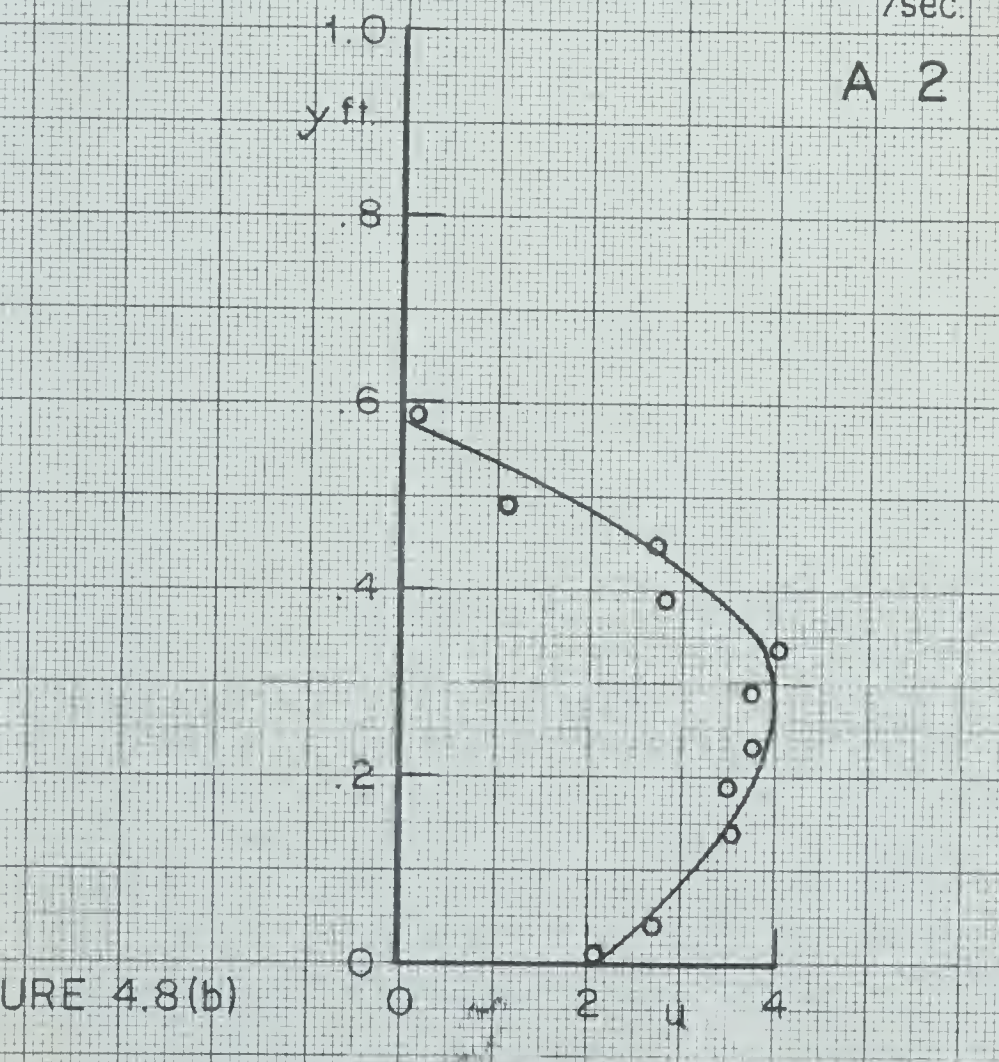

FIGURE 4.8(b)

VELOCITY DISTRIBUTION PLOTS

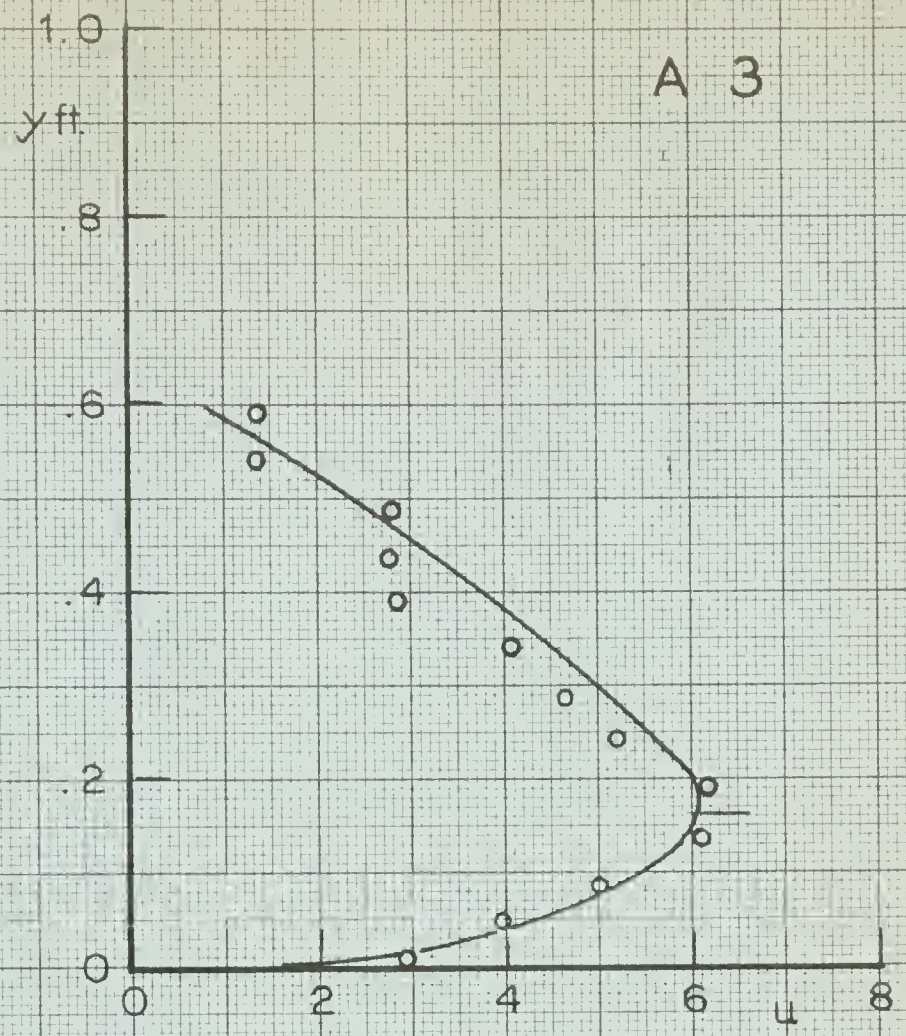

FIGURE 4.8(c)

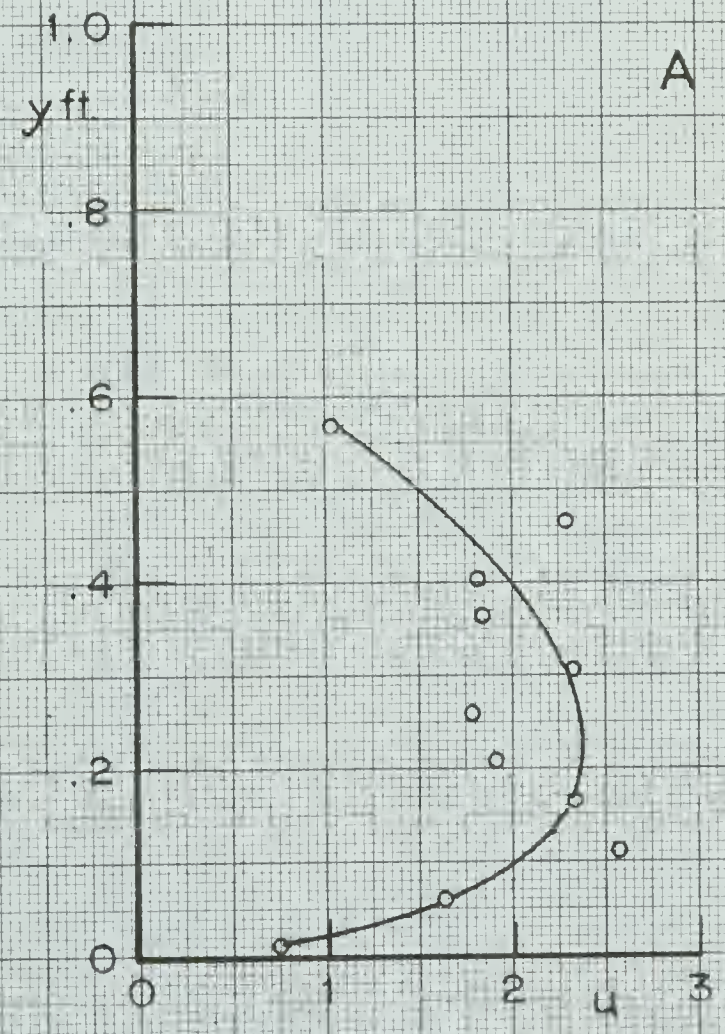

FIGURE 4.8(d)

VELOCITY DISTRIBUTION PLOTS

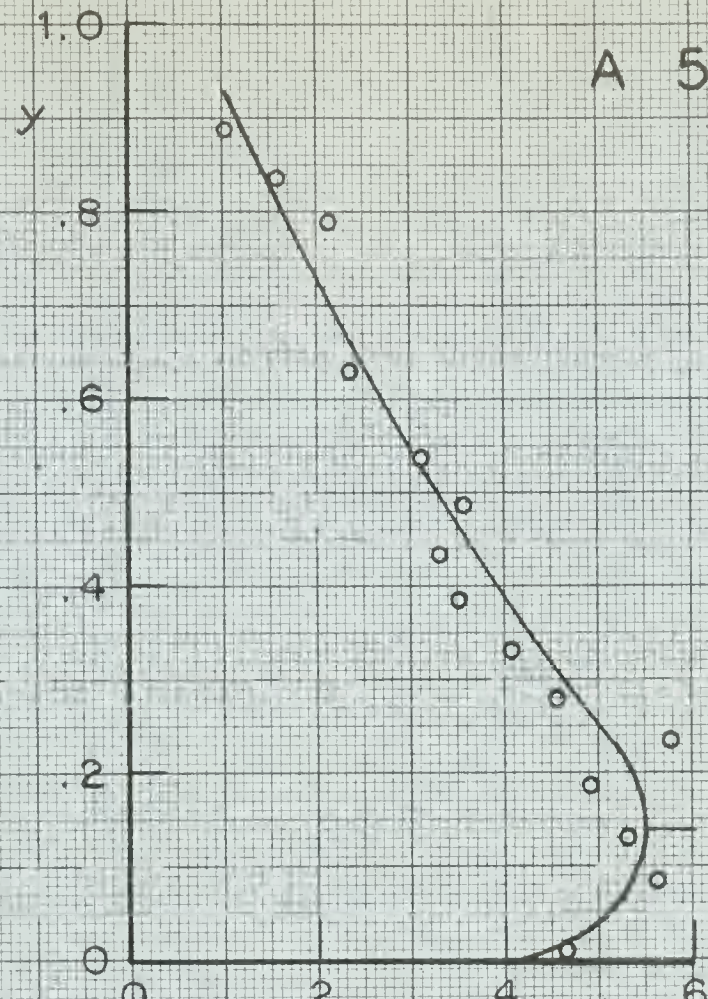

FIGURE 4.8 (e)

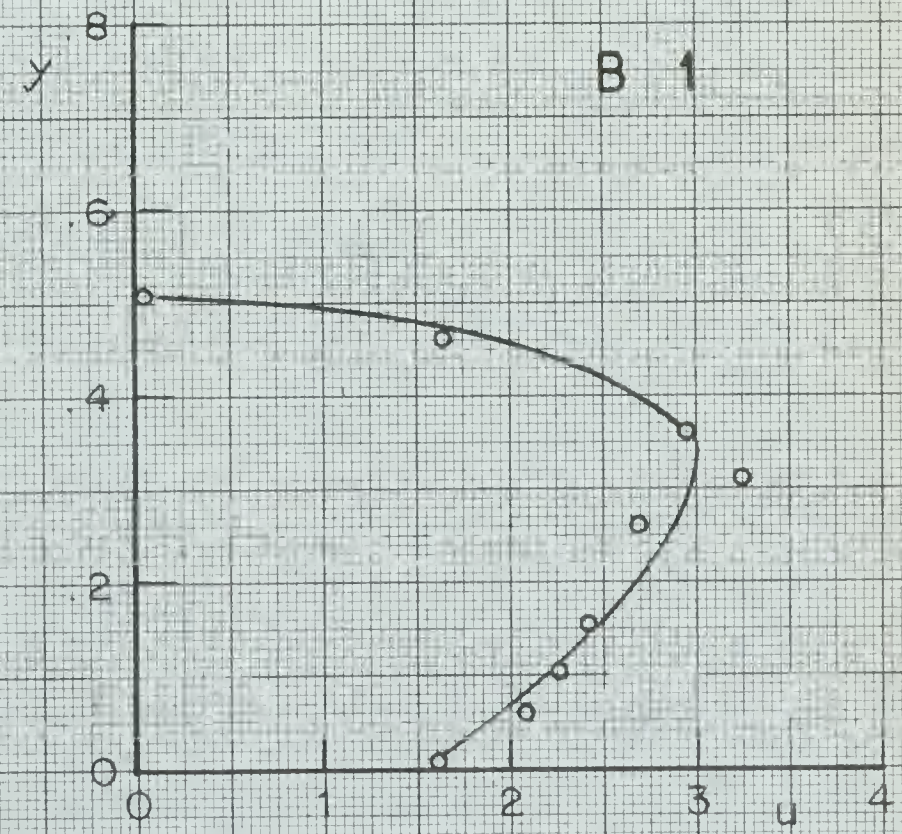

FIGURE 4.8 (f)

VELOCITY DISTRIBUTION PLOTS

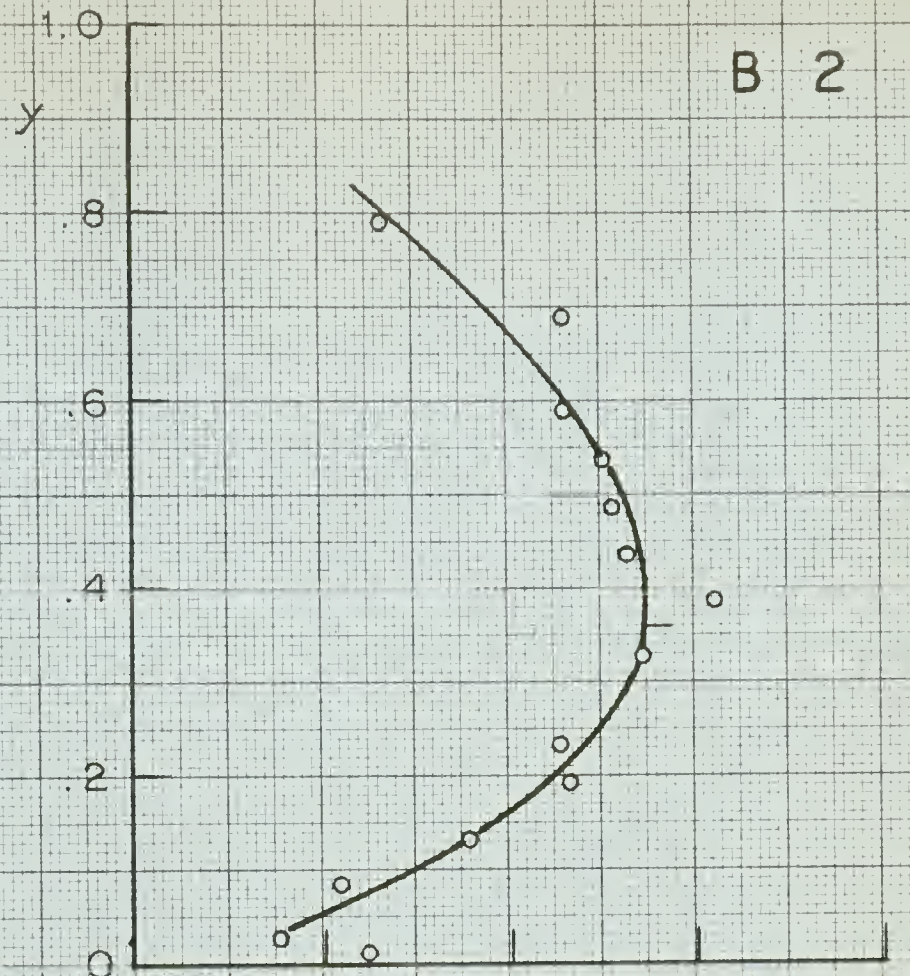

FIGURE 4.8(g)

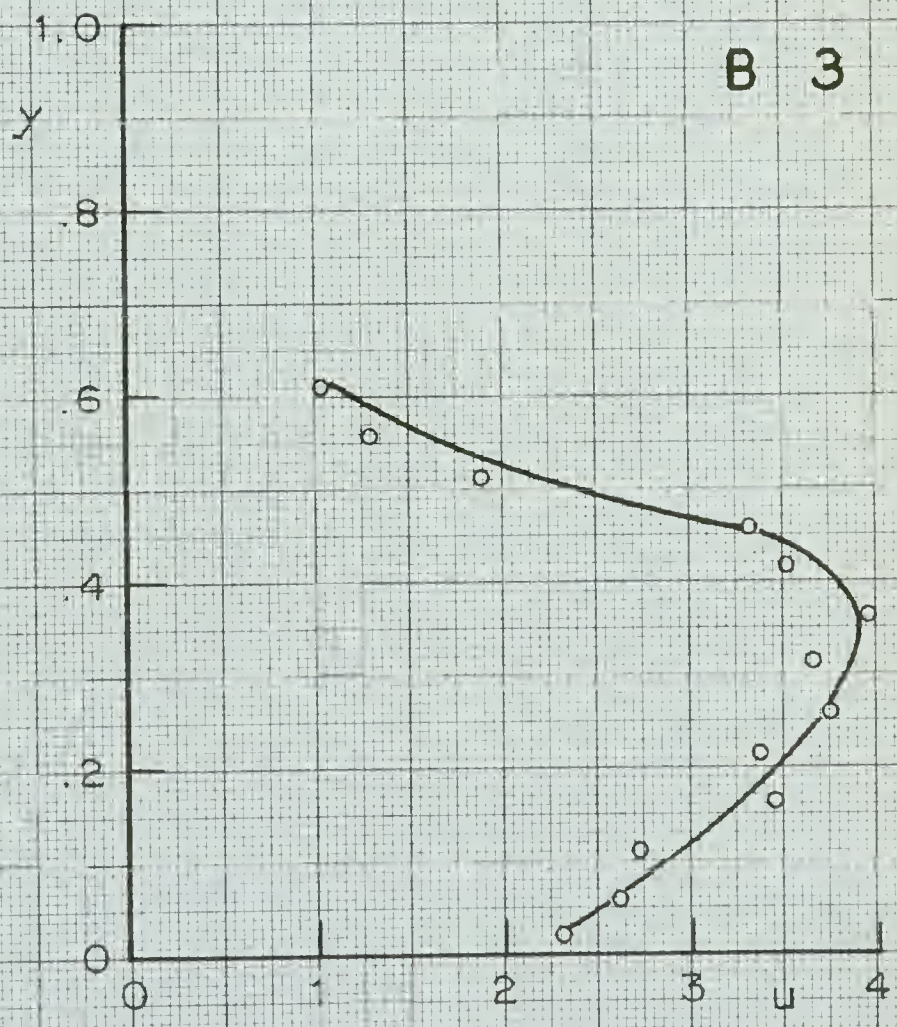

FIGURE 4.8(h)

VELOCITY DISTRIBUTION PLOTS

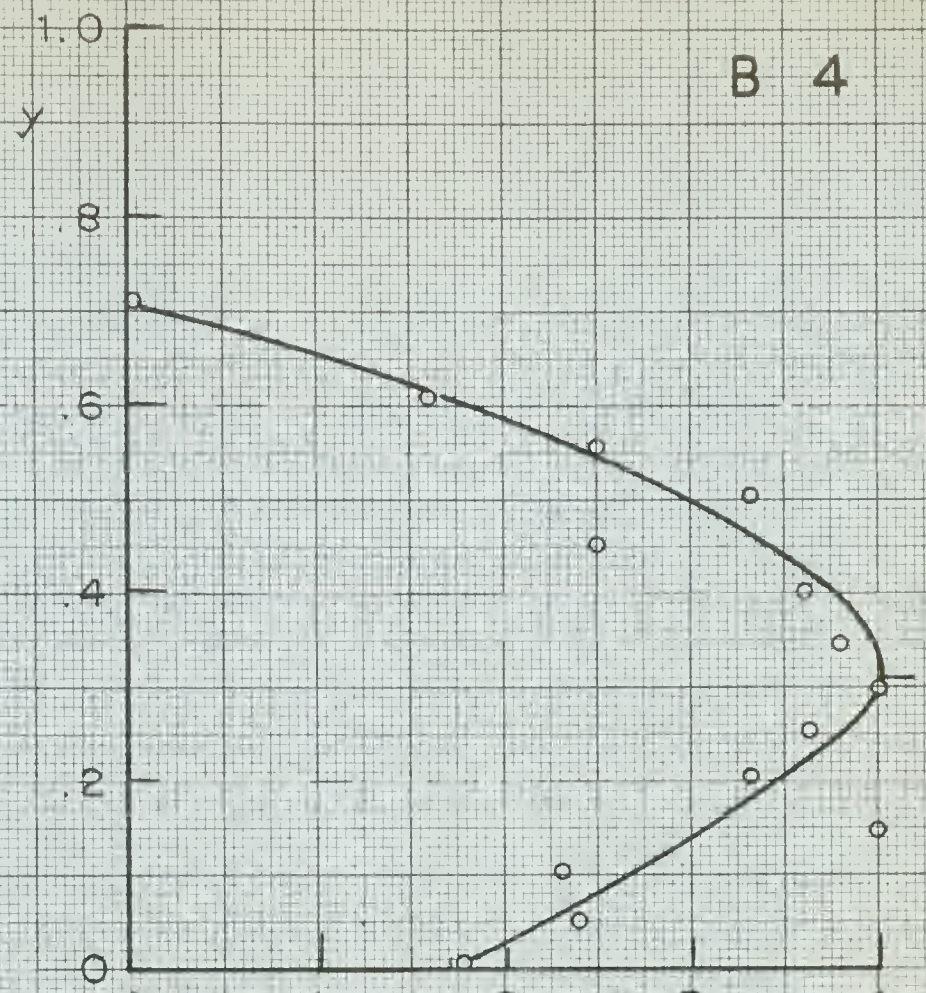

FIGURE 4.8(j)

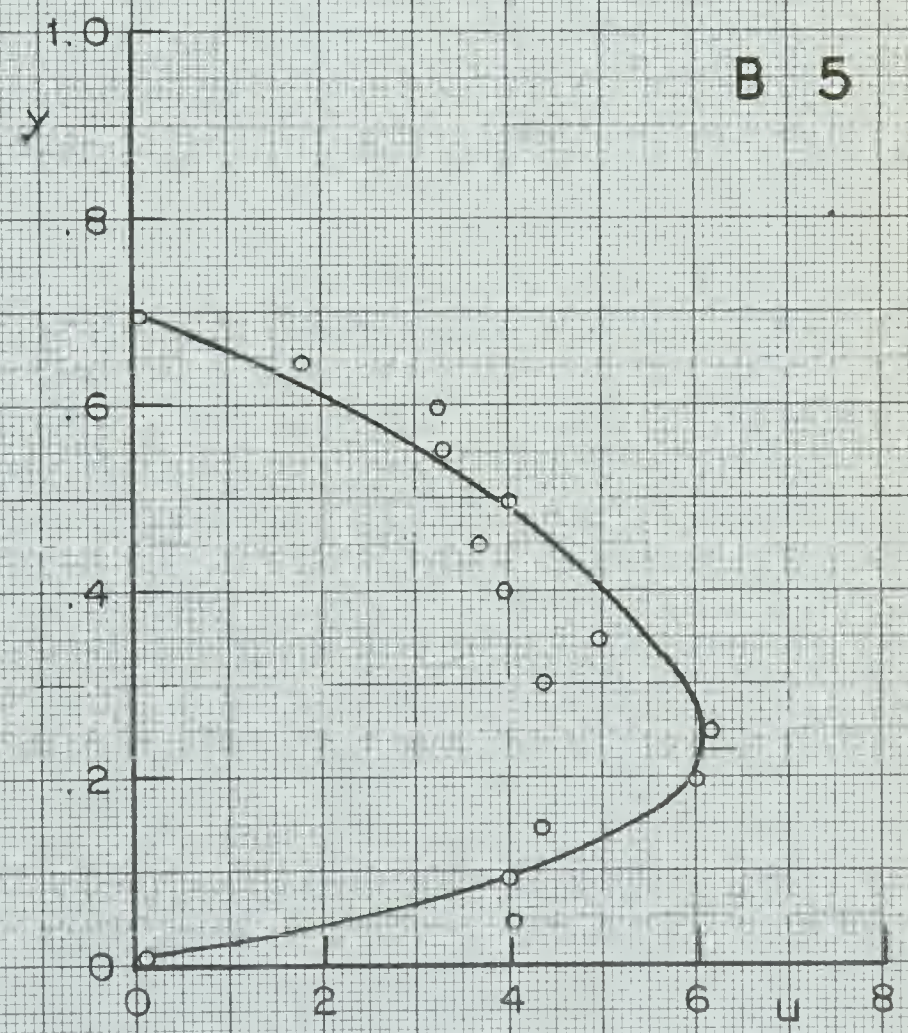

FIGURE 4.8(k)

VELOCITY DISTRIBUTION PLOTS

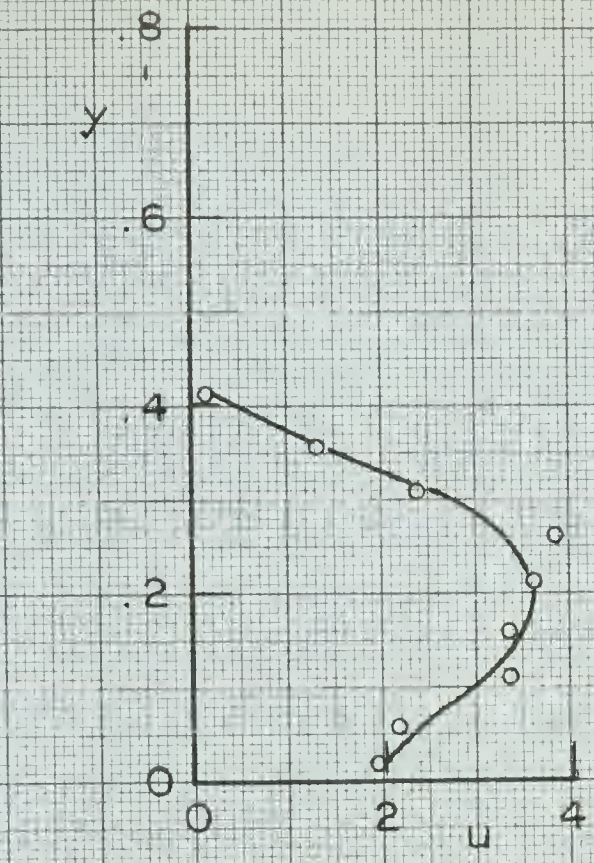

FIGURE 4.8 (l)

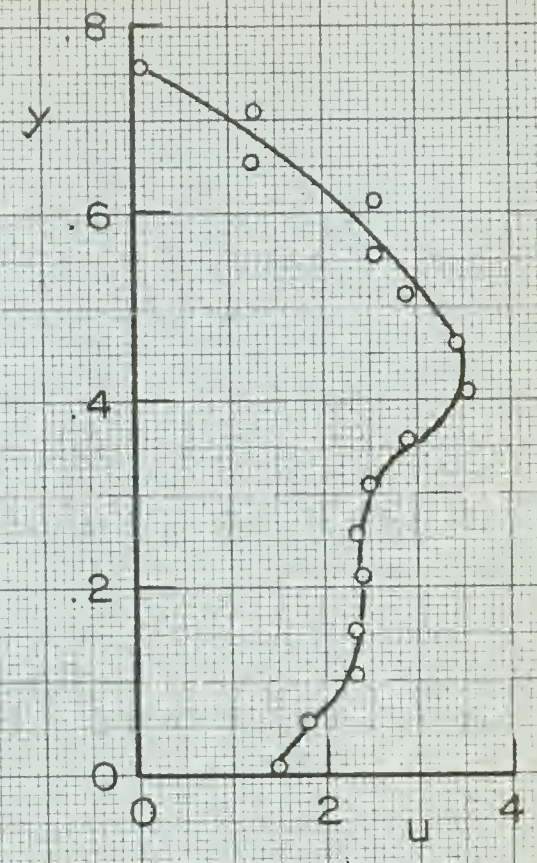

FIGURE 4.8 (m)

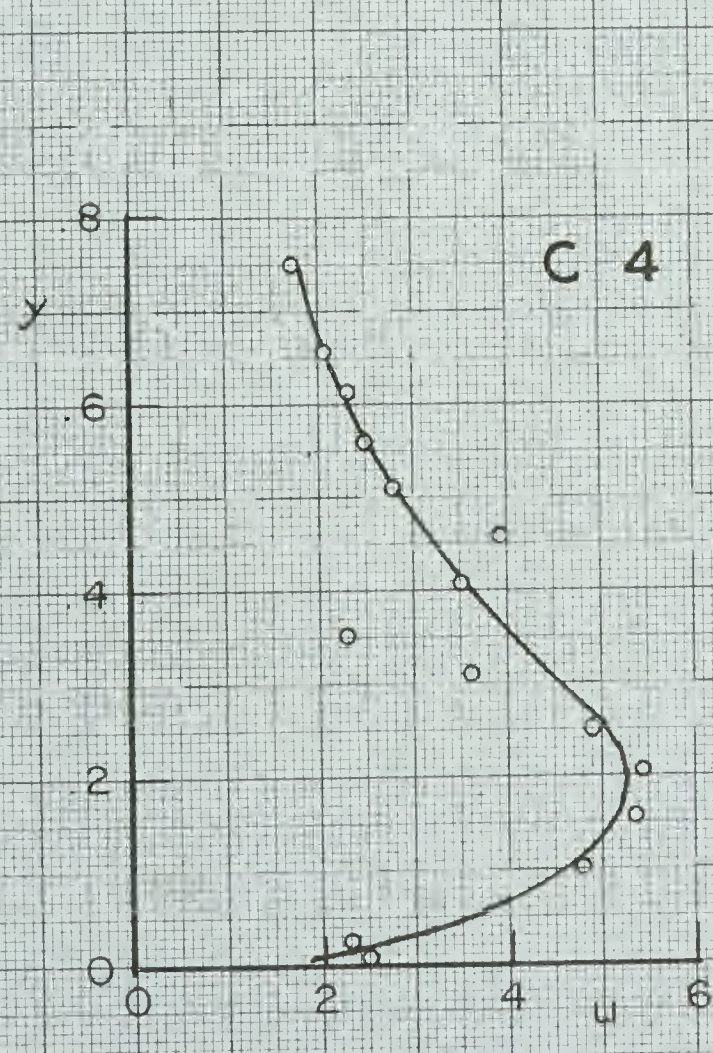

FIGURE 4.8 (n)

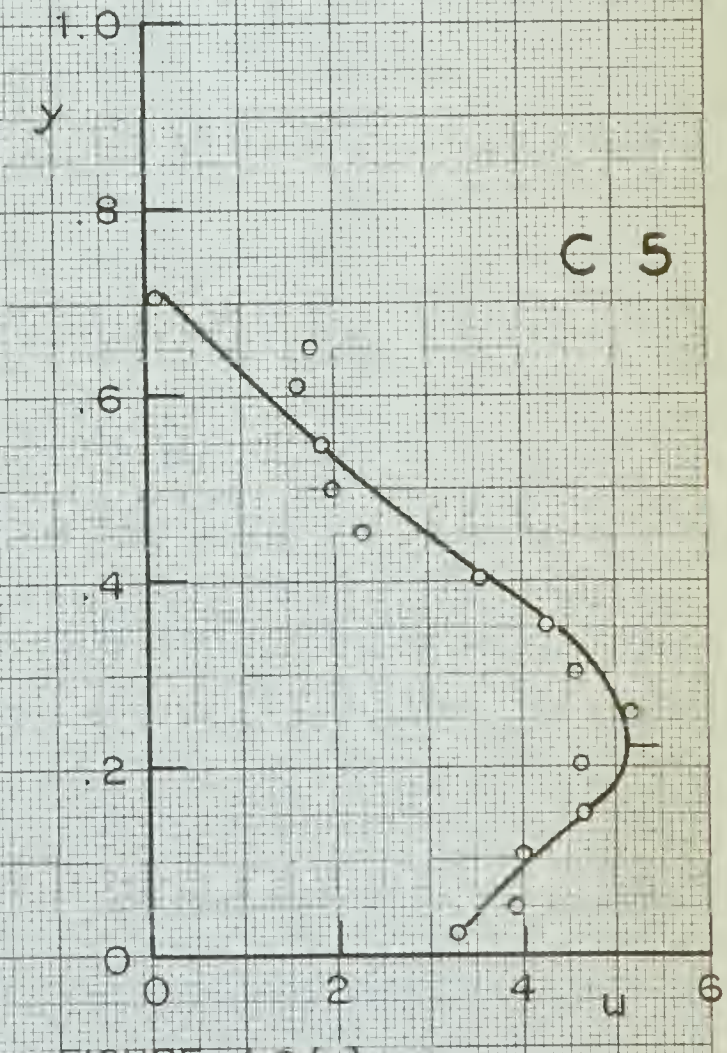

FIGURE 4.8 (o)

VELOCITY DISTRIBUTION PLOTS

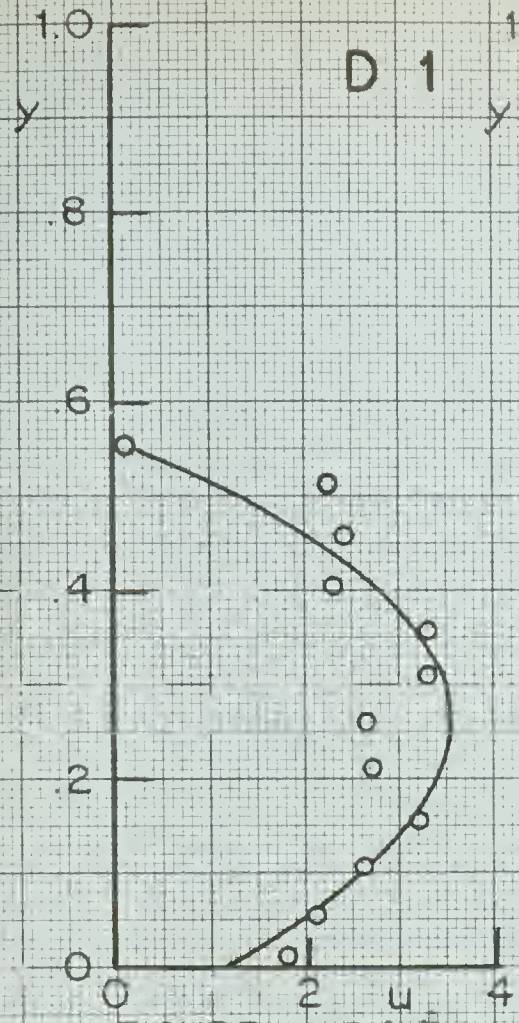

FIGURE 4.8 (p)

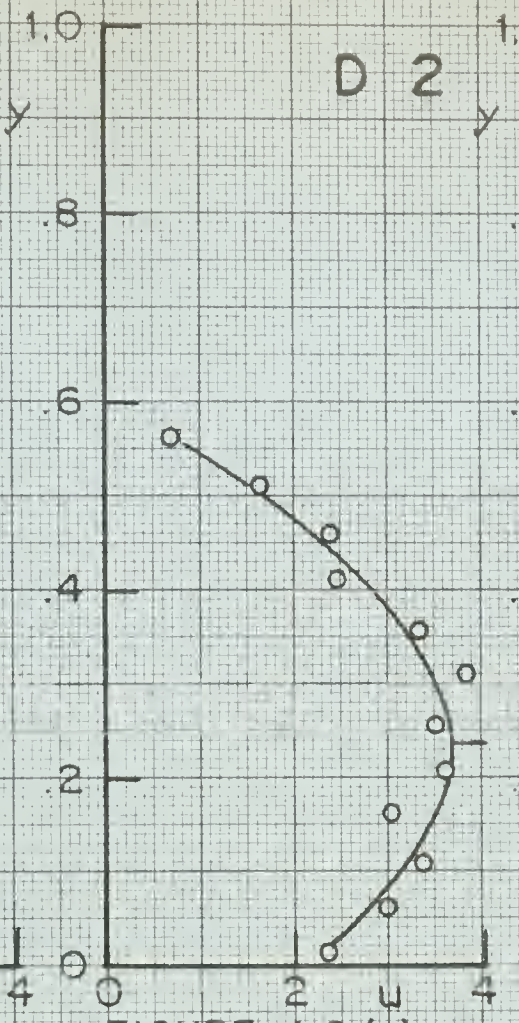

FIGURE 4.8 (r)

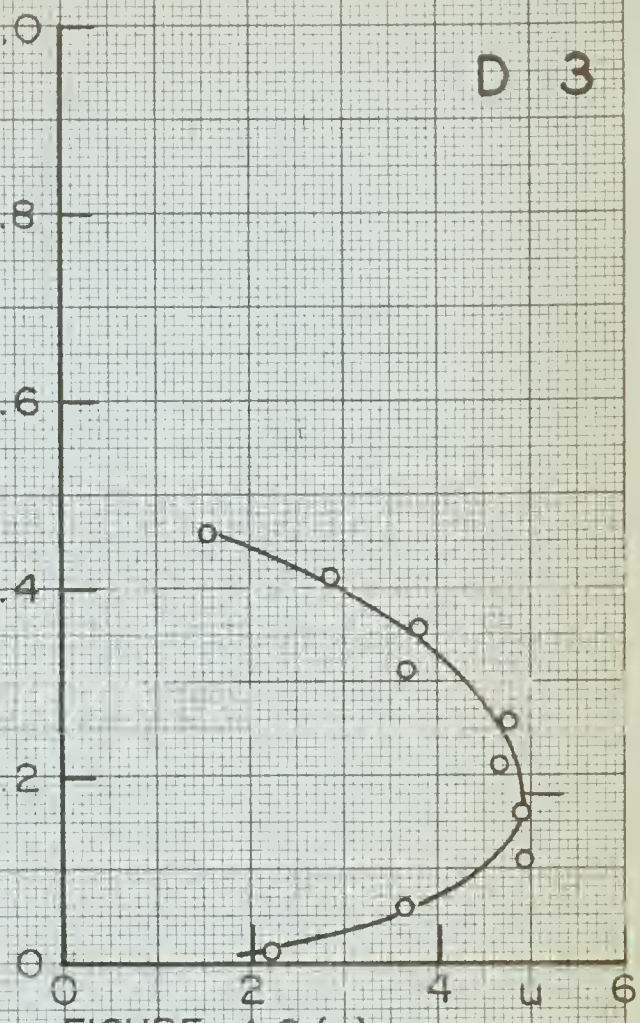

FIGURE 4.8 (s)

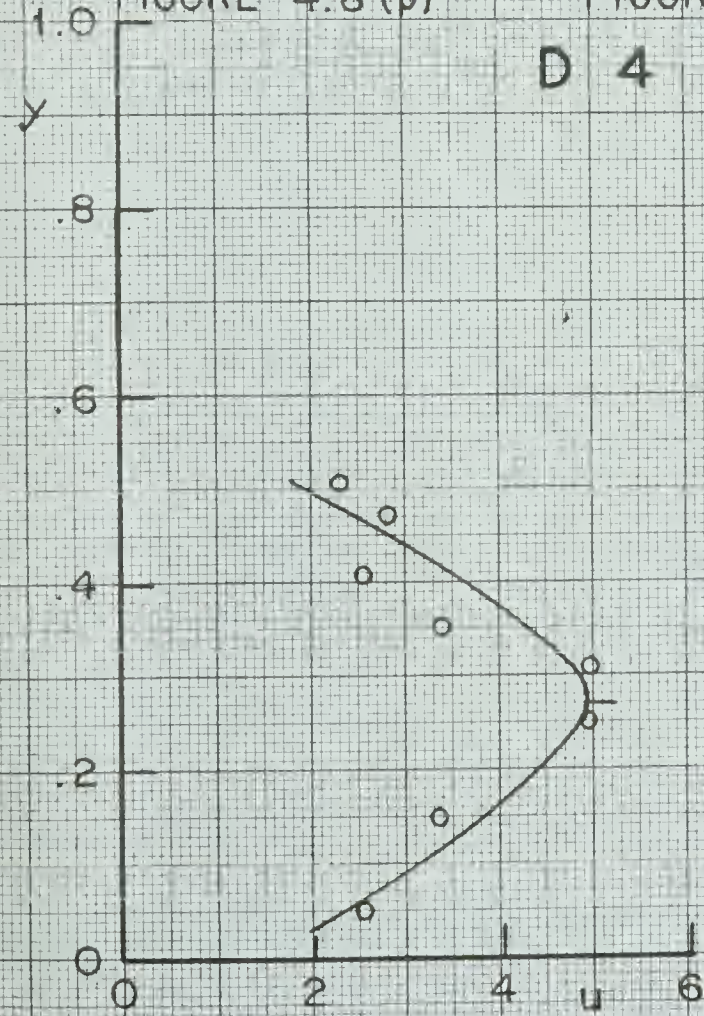

FIGURE 4.8 (t)

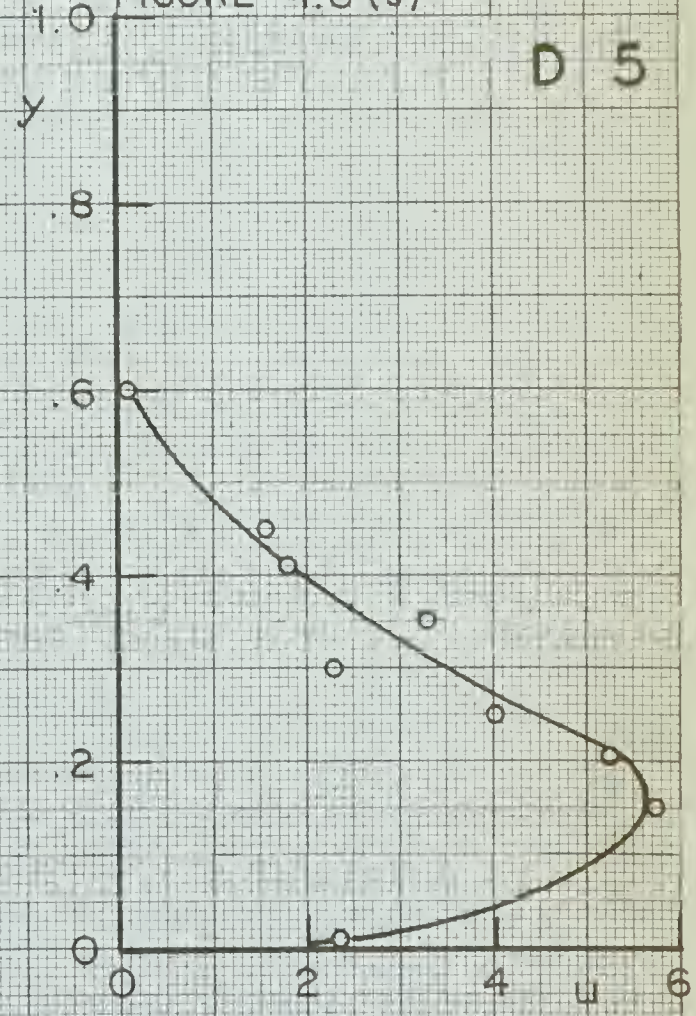

FIGURE 4.8 (u)

VELOCITY DISTRIBUTION PLOTS

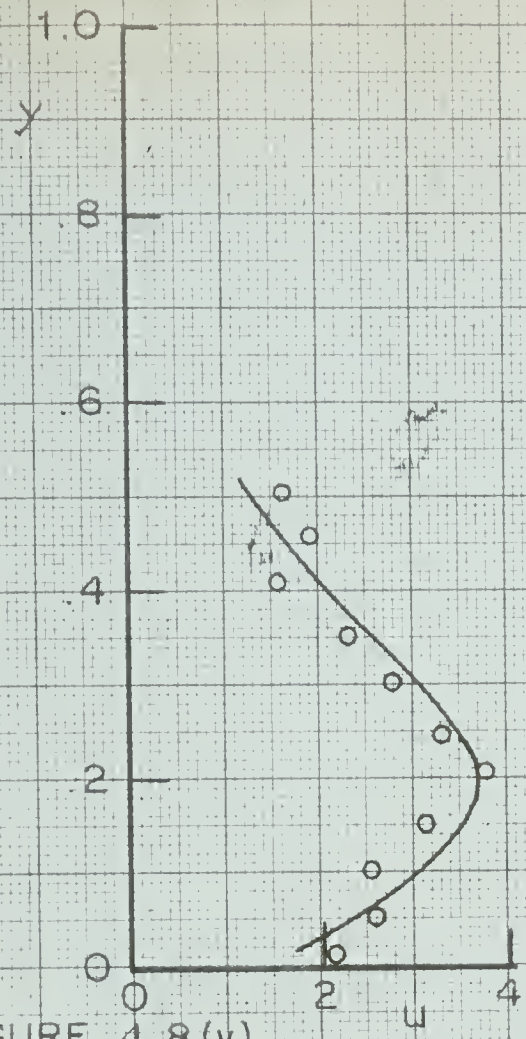

FIGURE 4.8 (v)

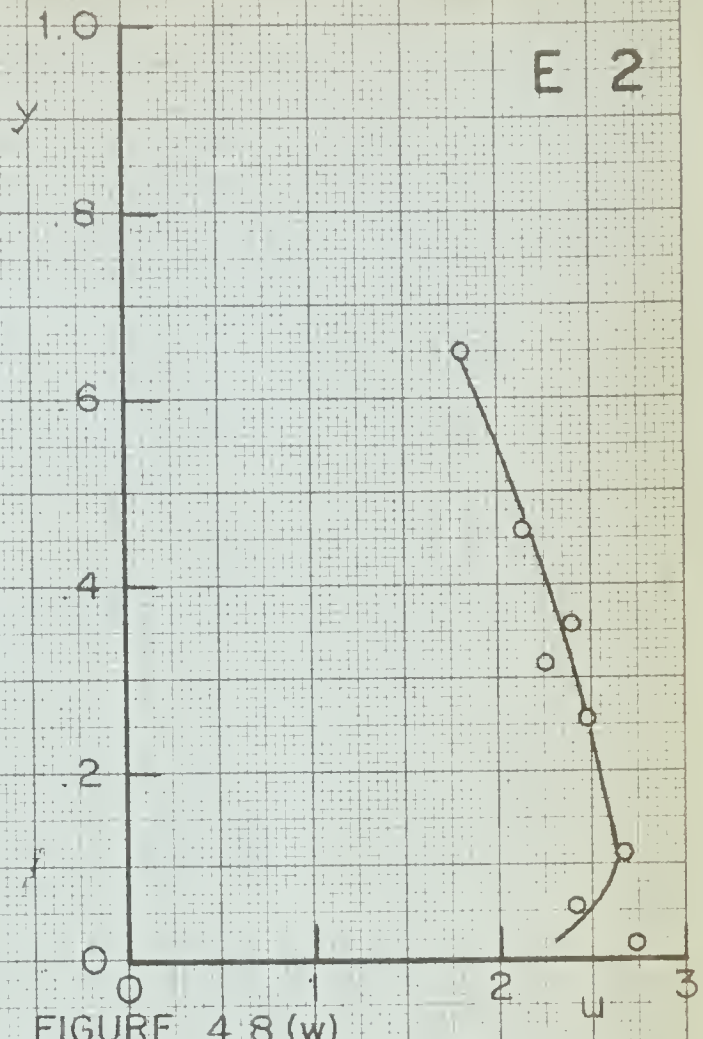

FIGURE 4.8 (w)

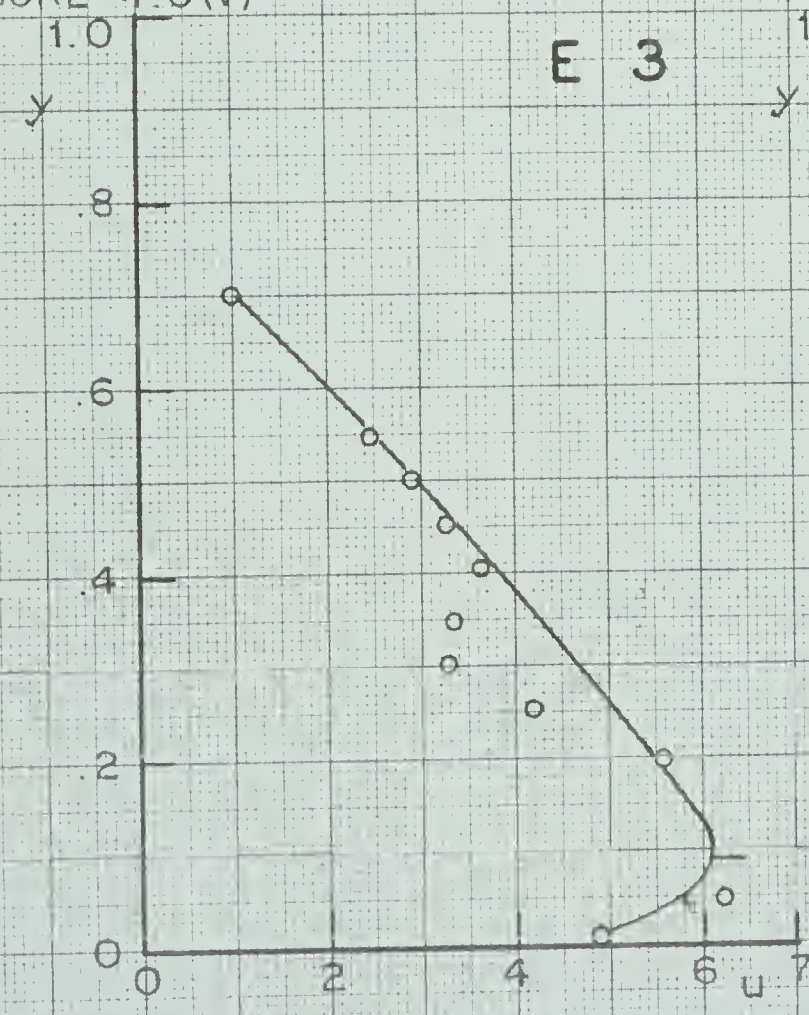

FIGURE 4.8 (x)

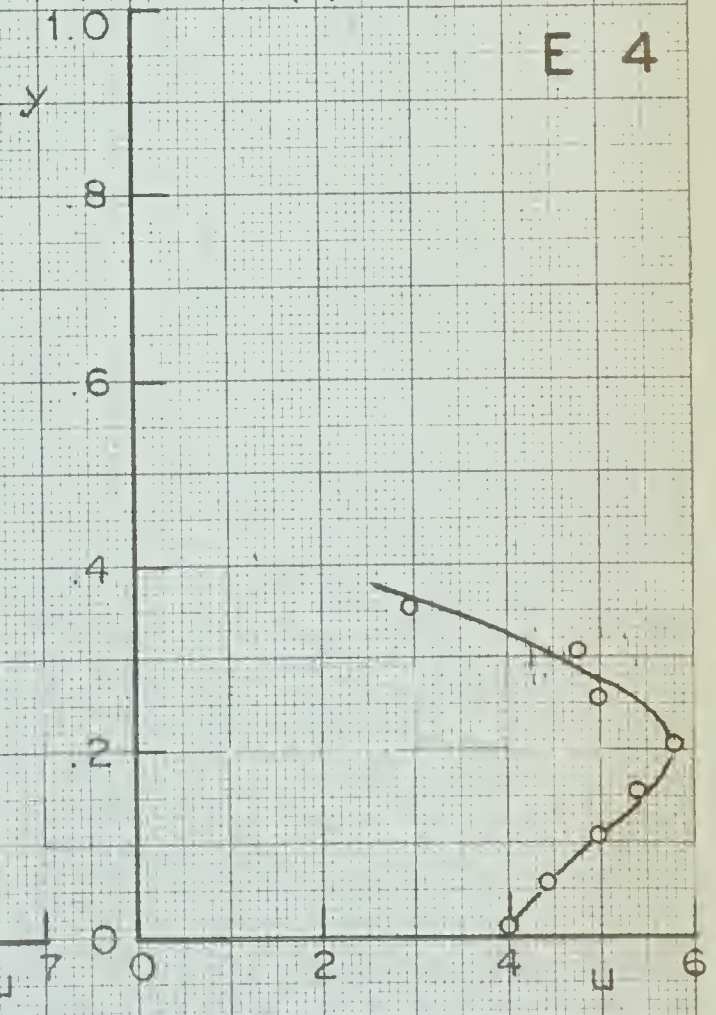

FIGURE 4.8 (y)

VELOCITY DISTRIBUTION PLOTS

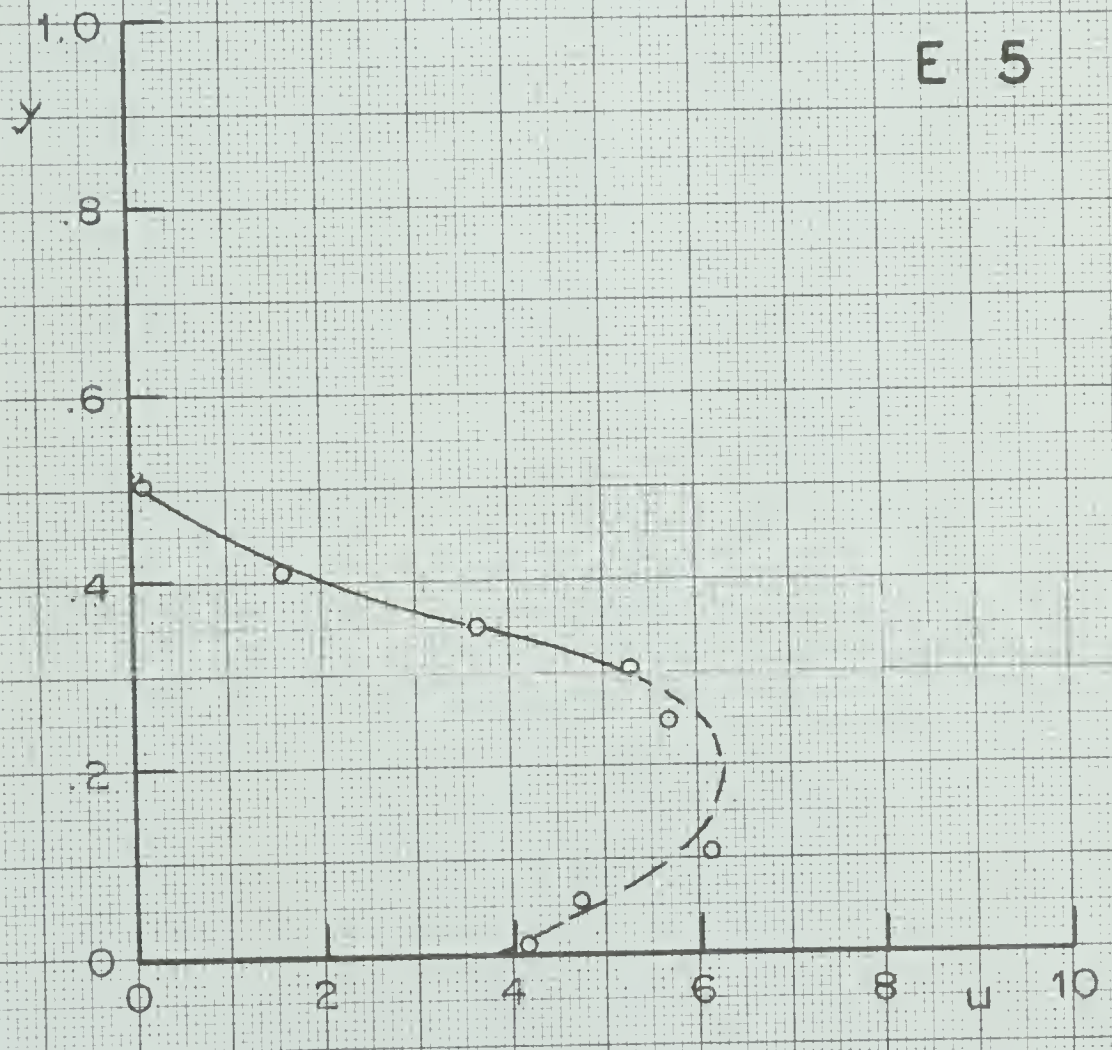

FIGURE 4.8 (z) VELOCITY DISTRIBUTION PLOT